Biophysicochemical properties of the 28-kDa *Schistosoma haematobium* and pseudo-26-kDa *Schistosoma haematobium/bovis* glutathione transferase

by

Neo Padi

(1482699)

A dissertation

Submitted in fulfilment of the requirements for the degree

Master of Science

in

Molecular and Cell Biology

in the Faculty of Science, University of the Witwatersrand, Johannesburg, South Africa

Supervisor: Dr Ikechukwu Achilonu

Sep 2022

DECLARATION

I, **Neo Padi (1482699)**, am a student registered for a **Master of Science in biochemistry and cell biology by dissertation** in the academic year **2021**. I hereby declare the following:

- I am aware that plagiarism (the use of someone else's work without their permission and/or without acknowledging the source) is wrong.
- I confirm that the work submitted for assessment for the above degree is my unaided work except where explicitly indicated otherwise.
- I have not submitted this work before for any other degree or examination at this or any other University.
- I have followed the required conventions in referencing the thoughts and ideas of others.
- I understand that the University of the Witwatersrand may take disciplinary action against me if there is a belief that this is not my unaided work or that I have failed to acknowledge the source of the ideas or words in my writing.

Signature  , 19th day of __Sep__ 2022

PUBLICATION

Part of the results presented in this dissertation have been published:

Padi, N., Akumadu, B.O., Faerch, O., Aloke, C., Meyer, V. and Achilonu, I., (2021). Engineering a Pseudo-26-kDa Schistosoma Glutathione Transferase from *bovis/haematobium* for Structure, Kinetics, and Ligandin Studies. *Biomolecules*, 11(12), 1844.

ABSTRACT

Schistosomiasis is a debilitating parasitic worm-induced, neglected tropical disease with veterinary and medical concerns in areas with poor socio-economic establishments. *S. haematobium* is one of the species that mainly affect humans and it has a zoonotic character enabling it to form hybrids with *S. bovis* thus justifying their common ancestor. In schistosomes, GSTs are primary detoxification enzymes. Moreover, they are involved in host immune response which makes them attractive drug candidates. However, studies are limited by an incomplete sequence of *S. haematobium* and there is a drug-resistant threat that calls for a new generation of anthelmintics. In this study, we designed a pseudo-Sbh26GST to elucidate its structural and functional properties in response to potential inhibitors, praziquantel (PZQ); artemisinin (ART) and bromosulfophthalein (BSP) in comparison to the well-studied Sh28GST. Several sequence analysis tools were used to complete the sequence of *S. haematobium/bovis* and generate the pseudo-Sbh26GST which was overexpressed successfully in *E. coli* with vector, pMAL-c5x while Sh28GST was expressed in pET-11a. All proteins were in the soluble fraction and then purified to >95% homogeneity. Functional characterisations were based on the classical GSTs glutathione (GSH) and 1-chloro-2,4 (CDNB) conjugation assay. Sh28GST had a higher 44 µmol/min/mg activity towards CDNB relative to 13 µmol/min/mg for Sbh26GST. PZQ and ART slightly increased the activity insignificantly while BSP inhibited Sbh26GST with an IC_{50} of 27 µM and 0. 88 µM for Sh28GST. The mode of inhibition, determined by kinetics was found to be random and non-competitive respectively. Structural characterisations were studied through Far-UV circular dichroism which showed that both proteins have a predominantly α-helical secondary structure content. Fluorescence spectroscopy studies showed that BSP and ART disturbed the local Trp environment whereas PZQ had an insignificant effect, all in the presence and absence of co-substrate, GSH and its similar structure, S-hexylglutathione (GTX). Additionally, extrinsic 8-anilino-1-naphthalenesulfonate fluorescence proved that BSP outcompetes it, while PZQ enhances it thus showing competition for the dimer interface and hydrophobic binding site. Thermodynamics parameters obtained by isothermal titration calorimetry indicate that the interaction between dimeric Sbh26GST and Sh28GST with one molecule of BSP is spontaneous and enthalpically driven, with additional entropy support in Sbh26GST but entropy cost in Sh28GST. Stability inferences from SYPRO Orange-based thermal shift assay demonstrated Sbh26GST had increased stability in the presence of BSP and GSH. BSP proved to bind and inhibit both proteins which translate to possibly rationalized new generation anthelmintics for the treatment of schistosomiasis.

“To God who was faithful to complete the good work, he began”

Family and friends who were there since day one

ACKNOWLEDGEMENTS

I could have not done it all alone, it was only by the grace of God. I would like to pass on my special gratitude to the people I encountered through my MSc journey, from family, colleagues, and friends to strangers. The love was something else.

My supervisor, Dr Ikechukwu Achilonu always pushed me to reach my full potential through constructive criticism. While simultaneously, being gentle by taking every step with me under his wings on a personal and professional level (going the extra mile). It was an honour to be acquainted with an expert who was patient with me and understanding.

Protein Structure-Function Research Unit (PSFRU) for being a conducive place that promotes learning under the guidance of the founder, Professor H.W. Dirr; director, Professor Yasien Sayed; and the leadership of Dr Sylvia Fanucchi. The ESKAPE group which is also involved in GSTs projects, in particular Blessing Oyiogu and Kagiso Pooe for guidance and advice as they have worked with *Schistosoma* GSTs. My experienced colleague who went before me, Dr Monare Thulo for taking off his time to teach me a valuable technique, isothermal titration calorimetry, and interpretation guidance. The rest of the unit members shared their knowledge and critics over small chats during data collection and analysis.

The department of Water and Sanitation (DWS) for funding my studies and providing additional financial support for a smooth varsity life. The bursary was one of the motivations that kept me going.

My family for always supporting me and believing in me when the world tells me otherwise. The prayers of my parents have kept me thus far. My siblings were my first teachers of fairness, cooperation, kindness and caring. Friends who turned into a family for lending me their ears.

To God be the glory for successfully completing my MSc research.

TABLE OF CONTENTS

DECLARATION II

PUBLICATION III

ABSTRACT IV

ACKNOWLEDGEMENTS VI

TABLE OF CONTENTS VII

LIST OF ABBREVIATIONS AND ACRONYMS XI

LIST OF FIGURES XIV

LIST OF TABLES XVI

CHAPTER 1: INTRODUCTION 1

1.1. Background 1

1.2. Problem statement 1

1.3. Rationale 2

1.4. Aims and objectives 2

1.5. Novelty 3

1.6. Limitation scope of the study 3

CHAPTER 2: LITERATURE REVIEW 5

2.1. Schistosomiasis epidemiology 5

2.2. The life cycle of schistosomes 7

2.3. Pathology of schistosomiasis 9

2.4. Treatment of Schistosomiasis 11

2.5. Parasitic glutathione transferases 12

2.6 Activity properties of GSTs- substrate specificity and inhibition 16

CHAPTER 3: OVER-EXPRESSION AND PURIFICATION OF SBH26GST AND SH28GST 18

3.1. Introduction 18

3.2. Materials 18

3.3. Methods 18

3.3.1. Gene construction of Sbh26GST 18

3.3.2. Design of vectors enabling expression of Sbh26GST and Sh28GST 19

3.3.3. Transformation of T7 E. coli cells with vectors, pMAL-c5X and pET-11a for expression of Sbh26GST and Sh28GST 20

3.3.4. Qualitative analysis of Sbh26GST and Sh28GST on gels 22

3.3.5. Overexpression of Sbh26GST and Sh28GST 23

3.3.6. Affinity chromatography purification of Sbh26GST and Sh28GST 24

3.3.7. Protein concentration determination 26

3.4. Results 27

3.4.1 Sbh26GST gene construct 27

3.4.2. Overexpression of Sbh26GST and Sh28GST 30

3.4.3. Affinity chromatography purification of Sbh26GST and Sh28GST 30

3.4.4. Protein quantification 33

3.5. Discussion 34

CHAPTER 4: STRUCTURE-FUNCTION CHARACTERISATION OF GSTS FROM *S. HAEMATOBIUM*/*BOVIS* 37

4.1. Introduction 37

4.2. Materials 37

4.3. Methods 37

4.3.1. Enzyme activity studies 37

4.3.2. Inhibition analysis-IC_{50} of BSP 38

4.3.3. Enzyme steady-state kinetics 39

4.3.4. Secondary structure 40

4.3.5. Tertiary structure 41

4.3.5.1 Intrinsic tryptophan fluorescence spectroscopy 41

4.3.5.2 Extrinsic ANS fluorescence spectroscopy 42

4.4. Results 43

4.4.1 Functional characterisation 43

4.4.1.1 Catalytic activity of Sbh26GST and Sh28GST 43

4.4.1.2 Inhibition studies for IC_{50} determination 45

4.4.1.3 Enzyme kinetics of GSTs' GSH-CDNB conjugation 45

4.4.2 Structural characterisation 48

4.4.2.1 Far-UV circular dichroism spectropolarimetry 48

4.4.2.2 Intrinsic tryptophan fluorescence 48

4.4.2.3 Extrinsic ANS fluorescence 51

4.5. Discussion 53

CHAPTER 5: THERMODYNAMICS OF BSP-SBH26GST/SH28GST INTERACTION ... 57

5.1. Introduction 57

5.2. Materials 58

5.3. Methods 58

5.4. Results 59

5.5. Discussion 61

CHAPTER 6: STABILITY OF GSTS FROM *S. HAEMATOBIUM*/*BOVIS* 64

6.1. Introduction 64

6.2. Materials 64

6.3. Methods 64

6.4. Results 66

6.5. Discussion 66

SCHAPTER 7: SUMMARY, CONCLUSION, AND POSSIBLE FUTURE DIRECTIONS 70

REFERENCES 73

APPENDIX 83

Supplementary material 83

LIST OF ABBREVIATIONS AND ACRONYMS

A_{280}	absorbance at 280 nm
ANS	8-anilino-1-naphthalenesulfonate
CD	circular dichroism
CDNB	1-chloro-2.4-dinitrobenzene
C-terminal	carboxylic acid terminal
Da	dalton
DNA	deoxyribonucleic acid
DTT	dithiothreitol
EC	enzyme class
E. coli	*Escherichia coli*
EMBL	European molecular biology laboratory
EDTA	ethylenediaminetetraacetic acid
ΔH	enthalpy change
ΔS	entropy change
ΔG	Gibbs free energy
GSH	reduced L-glutathione
G-site	glutathione binding site
GST	glutathione S-transferase
H-site	hydrophobic electrophilic substrate binding site
IC_{50}	50% inhibitory concentration
IMAC	immobilised metal affinity chromatography
IPTG	isopropyl-β-D-thiogalactopyranoside
ITC	isothermal titration calorimetry

pI	isoelectric point
kDa	kilodalton
k_d	dissociation constant
k_{cat}	turnover number
k_{cat}/K_M	catalytic efficiency
K_M	Michaelis-Menten constant
kJ/mol	kilojoules per mole
mdeg	millidegrees
Mw	molecular weight
NTD	neglected tropical disease
N-terminal	amino-terminal
µL	microlitre
µm	micrometre
µM	micromolar
nm	nanometre
nM	nanomolar
L-site	non-substrate ligand binding site in GSTs
ε	molar extinction coefficient
[θ]	mean residue ellipticity
MCS	multiple cloning site
OD	optical density
PBS	phosphate buffer saline
RMSD	root mean square deviation
rpm	revolution per minute

Sb26GST	*Schistosoma bovis* 26 kDa glutathione transferase
Sbh26GST	*Schistosoma bovis*/*haematobium* 26 kDa glutathione transferase
Sj26GST	*Schistosoma japonicum* 26 kDa glutathione transferase
Sh28GST	*Schistosoma haematobium* 28 kDa glutathione transferase
SDS-PAGE	sodium dodecyl sulphate polyacrylamide gel electrophoresis
TCEP	tris(2-carboxyethyl)
TEMED	*N, N, N', N'* tetramethylethylenediamine
Tris-HCl	tris(hydroxymethyl) aminomethane hydrochloric acid
UV	ultraviolet
v/v	volume per volume
w/v	weight per volume

Amino acids are named according to the three-letter codes of the International Union of Pure and Applied Chemistry (IUPAC).

LIST OF FIGURES

Figure 2.1. Global distribution of schistosomiasis.....6

Figure 2.2. The lifecycle of Schistosoma parasite. 8

Figure 2.3. Pathologies of schistosomiasis. 10

Figure 2.4. Cartoon homology model of Sj26GST for Sbh26GST elucidation.....15

Figure 2.5. 2D structural illustration of the three ligands used in the study 17

Figure 3.1 Schematic diagram of pMAL-c5X and pET-11a vector maps 21

Figure 3.2. Sequence alignment of the putative 26 kDa GSTs from S. bovis and S. haematobium fragments.....28

Figure 3.3. Protein sequence alignment of 26 kDa GSTs from Schistosoma bovis with homologous species.. 29

Figure 3.4. Synthesized Sbh26GST 29

Figure 3.5. The overexpression of Sbh26GST and Sh28GST 31

Figure 3.6. Affinity chromatography of Sbh26GST and Sh28GST.. 32

Figure 3.7. Absorbance spectra of Sbh26GST and Sh26GST.. 33

Figure 3.8. Protein quantification of Sbh26GST and Sh26GST.....34

Figure 4.1 Schematic description of CDNB conjugating assay.....38

Figure 4.2. 2D illustration of the structures of 8-anilino-1-naphthalenesulfonate.....42

Figure 4.3. Specific activity towards GSH-CDNB conjugation 44

Figure 4.4. The inhibitory concentration of BSP on Sbh26GST and Sh28GST.....45

Figure 4.5. Michaelis-Menten curve of Sbh26GST and Sh28GST towards GSH.....47

Figure 4.6. Far-UV CD spectra of Sbh26GST and Sh28GST.. 49

Figure 4.7. Trp fluorescence emission spectrum of Sbh26GST vs Sh28GST.....50

Figure 4.8. ANS fluorescence emission spectrum of Sbh26GST vs Sh28GST.....52

Figure 5.1. Schematic diagram of ITC concept. 58

Figure 5.2. ITC titration of BSP into Sbh26GST and Sh28GST.....60

Figure 6.1 Visual representation of thermal shift assay layout.....65

Figure 6.2. Thermographs of Sbh26GST.....67

Figure 6.3. Melting temperatures for Sbh26GST in varying ligands 68

Figure S1. Thrombin cleavage trials.....83

Figure S2. Absorbance spectrum of ligands used in the study (PZQ, ART and BSP). 83

Figure S4. Linear-plots of Michaelis-Menten kinetics for Sbh26GST and Sh28GST. 85

Figure S5. k_{cat} determination of Sbh26GST and Sh28GST......86

Figure S6. Trp fluorescence emission spectra of Sbh26GST in the presence of GSH (A) and GTX (B) as well as Sh28GST in the presence of GSH (C) and GTX (D).. 87

Figure S7. ANS fluorescence emission spectra of Sbh26GST in the presence of GSH (A) and GTX (B) as well as Sh28GST in the presence of GSH (C) and GTX (D).. 89

Figure S8. Thermogram and isotherm of Sbh26GST and Sh28GST interacting with BSP.. ..91

Figure S9. Thermogram of Sbh26GST......92

LIST OF TABLES

Table 4.1. Kinetic parameters of Sbh26GST and Sh28GST 46

Table 4.2. Dichroweb data for secondary structure content of Sbh26GST and Sh28GST.....49

Table 5.1. Thermodynamic parameters of the interaction between BSP and protein, Sbh26GST and Sh28GST in the presence and absence of GSH (co-substrate), respectively 61

Table S1. The variation of Michaelis-Menten Kinetic parameters of Sbh26GST and Sh28GST based on different arrangements of the linear plots for error analysis.....86

Table S2. Impact of ligand binding on Trp fluorescence emission of Sbh26GST and Sh28GST with respect to PZQ, ART and BSP in the presence and absence of GSH and GTX.....88

Table S3. Impact of ligand binding on ANS fluorescence emission of Sbh26GST and Sh28GST with respect to PZQ, ART and BSP in the presence and absence of GSH and GTX.....90

Table S4. Thermodynamic parameters of BSP interaction with Sbh26GST and Sh28GST in the presence and absence of GSH based on multiple sites model fitting (H-site vs L-site).....91

Chapter 1
Introduction

1.1. Background

Schistosoma haematobium is a parasitic trematode that causes urogenital schistosomiasis, a neglected tropical disease most prevalent in sub-Saharan Africa and affects over 230 million people worldwide (Chitsulo *et al.*, 2000; Steinmann *et al.*, 2006; King and Dangerfield-Cha, 2008; Vos *et al.*, 2012). The infection results in an induced range of chronic pathologies that include anaemia, impaired cognition, growth stunting, organ fibrotic damage and cancer as well as enhanced susceptibility to other infections such as HIV/AIDS (Kallestrup *et al.*, 2006; Burke *et al.*, 2009; Downs *et al.*, 2012; Secor, 2012). For over a decade, schistosomiasis control has been driven by the mass administration of praziquantel (PZQ) treatment. Still, it is under pressure with a fairly unchanged significant disease burden of helminths.

1.2. Problem statement

There have been several attempts to contain the transmission of schistosomiasis infections. One of the World Health Organisation (WHO) programmes proposed reducing the densities of intermediate hosts (snails) using molluscicides, but the plan was abandoned as it proved to be a high cost linked to environmental hazards (Utzinger *et al.*, 2009). Alternatively, chemotherapy and several drugs were used for the treatment of schistosomiasis as well as good hygiene. Unfortunately, affected populations could hardly afford the costs, and some drugs were not effective except as supplements (Caffrey, 2007; Doenhoff *et al.*, 2008). The only standing treatment for schistosomiasis is PZQ, which is majorly effective against adult worms and not early-stage immature worms (Colley *et al.*, 2014)

Moreover, its mode of action is not fully understood, and it has a short half-life (1-2 hrs) that does not promote combination therapy in some cases such as chemoprophylaxis (Ross *et al.*, 2002). Available helminths controls are held back by drug tolerance or failure and post-treatment reinfections as supported by reports of some *Schistosoma* species displaying drug resistance against PZQ in endemic countries and laboratory models (Doenhoff *et al.*, 2008). Hence, the burden of some *Schistosoma* species remains unchanged. There is a need to identify and develop new approaches for a rationalised new generation of anthelmintics

1.3. Rationale

It is essential to develop new therapeutics to control schistosomiasis due to the threat of PZQ resistance that might cause breakouts and re-infections that are not decreasing the disease burden. An attractive drug target candidate in schistosomes is their glutathione S-transferase enzymes (Connelly *et al.*). They are primarily essential for detoxification in parasitic helminths for survival (Ramsay and Dilda, 2014). GSTs also exhibit a high capacity to bind various non-substrate with different affinities to render their uptake and transportation. Additionally, this ligandin function has been associated with the regulation of GSTs activity as ligand binding can inhibit the catalytic properties of these enzymes.

Ligands such as bromosulfophthalein (BSP) and ellagic acid (EA) were reported to bind at the dimer interface and inhibit the activity of the closely related 26 kDa *S. japonicum* GSTs (Sj26GST) (Yassin *et al.*, 2004; Akumadu *et al.*, 2020; Pooe *et al.*, 2021). Similarly, PZQ has been shown to bind at the dimer interface of Sj26GST but with no inhibition (McTigue *et al.*, 1995; Milhon *et al.*, 1997). This phenomenon of ligands binding at the dimer interface is not common in human GSTs, so the binding could be accounted for by the structural variations of *Schistosoma* GSTs being more hydrophobic, thus forming the structural backbone required for rational drug design of substrate analogue inhibitors. The structural profile of the protein of interest, *S. haematobium* 26 kDa GST is limited as its open reading frame (ORF) is incomplete unlike the 28 kDa isoform and it has previously impeded its research progression. However, we completed the sequence through common ancestor homology analysis in this study, thus yielding a pseudo-26 kDa *S. haematobium*/*bovis* GST (Sbh26GST). All in all, to introduce potential inhibitors against *Schistosoma* GSTs for the control of schistosomiasis, namely ART and BSP which are all available in the market thus decreasing the cost and time of drug discovery.

1.4. Aims and objectives

This study aimed to determine the structural and functional characterisation of a pseudo-Sbh26GST and Sh28GST in the presence and absence of potential inhibitors namely PZQ, ART and BSP. The following objectives were used to address the research question:

- To recombinantly overexpress pseudo-Sbh26GST and Sh28GST with pMALc5X and pET-11a vector respectively, in an *Escherichia coli* (*E. coli*) system.
- To purify the recombinant proteins with various affinity chromatography, namely maltose-binding protein (MBP) and immobilised metal affinity chromatography (IMAC)

- To perform a quality assessment of the expression and purification using sodium dodecyl sulphate polyacrylamide gel electrophoresis (SDS-PAGE)
- To determine the concentrations of the purified recombinant enzymes spectrophotometrically
- To conduct structural and functional characterisation of Sbh26GST and Sh28GST by performing:
    - CDNB/GSH conjugation assay for its specific activity and effects of ligands
    - The far-UV circular dichroism for secondary structure content
    - Fluorescence spectroscopy to analyse solvent accessibility of intrinsic Trp residues and extrinsic 8-anilino-1-naphthalenesulfonate binding in the presence and absence of ligands
- To Obtain the IC_{50} of potential GSH-CDNB conjugation assay inhibitors
- To determine kinetic parameters (V_{max}, K_M, k_{cat}, k_{cat}/K_M) of Sbh26GST and Sh28GST in the presence and absence of ligands
- To understand the energetics of binding through thermodynamic parameters (ΔH, ΔS, ΔG and K_d) using isothermal titration calorimetry.
- To perform conformational stability studies via thermal shift assay in response to ligands

1.5. Novelty

GSTs are highly conserved across different schistosomes thus rendering them suitable targets for drug therapy. They play a critical role in detoxification; hence targeting GSTs would cause catastrophic metabolic deficits in parasites that would lead to cell death. However, the gene sequence of some GST species such as *S. haematobium* is incomplete, which has previously limited studies. The sequence design of a complete open ORF of Sh26GST was based on closely related homologous species to produce a pseudo-Sbh26GST, a concept that has never been explored. These were performed to achieve high yields of soluble Sbh26GST that is easy to purify and active for characterisation of structural and functional insights using biophysical and chemical strategies.

1.6. Limitation scope of the study

The native structure of *S. haematobium* is unknown so we made structural and functional characterisation inferences based on a pseudo-design that is not a 100% true reflection of the *Schistosoma* species at hand. Furthermore, some ligands used were not soluble at high

concentrations in aqueous nor organic solvents at a percentage that was not detrimental to proteins and hence not incorporated in some cases. Given that ligands were dissolved in DMSO which causes a lot of background noise when it comes to CD studies, the effects of BSP and PZQ on the secondary structure of proteins of interest were not persuaded. Lastly, the GSH-CDNB conjugation assay used for kinetic studies was not useful for the determination of the H-site mode of inhibition as CDNB is not a natural substrate of GST and could not reach saturation.

Chapter 2
Literature review

2.1. Schistosomiasis epidemiology

Helminths are ancient scourges of humans with insidious impact. They are usually characterised by chronic diseases that gradually deteriorate one's health, unlike bacterial and viral diseases that mostly produce acute illness (Abraham *et al.*, 2018; Stutzer *et al.*, 2018). Amongst species of concern, Schistosomiasis infections are one of the major threats. Schistosomiasis (bilharziasis) is a waterborne disease instigated by parasitic blood flukes (trematodes) from *Schistosoma*. Amongst neglected tropical diseases (NTD), schistosomiasis is one of the most debilitating diseases and comes second to malaria (Sangweme *et al.*, 2010). This parasitic infection tackles both humans and animals, thus posing an alarming medical and veterinary concern that strains the socio-economic state of affected regions. Worldwide conservative estimates revealed that over 230 million people are infected with schistosomiasis, of which 200 000 die annually, and 800 million people are at risk (Hotez *et al.*, 2014; McManus *et al.*, 2018). In addition, schistosomiasis is responsible for at least 3.3 million disability-adjusted life years (DALYs) due to clinal and subtle morbidities associated with the infection (King *et al.*, 2005; Vos *et al*., 2012). The most affected groups are school-aged children and pregnant women in tropical regions such as sub-Saharan Africa. These areas where schistosomiasis is prevalent, are usually associated with indigent and rural societies that are resource-deprived with low incomes or large segments of world populations (Chitsulo *et al*., 2000; Colley *et al*., 2014; Anisuzzaman and Tsuji, 2020). In terms of livestock, schistosomiasis has been estimated to affect 165 million cattle (De Bont and Vercruysse, 1997). Animal schistosomiasis does not receive as much attention as human schistosomiasis. However, there is some evidence of bidirectional introgressive hybridisation between a bovine and human *Schistosoma* due to environmental changes (Huyse *et al.*, 2009). This poses a threat of heterosis, which can negatively impact schistosomiasis prevalence, pathology, and treatment.

Schistosomes were first discovered in 1851 by Theodor Bilharzia. There are several *Schistosoma* species of attention flagged by the WHO with distinct geographic distributions, tissue localisation and clinical manifestations: *S. mekongi, S. intercalatum, S. bovis, S. matteei, S. japonicum, S. mansoni* and *S. haematobium.* The latter three predominate human infections, *S. mansoni* occurs in Arabia, South America, the Caribbean, and Africa; intestinal *S. japonicum* in the Philippines, China and Japan; and urinary *S. haematobium* in the Middle

East and Africa as depicted in Figure 2.1. The schistosomes species also have their respective intermediate snail species that determine their prevalence: *Tricular* (*Neotricular aperta*) for *S. mekongi*, *Biomphalaria* for *S. mansoni*, *Oncomelania* for *S. japonicum* and *Bulinus* for *S. haematobium* and *S. intercalatum*.

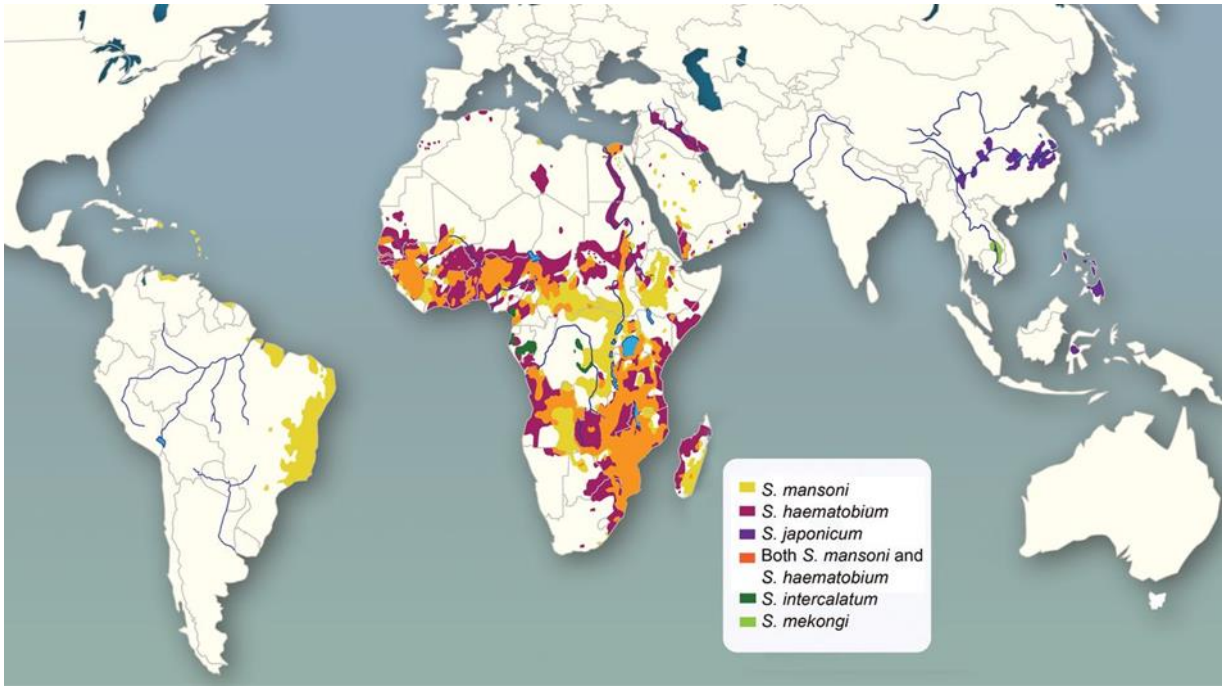

Figure 2.1. Global distribution of schistosomiasis. Amongst the areas that various *Schistosoma* species dominate, *S. mansoni* is local to sub-Saharan Africa, Surinam, the Arabic peninsula, lower and middle Egypt, Venezuela, northeast Brazil, and the Caribbean; *S. haematobium* is endemic in sub-Saharan Africa, Egypt to Sudan (Nile river), the Arabian Peninsula and the Maghreb; *S. japonicum* dominates China (River Yangtze and central lakes), small pockets in Indonesia, Mindanao, Leyte, and some other Philippian islands; *S. mekongi* is frequent in central Mekong Basin in Laos and Cambodia; *S. intercalatum* is central to the pockets in the west and central Africa. https://journals.asm.org/doi/10.1128/cmr.00137-14.

These parasitic worms attack their definitive host through skin penetration and migrate to their respective site of infection (bladder or intestine) via the blood circulatory system. In the process, the schistosomes undergo various morphological, physiological, and biochemical changes that further develop them into male and female mature worms that eventually pair up and lay eggs. However, the changes are accompanied by high hazardous oxidative stress caused by internal and external host immune responses (Alger and Williams, 2002). Therefore, schistosomes promote survival by releasing immunomodulating molecules that paralyze the highly orchestrated defence mechanism of the host during the invasion and express a syncytial tegument with detoxification systems. This unique host-interaction layer has gained attention in research due to the expression of potential drug and vaccine targets (Ressurreição *et al.*, 2016). These include three antioxidant enzymes, namely: super-oxidase

dismutase responsible for dividing toxic superoxide (O_2^-) radicals into oxygen (O_2) and hydrogen peroxide (H_2O_2) via oxidative metal potential (Mkoji *et al.*, 1988); glutathione peroxidase that reduces hydrogen peroxide to water and oxygen as well as peroxide radicals to alcohols and oxygen via GSH oxidation (Arthur, 2000). Lastly, GST participates in the conjugation of electrophilic xenobiotics compound with GSH neutralising reactive oxidative species from lipid peroxidation. The link of parasitic GSTs to membranes explains their participation as the first line of defence against host immune response thus making them crucial in schistosomes to tolerate oxidative stress (Zelck and Von Janowsky, 2004). GSTs are also responsible for synthesising prostaglandin D2 (PGD2), which is essential for parasitic fertility and escaping the host's immune response through inhibition of the migration of Langerhans cells during infection (Baiocco *et al.*, 2006).

2.2. The life cycle of schistosomes

Schistosoma species have a two-host lifecycle as illustrated in Figure 2.2. The male and female adult worm co-exist whereby the male holds the female in a gynecologic canal groove in his body (A). The pair copulate and lay eggs within the mesenteric venules of the vertebrate host. In the case of *S. mansoni*, it dominates the large intestine, whereas *S. japonicum* goes for the small intestines, and *S. haematobium* uses the perivascular and rectal venules. The eggs are eliminated to the environment through urine (*S. haematobium*) or faeces (*S. mansoni* and *S. japonicum*) but when retained in human tissues, they thrive by feeding on erythrocytes and producing energy through glucose metabolism. The trapped eggs in the body re-enter the liver and heighten immune responses such as inflammation as the eggs build up. Once the eggs reach an optimal environment, they hatch and release a free-living ciliated larva called miracidia (C). The miracidia penetrate an intermediate host, snail tissue and mature into sporocysts which reproduce asexually and release multiple motile cercariae into water within 4-6 weeks (D). Upon release, infectious cercariae penetrate the unbroken skin of their definitive host, the ruminants/humans and lose their forked tail to develop into schistosomulae (E). The schistosomulae travels to the liver via the portal blood circulation to mature into adult worms and spread to their distinct residence depending on the species.

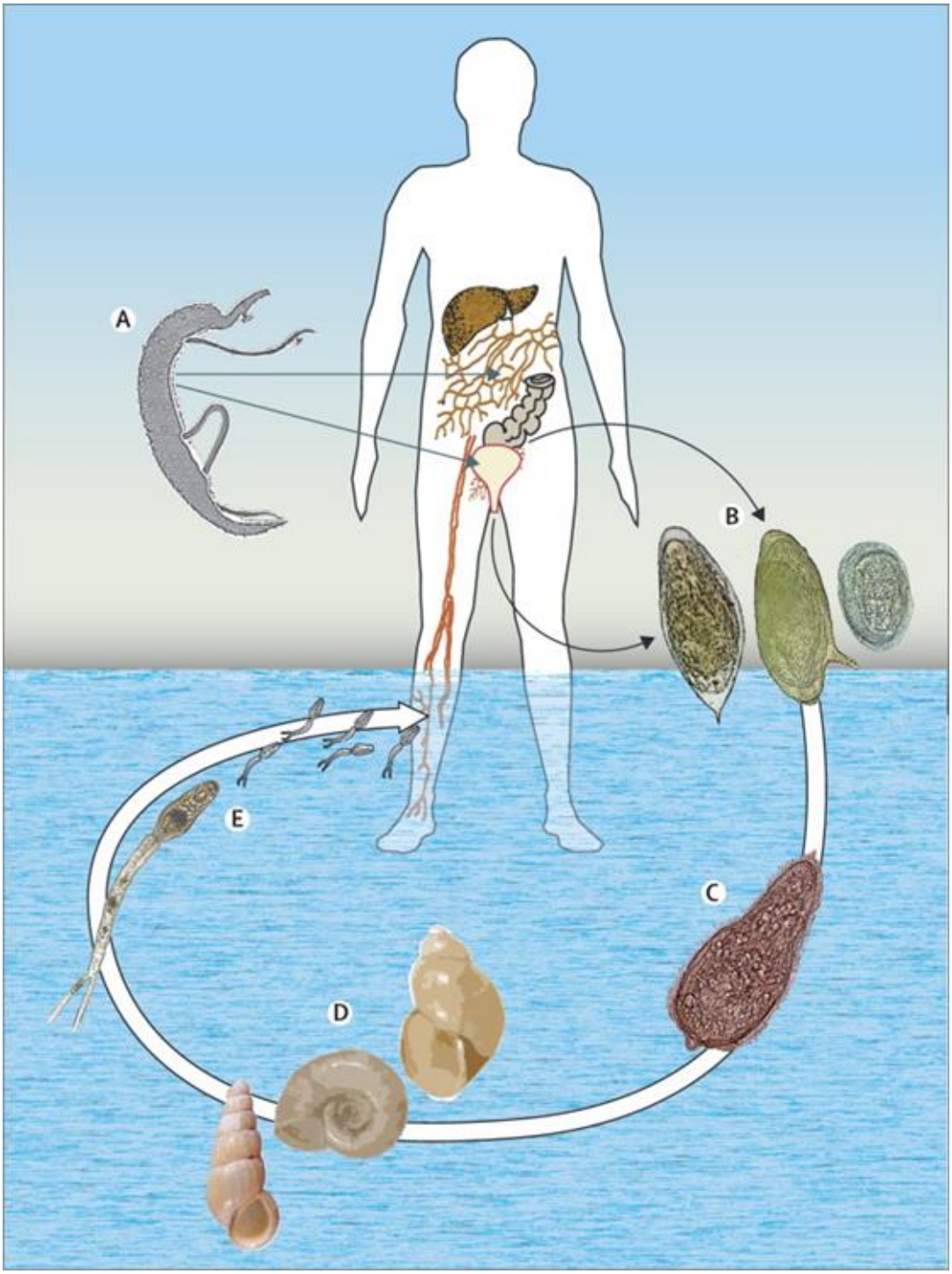

Figure 2.2. The lifecycle of *Schistosoma* parasite. **A**. Paired adult worms live and produce distinct eggs according to different species **B**. *S haematobium*, *S mansoni*, *S japonicum* (left to right). **C**. A ciliated miracidium matures and penetrates respective **D**. Intermediate host snails: *Oncomelania*, *Biomphalaria*, *Bulinus* (left to right) for asexual reproduction. **E**. Cercariae (Colley *et al*., 2014).

2.3. Pathology of schistosomiasis

The condition of schistosomiasis begins with the migratory stage (cercarial dermatitis and swimmer's itch) upon cercariae skin penetration, followed by acute Katayama syndrome within two to twelve weeks after infestation (Ross *et al*., 2002) and eventually becomes chronically organ-specific if left untreated. The worms mature and produce eggs that secrete antigens that induce an immune response of granulomatous inflammatory reactions, fibrosis, and obstruction as depicted in Figure 2.3 characterised by T-helper 2 cytokines, eosinophils and activated macrophages that result in clinical diseases (Burke *et al*., 2009). Clinical manifestation ranges from pain, lesions, gastrointestinal bleeding, tissue damage, and seizures to cancer depending on the *Schistosoma* species as they have varying locations and frequencies or times of egg production. The eggs embedded in the intestines, liver, bladder, or urogenital system rather than adult worms account for observed morbidities in *Schistosoma* infections. Childhood development is heavily compromised at both cognitive and physiological levels in cases of re-infection as well as in pregnant women, which leads to anaemia, malnutrition, splenomegaly, infants with low birth weight etc. Genital schistosomiasis is underappreciated despite being debilitating in females, resulting in infertility, menstrual disorders, and dyspareunia. In severe cases, schistosomiasis leads to tissue damage and disfigurement of limbs, increasing the susceptibility to other infections such as HIV. This was supported by studies that respectively showed that genital schistosomiasis infection was an apparent co-factor in the transmission of HIV (Downs *et al*., 2012; Secor, 2012), and patients with HIV showed a poor response to schistosomiasis chemotherapy (Kallestrup *et al*., 2006).

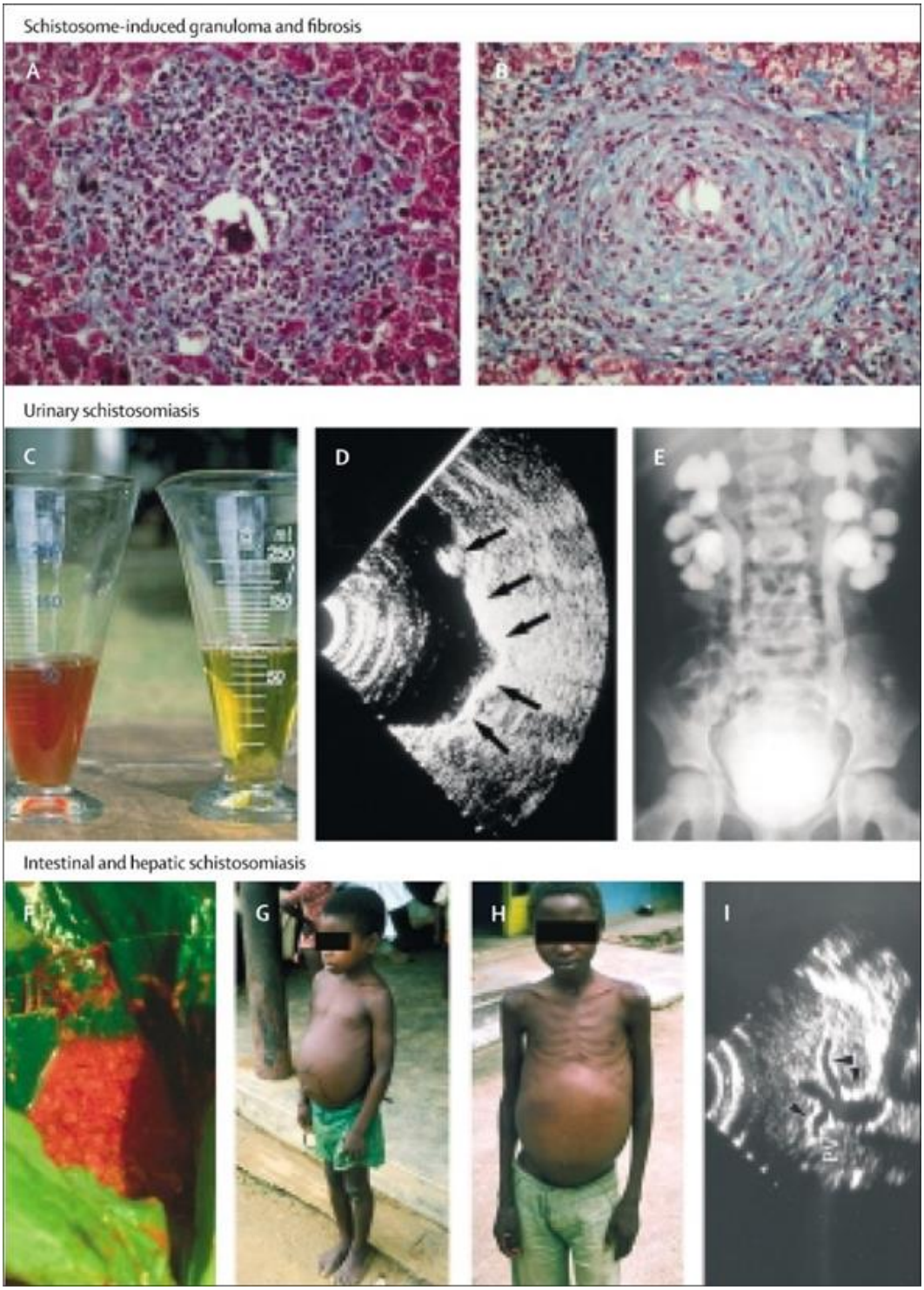

Figure 2.3. Pathologies of schistosomiasis. A. The liver of an experimental mouse showing acute granuloma from an infection of *S. mansoni* egg affecting eosinophils, lymphocytes, and some macrophages, but large red cells of murine hepatocytes were intact. **B** The progression to chronic liver granuloma surrounding the remaining schistosome egg in mouse liver where blue regions represent dominant fibrous tissue. **C** A closer look at urinary schistosomiasis depicting macrohaematuria caused by bladder wall ulceration. **D**. Irregular bladder wall and polyp captured with ultrasonography. **E**. Intravenous pyelography of bilateral hydroureter and hydronephrosis. **F** Severe bloody diarrhoea at late stages of *S. mansoni* infection. **G**. A minor with gross reactive hepatosplenomegaly. **H**. An adult depicting symptoms of chronic fibrotic hepatic schistosomiasis (splenomegaly, external varices, and growth retardation). **I.** An ultrasonography image of an advanced periportal fibrosis and portal venodilatation (Colley *et al*., 2014).

2.4. Treatment of Schistosomiasis

The treatment of schistosomiasis currently relies heavily on one drug, the anti-helminthic praziquantel (PZQ) ($C_{19}H_{24}N_2O_2$, M_W 312.41 g/mol) (Figure 2.5 A) which was discovered in 1982. The drug is specific to trematodes and cestodes by targeting the calcium ion channels of schistosomes for a Ca^{2+} influx that disrupts the permeability of cell membrane, resulting in contractions, vacuolization and disintegration of their tegument that signals an immune response. Secondary effects include glucose uptake inhibition, decreased glucose levels and enhanced lactate release. However, PZQ's activity is ideal under an effective host antibody response caused by adult schistosome worms producing eggs rather than poorly detected juvenile schistosomes (Colley *et al*., 2014). The mode of action that PZQ uses is not well understood (Doenhoff *et al*., 2008), despite having a well-tolerated administered dose of 40 mg/kg with minimal side effects that yields an outcome of 60% cure within 1-2 months of treatment (Kramer *et al.*, 2014). Alternative drugs for schistosomiasis include oxamniquine which only attacks *S. mansoni* (Fenwick *et al.*, 2003) and metrifonate for *S. haematobium* (Feldmeier and Chitsulo, 1999), but the high specificity of these drugs comes at the cost of high operational dose that causes remarkable side-effects like epileptic seizures, drowsiness etc. which poverty and underdevelopment associated endemic regions cannot afford. In addition, antimalarial drugs such as artemether and artesunate derivatives of artemisinin are also active against *Schistosoma* worms that are not fully developed to the adult stage (Utzinger *et al.*, 2000). Hence, artemisinin derivatives and praziquantel could be used together to enhance treatment in regions of high re-infection rates.

Despite inexpensive high cure rates of PZQ yielding a reduction in transmission and morbidity, mass administration for over four decades has placed pressure on the inevitable route of drug resistance (Cioli *et al.*, 2014). There are reported cases of PZQ tolerance in endemic regions by *S. mansoni* and laboratory-induced resistance cases of other species to back up the concern (Wang *et al.*, 2012). Another factor is the high chances of re-infection by unattacked immature schistosome larvae (Rollinson, 2009). Hence the need to identify new drugs with a well-understood mode of action that can be used solely or co-administered with other anti-helminths in integrated control programs. So far, the major vaccine and drug target against schistosomiasis is the primary detoxification enzyme, glutathione *S*-transferase with vaccines that have made it to clinical trials being Sh28GST (Bilhvax) and Sm14 (Ricciardi and Ndao, 2015). Nevertheless, the complicated life cycle of *Schistosoma* makes it challenging to control and eradicate this parasitic disease. Additional attractive stages that can be reduced include snail infections, human penetrations and pairing of adult worms but measures

in place are either costly, ineffective, or harmful. The key is to develop medication by analyzing the structure and function of a target molecule rather than using arbitrary drugs in the hope of eliciting a therapeutic effect.

2.5. Parasitic glutathione transferases

Glutathione S-transferases (EC 2.5.1.18) are a multifunctional superfamily of enzymes that form part of intracellular multi-gene isoenzymes responsible for phase II detoxification (Jakoby and Ziegler, 1990) of electrophilic compounds through GSH tripeptide (γ-Glu-Cys-Gly) conjugation to inactivate toxic molecules. This is achieved by increasing the solubility of electrophiles and eventually excreting them via a mercapturate pathway (Boyland and Chasseaud, 1969). However, the role of GSTs is not always catalytic, and they tend to bind a wide range of endo and exogenous ligands: alkyl or aryl halides, activated alkenes, epoxides, olefins, sulphate esters, quinones and organic peroxides for transportation; prostaglandin and leukotriene biosynthesis; catabolism of aromatic amino acids; isomerisation, modulation and/or development of ion channels and regulation of cell signalling transduction pathways responsible for cell survival and apoptosis via protein-protein interactions (Torres-Rivera and Landa, 2008). GSTs are classified into different groups based on their localisation, sequence similarities and interactions with substrates. This includes the mitochondrial GSTs, microsomal GSTs or MAPEG (membrane proteins associated with eicosanoid and glutathione metabolism) and cytosolic GSTs. The mitochondrial group includes Kappa (κ) (Pemble *et al.*, 1996), which plays a major role in the β-oxidation of fatty acids and lipid peroxidase. The microsomal GSTs are not well characterised like other groups despite studies that showed there are four groups (I, II, III, IV) (Jakobsson *et al.*, 1999; Frova, 2006). The cytosolic GSTs are further divided according to ubiquitous groups of Alpha (α), Mu (μ), Pi (π) (Mannervik *et al.*, 1985), Sigma (σ) (Buetler and Eaton, 1992), Theta (θ) (Meyer *et al.*, 1991), Omega (ω, Ω) and Zeta (ζ, Z) (Board, 2011). GSTs are composed of homo or heterodimers with a molecular weight of ~50 kDa made up of ~25 kDa subunits. The dimerization is essential for catalytic functionality since one subunit needs secondary structural elements from the neighbouring subunit. It also creates an allosteric binding site buried at the subunits interface that accommodates non-substrate ligands (L-site) (Dirr *et al.*, 1994). In each subunit, there is an independent catalytic site that is catered for the binding of GSH (G-site) and hydrophobic electrophiles (H-site). Furthermore, the H-site can accommodate a wide range of molecules due to its low specificity for substrates.

GSTs are of utter importance to schistosomes due to the lack of alternative detoxification mechanisms such as Phase I, cytochrome P-450 (use heme as a cofactor for monooxygenases) in parasitic helminths (McTigue et al., 1995). They tend to be mostly expressed in response to drug therapy (Sheehan *et al.*, 2001), thus their popular use as targets for developing a vaccine and chemotherapeutic drugs. The activity levels of other detoxification enzymes are low relative to other organisms such as humans. This difference in schistosomes is compensated by having two types of one enzyme, particularly the 26 and 28 kDa *Schistosoma* GST isoforms. *S. mansoni* has five GST isoforms (two being the 26 kDa ones (1 and 2). The other three are 28 kDa (GST 1, 2, 3) which are similar to the 26 kDa and 28 kDa isoform found in *S. japonicum* (Wright *et al.*, 1991), and all homologous to Mu GSTs of the mammalian class that is similar to Pi and Alpha GSTs (Walker *et al.*, 1993).

Interestingly, it has been discovered that the 28 kDa of *S. haematobium* is similar to the one found in *S. bovis* (Trottein *et al.*, 1992). The isoforms have varying kinetic properties and substrate-binding functions thus different responses to inhibitors. Furthermore, their different locations in parasites explain the respective metabolic pathways routes taken. The isoforms are found in the tegument and subtegumentary parenchymal cells. The 26 kDa is based in the finger-like part of the cytoplasm confined at the apical chamber outlined via the body of the flame cell. The 28 kDa dominates the surface of undeveloped germinal cells of the male and female as well as ootype in the female genitals. In schistosomes, GSTs are highly expressed during the egg stage to aid fecundity. The silencing of the 28 kDa isoform has been proven to compromise egg growth due to redox reaction imbalance and eventually decreases prolificacy (Walker *et al*., 1993; Huyse *et al*., 2009).

Conversely, the 26 kDa isoform plays a role in toxin storage and transportation. This includes minimising (I) lipid peroxidation, which causes oxidative damage (Walker et al., 1993), and (Board *et al.*) heme built up during host erythrocyte metabolism that would otherwise form hematin and block the parasite's gut (Toh *et al.*, 2010; Zhan *et al.*, 2010). In conclusion, GST inhibition in schistosomes would interrupt metabolic processes in crucial areas; otherwise, they would protect parasites from the toxic impact of anthelmintics (Huang *et al*., 2012).

The lack of complete genome and transcriptome information for *S. haematobium* GST as well as its difficulty to maintain in the lab hinders research. Distinctively, the zoonotic characters of *S. haematobium* promote the natural interaction of bidirectional introgressive hybridization with *S. bovis* which supports the close relationship between the two species and an insignificant phylogenetic distance (Huyse *et al*., 2009; Rollinson, 2009). What is frighten-

ing is that *Schistosoma* hybrids tend to depict heterosis (diverse intermediate host, faster maturation, and increased fecundity) (Taylor, 1970), which might collapse the available treatment for schistosomiasis. Unfortunately, studies on GSTs of these species have been confined by the lack of a complete open reading frame (ORF) encoding the 26-kDa isoforms in both *S. haematobium* and *bovis*. In particular, 12 residues are missing from the N-terminus Met, despite the sequence of *S. bovis* being less partially complete (Hsu *et al.*, 1966; Agnew *et al.*, 1989; Djuikwo-Teukeng *et al.*, 2019). Preliminary studies have shown that the sequence encoding the putative 26-kDa GST in *S. haematobium* and *bovis* appears to be ~100% identical in both amino acid sequence and mRNA sequence.

The 3-dimensional structure of Sbh26GST has not been elucidated thus, the use of the well-studied homologous Sj26GST as a model but the one for Sh28GST has been solved. The classical GSTs structure contains 218 amino acids which take on a fold of two distinct domains namely, the small (1-76 residues) N-terminal domain with a βαβαββα topology (thioredoxin-like fold) that forms the hydrophobic core of the protein to house the G-site in proximity to the dimer interface and the larger C-terminal which consists of five α helices and an extended linker coil (residue 195-218) to yield the H-site (Figure 2.4). In particular, the dimer interface is lined by residue 50–53 (β-turn), 63-66 (β4), 67- 76 (α3), 77-85 (loop), 88-109 (α4) and 129-136 (α5) of which Asp77-Arg89 and Glu51-Arg136 form two salt bridges.

In schistosomes, the hairpin loop formed by residue 211-218 (Gly-Gly-Gly-Asp-His-cis Pro-Pro-Lys) makes their GSTs distinct from human GSTs (McTigue *et al.*, 1995). Moreover, the active site in each monomer is characterized by fewer polar residues in the H-site than in human GSTs, thus rendering this site more hydrophobic with a different substrate sensitivity. This also explains the unique orientation of catalytic Tyr103 in Sj26GST (Cardoso *et al.*, 2003). Subsequently, the dimer interface of these schistosomes (residue 33-41 and 200-218) can bind non-substrates/xenobiotics without affecting catalysis, as proven by the study of PZQ binding in Sj26GST, and this site is usually not implicated in human GSTs (McTigue *et al*., 1995; Sheehan *et al*., 2001; Rufer *et al.*, 2005; Baiocco *et al*., 2006). Additionally, some ligands such as ellagic acid (EA) and BSP have been shown to bind at the dimer interface, with detrimental effects on the enzymes that decrease their enzyme activity (Akumadu *et al.*, 2020; Pooe *et al.*, 2021). The residues that may be involved in binding at the long (40 Å) narrow cleft dimer interface include Phe52, which makes the main hydrophobic contact found in α4 and α5. In contrast, the polar contacts contributions are from residues Ser, Gln, Arg107, Tyr103, Asp, Leu100 and Met69 lining the active sites. Despite similarities in mammalian and parasitic GSTs such as the position of $117C^{\alpha}$ location from α helices and β

strands, there exist adequate structural differences between them as demonstrated (McTigue et al., 1995), thus giving a selective rational structural backbone for designing novel generation of anthelmintics drugs.

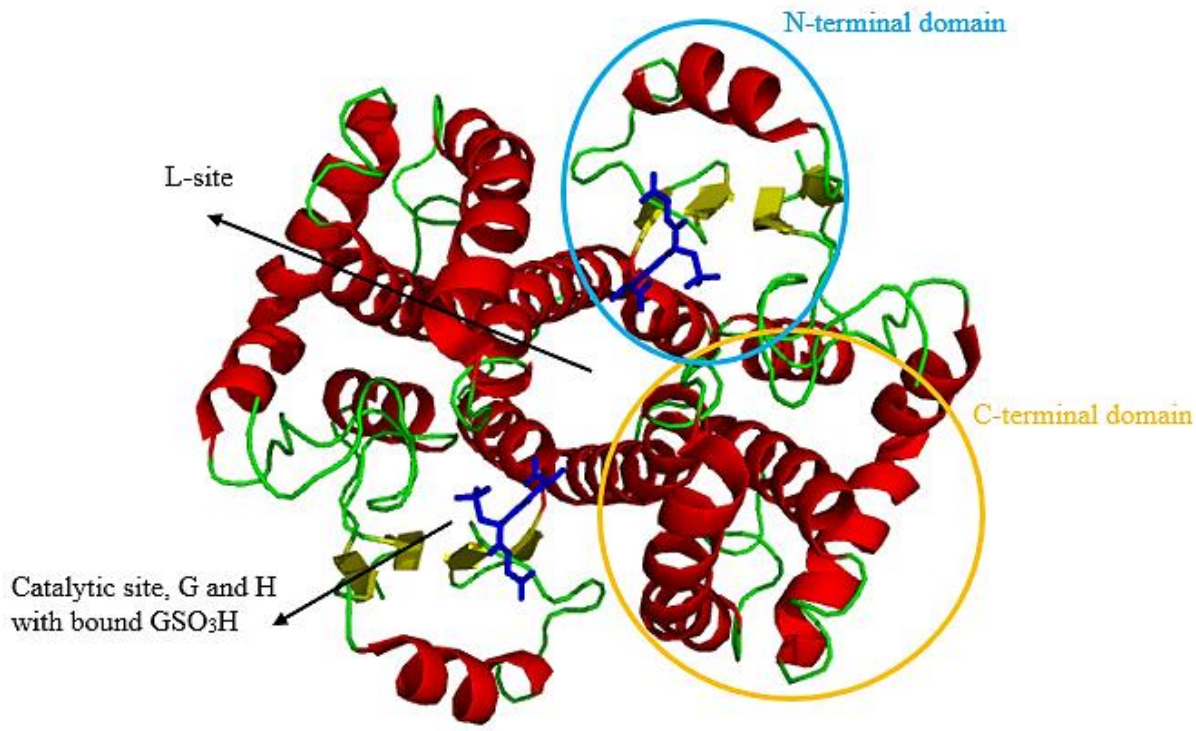

Figure 2.4. Cartoon homology model of Sj26GST for Sbh26GST elucidation. The primary sequence of Sj26GST when read from the N to C-terminus yields a secondary structure fold that is predominantly α-helical (red) with few β-sheets (yellow) entangled in coils (green). The enzyme houses the catalytic binding site, G and H with bound glutathione sulfonic acid (GSO_3H) as well as the allosteric L-site. The image was generated with PyMOL (PDB 1m99).

The native structures of GSTs have varying stability, Sj26GST conforms to the co-operative two-state transition involving the native dimer at ~ 25 kcal/mol and the unfolded monomer with no presence of thermodynamically stable intermediates (Kaplan *et al*., 1997). Higher stability is observed in the class Alpha/Pi/Mu/Sj26GST compared to Sigma and Theta due to the differences in the dimer interface. The latter lacks stabilising hydrophobic interaction since their dimer interface is lined by a network of polar residues. Therefore, the quaternary interactions have a more significant role in these classes for subunit stabilisation than those that show intermediates of molten globule-like inactive monomers. This supports that the evolution of GSTs is towards the functionality of the protein dimer than enhancing subunit stability.

2.6 Activity properties of GSTs- substrate specificity and inhibition

Enzymes speed up the rate of reactions through tight regulations of specificity for substrates. GSTs are bi-substrate enzymes where the isoform determines the order and mode of reaction. Sj26GST tends to follow a sequential displacement catalytic mechanism with preferential binding to GSH (Stefanidis *et al.*, 2018). GSTs, conduct their catalytic role by deprotonating the thiol group of GSH by using a hydrogen bond donor which results in a highly reactive thiolate group that can easily attack electrophiles. This is achieved by lowering the p*K*a of GSH by two or three pH units in the enzyme-substrate complex.

The G-site's critical residues accessible to the solvent include Tyr7, Asn54, Leu55, Gln67, Ser68 and Asp101 which stabilise orientations for alignment and interactions (Cardoso *et al*., 2003). Hydrophobic pockets form the H-site that houses xenobiotics and other endogenous substrates in domain II, namely the α4 helix (Arg103, Tyr104, Ser107, Tyr111), the loop of β1-α1 (Tyr7, Trp8, Ile10, Gly12, Leu13) and the coil at the C-terminus (Gln204, Gly205, Trp206, Gln207) (Cardoso *et al*., 2003) that either takes on the in or out conformation which determines the variability of substrates. On the other hand, the catalysis and thermodynamics of the L-site are not well-understood, especially for parasites and it is the site that accommodates a wide range of non-substrate such as PZQ in a non-competitive manner towards GSH-CDNB conjugation.

Anthelminthic compounds targeted at GSTs inhibit or modulate their activity thus leaving parasites with no shield against oxidative stress and harmful xenobiotics that would otherwise be metabolised. A potent inhibitor of Pi, Mu and Alpha GSTs is the diuretic ethacrynic acid (EA) that disrupts electrolyte balance through binding at the H-site (Ploemen *et al.*, 1993). However, some inhibitors such as ellagic acid can bind both the H-site and dimer interface of Sj26GST. Ligands used in the study include PZQ, artemisinin (ART) and BSP, which all display bulky rings with some hydrophobic character. They are polyphenols with varying arrangements and are used as modulators of numerous biological processes.

BSP ($C_{20}H_8Br_4Na_2O_{10}S_2$, Mw 838.0 g/mol) properties from PubChem include being in an organic class called benzofuran with four rings, the water solubility of 7.99×10^{-3} mg/mL, a physiological charge of -2, an H-bond acceptor of nine and donor of four, rotatable bond count of four and three covalent bonds. BSP is an amphipathic anion dye initially used in liver function tests (Figure 2.5 B), whereby healthy patients show rapid sequestration from the blood through bile conjugates. However, it is also used as a probe for catalytic properties of GSTs, since it alters the intracellular concentration of GSH. BSP has been shown to bind at the hydrophobic cleft enthalpically, L-site in GST classes such as Alpha which results in con-

formational changes that hamper the activity of the enzyme (Sluis-Cremer *et al.*, 1998; Plaa, 2010), while in schistosomes, it favours binding at the dimer interface. This knowledge provides an alternative site for non-substrate xenobiotics to regulate GSTs.

ART ($C_{15}H_{22}O_5$, M_W 282.33 g/mol) (Figure 2.5 C), properties from PubChem include no H-bond donors but five acceptors, no rotatable bonds, no formal charge, and one covalently bonded unit. It has been evaluated for safety and efficacy. ART is a sesquiterpene lactone with organic peroxide derived from sweet wormwood to treat malaria, displaying effectiveness that can extend its anti-infective agent to phylogenetically unrelated parasites such as schistosomes (Krishna *et al.*, 2008). The mechanism of action for ART uses a heme-mediated decomposition of the endoperoxide bridge to produce carbon-centred free radicals thus their toxic selectivity to parasites, bacteria and viruses (Meshnick, 2002). Given the mentioned drugs are well studied and already available on the market, repurposing these for the treatment of schistosomiasis will be shorter and less costly than developing novel drugs.

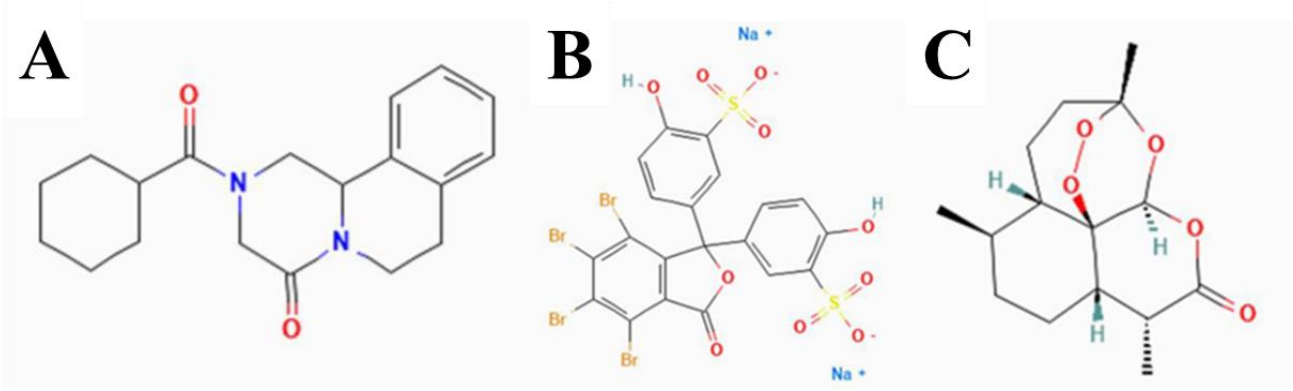

Figure 2.5. 2D structural illustration of the three ligands used in the study. A. Praziquantel, **B**. Bromosulfophthalein and, **C.** Artemisinin.

It is evident there is a need for rational drug discovery against schistosomes. Our approach uses GST enzymes as a drug target since there are critical for metabolism. However, to eradicate all species, it is essential to generate a complete picture of the biochemistry of both isoforms in all human *Schistosoma* parasites. Available sequence information on the putative 26 kDa GST in *S. haematobium, S. bovis* and the complete ORF sequences from other parasitic species were used to construct a pseudo-Sbh26GST. This was done to recombinantly expression and purify Sbh26GST using the pMAL-c5X in comparison to the well-known Sh28GST isoform. The structure, function, and ligandin enzyme's properties were studied to add to the body of knowledge on potential inhibitors that can be designed or re-purposed as new-generation anti-helminthics.

Chapter 3
Over-expression and purification of Sbh26GST and Sh28GST

3.1. Introduction

The machinery of *E. coli* was manipulated to produce high levels of recombinant pseudo-Sbh26GST and Sh28GST. Thereafter, the proteins of interest were isolated from other bacterial proteins, crucial for their survival. All based on the prior knowledge of basic properties of the respective proteins, extracted from ProtParam ExPASy. Sbh26GST is made up of 230 amino acids weighting 26.61 kDa with a theoretical isoelectric point (pI) of 7.16 (Ext. coefficient at 280 nm = 39880 $M^{-1}.cm^{-1}$ when all Cys residues are reduced) while Sh28GST is made up of 219 amino acids weighing 24.93 with pI 6.67 (Ext. coefficient at 280 nm = 22920 $M^{-1}.cm^{-1}$ when all Cys residues are reduced). All-inclusive of the extra N-terminal His-tag and MBP tag respectively. The chapter unfolds how proteins of interest were overexpressed and purified to produce high yields of active proteins for downstream analysis.

3.2. Materials

Escherichia coli (*E. coli*) T7 Express Competent Cells (New England Biolabs, Ipswich, MA, USA), expression vectors; pMAL-c5X for Sbh26GST and pET-11a for Sh28GST were supplied by GenScript, USA. Reagents and chemicals supplied by Sigma-Aldrich® St. Louis, MO, USA include isopropyl β-D-1-thiogalactopyranoside (IPTG), NaCl, yeast extract, tryptone, chloramphenicol, ampicillin, $NiSO_4$, Tween-20 and, BLUeye Prestained Protein Ladder (molecular weight marker). The agar was from Merck Biosciences. Electrophoresis apparatuses were from Bio-Rad suppliers (bromophenol blue, N, N, N,' N'-tetramethyl ethylenediamine (TEMED), bis-acrylamide, acrylamide, sodium dodecyl sulfate (SDS), β-mercaptoethanol, glycine, Coomassie Brilliant Blue G-250, Coomassie Brilliant Blue R-250, glacial acetic acid). Snakeskin™ dialysis tubing (10K MWCO, 22 mm) was purchased from Thermo scientific (South Africa). Other non-standard reagents used were of analytical grade.

3.3. Methods

3.3.1. Gene construction of Sbh26GST

Given the gene sequence of Sbh26GST is incomplete, Dr Ikechukwu Achilonu used several sequence analyses tools to generate the unknown region in its ORF. The construction of pseudo-Sbh26GST was based on the similarity of native Sh26GST and Sb26GST that

showed 99.9% sequence identity as shown in Figure 3.1. Resembling, they might have stemmed from a common ancestor which is inconsequential. The partially complete polypeptide and nucleotide sequences for Sh26GST (UniProtKB ID: A0A6A5D1Y9) and Sb26GST (UniProtKB ID: A0A430Q9J5) were extracted from the UniProtKB database. Furthermore, a program that searches for similarities in the sequence database (Clustal Omega) was used to confirm that the latter sequences are related to the well-known complete Sj26GST (EMBL ID: CAX71419), and the focus was on the 26 kDa isoform of *Schistosoma* GST, not the 28 kDa. However, the first 12 amino acids are missing in both sequences. In this study, the latter sequence was completed through BLAST which is used to identify evolutionary related sequences in the database whereby top scoring sequences were subjected to multiple sequence alignment analysis to identify a consensus first 12 amino acids sequence. The consensus was generated with CLC bio™ bioinformatics software which uses a computed score based on the Shannon entropy (Schneider and Stephens, 1990) to show each alignment position and sequence information. Thus, it helped determine the 12 initial amino acids missing in the sequence of Sbh26GST referred to as a pseudo-26 kDa *S. bovis-haematobium* GST (Sbh26GST).

3.3.2. Design of vectors enabling expression of Sbh26GST and Sh28GST

pMAL-c5X is an *E. coli* plasmid cloning vector that uses a pMAL protein fusion and purification system to enhance the expression and solubility of the target protein. This is achieved by translational fusion of maltose-binding protein (MBP) encoded by the malE gene to the N-terminus of the cloned target protein in the cytoplasm (Maina *et al.*, 1988). To overexpress Sbh26GST, its constructed gene was inserted in the multiple cloning sites of the pMAL-c5X vector via amplifying the DNA fragment with primers through polymerase chain reaction (PCR) and ligated to the vector after digestion with restriction enzymes, namely *BamHI* and *NdeI*. However, the cDNA was modified by adding a hexa-histidine tag to the N-terminus of the ORF to aid with the second round of purification. The promiscuous, factor Xa site was substituted for the thrombin cleavage site (Waugh, 2011). Similarly, the codon optimised gene of Sh28GST was cloned into the vector, pET-11a with a single modification of a His-tag. Inqaba Biotech ™ (Pretoria, South Africa) performed all sequencing whereby the mRNA was optimised through codon harmonisation of *E. coli* frequencies and the plasmids were synthesized by GenScript Corporation (Piscataway, NJ, USA).

In both vectors, protein synthesis is under the transcriptional control of a T7 tac promoter and the inducible lacIq promoter encoding RNA polymerase. This is advantageous

over the strain of lambda DE3 prophage since the wild-type lac promoter results in a lower basal expression in *E. coli* and it is monitored by the lacI repressor which inhibitory binds the lac operator. Moreover, protein synthesis before induction is restricted by co-expression of T7 lysozyme (Studier, 1991). The inhibition can be relieved by the addition of lactose or IPTG. The vectors also have an ampicillin resistance selective mechanism against other bacteria without plasmids of interest, on top of that the T7 cells are resistant to chloramphenicol (Kesik-Brodacka *et al.*, 2012).

3.3.3. Transformation of T7 E. coli cells with vectors, pMAL-c5X and pET-11a for expression of Sbh26GST and Sh28GST

E. coli is a well-studied Gram-negative bacterium widely used for recombinant protein technology due to the ease of genetic manipulations and rapid growth in low-cost media (Rosano and Ceccarelli, 2014). The T7 *E. coli* competent cells were transformed with vector, pMAL-c5X encoding Sbh26GST and pET-11a encoding Sh28GST by using the heat shock method to increase membrane permeability thus enabling the uptake of constructed vectors (Froger and Hall, 2007). The respective lyophilized vectors were reconstituted by allowing the vial to warm to room temperature (20 °C) for 30 min and centrifuged at 16 000 *g* for 5 min. After that, 100 µL of 0.2 µm filtered water was added to a final concentration of 40 ng/µL before vortexing for 1 min. Lastly, the vial was spined down for 10 sec and 25 µL was transferred into an 1.5 mL microfuge tube for use as stock stored at -20 °C. A 1.5 mL microfuge tube of 50 µL of T7 competent cells were thawed on ice followed by an addition of 5 µL of the vector (200 ng) and left for 30 min. The cells were then briefly placed on a heating block for 60 secs at 42 °C and back in ice for 10 min. The mixture was added to 1 mL of SOC media (Super Optimal broth with Catabolite repression made up of 0.5 % (w/v) yeast extract, 2 % (w/v) tryptone, 20 mM $MgCl_2$, 2.5 mM KCl, 10 mM glucose) for one h incubation at 37 °C and 250 rpm for aeration. Furthermore, the cells were centrifuged at 6800 *g* for 1 min whereby 80% of the supernatant was decanted and the pellet was resuspended. Transformed cells were plated on LB agar (1% tryptone, 0.5% yeast and 0.5% NaCl) supplemented with 50 µg. mL^{-1} ampicillin as well as 35 µg. mL^{-1} chloramphenicol and incubated overnight (12-16 h) at 37 °C and 230 rpm.

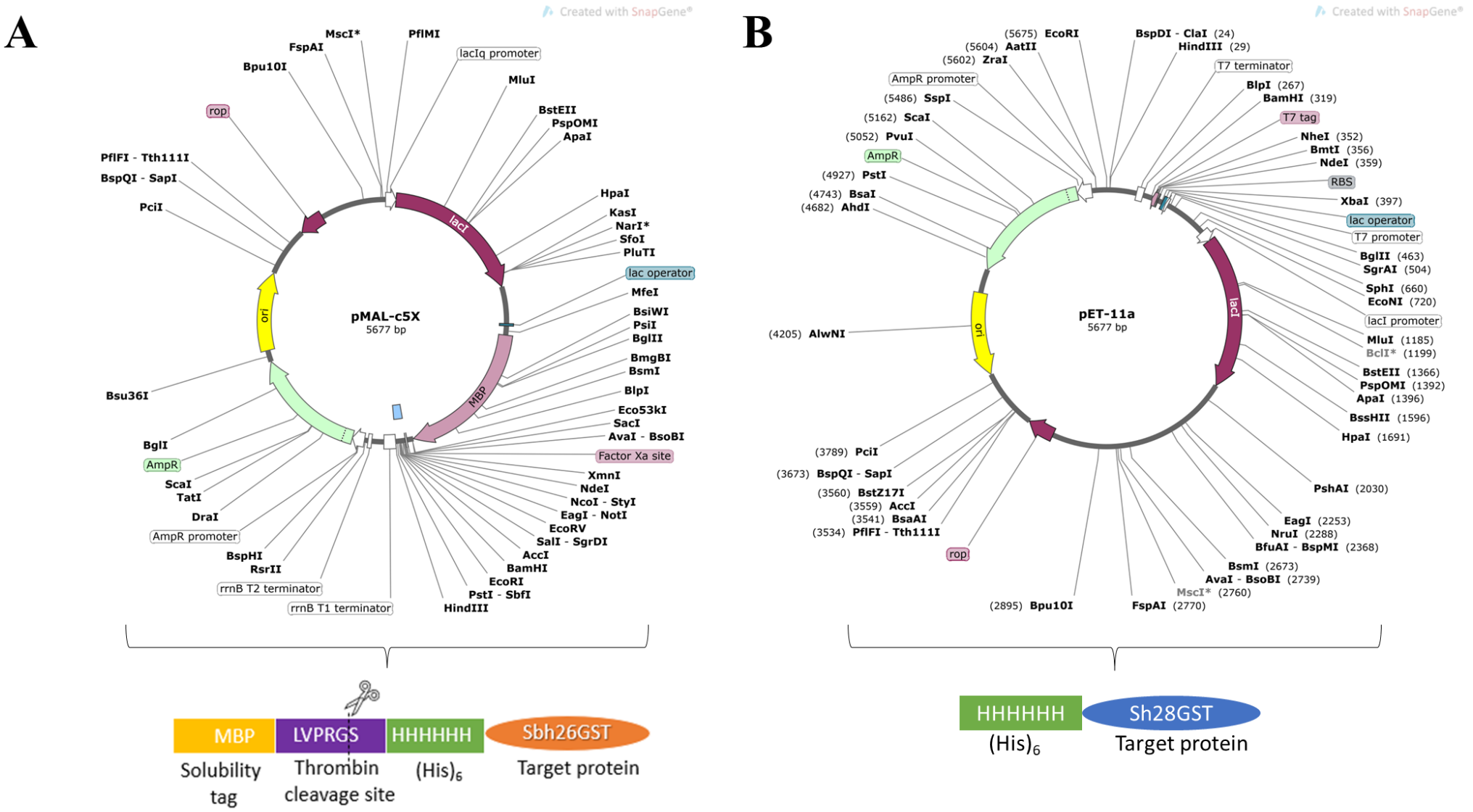

Figure 3.1 Schematic diagram of pMAL-c5X and pET-11a vector maps. A. The gene of Sbh26GST incorporated with *BamHI* and *NdeI* restriction enzyme to the multiple cloning sites of pMAL-c5X yields maltose binding protein (MBP) fusion proteins. **B** The gene of Sh28GST, on the other hand, was inserted in between the T7 promoter and terminator of pET-11a along with a histidine tag.

To expression the respective proteins, three single colonies were individually grown overnight in 50 mL of 2X YT media (1.6 % (w/v) tryptone, 1.0 % (w/v) yeast extract and 0.5 % (w/v) NaCl) augmented with 50 μg. mL^{-1} ampicillin and 35 μg. mL^{-1} chloramphenicol at 37 °C and 230 rpm. Some overnight cultures were used to make glycerol stocks (5 per colony) by adding a 1:1 ratio of culture and 80% (v/v) glycerol. At the same time, the rest of the cultures were diluted 50X into 100 mL 2X YT in 500 mL Erlenmeyer flasks and grown under the same conditions until they reached the mid-log phase (an OD_{600} between 0.45 and 0.55). Subsequently, the flasks were chilled on ice for 10 min. Each culture was split into 50 mL of uninduced cells and 50 mL of induced cells with 0.5 mM IPTG (an allolactose analogue that remains constant in the media due to the unhydrolyzed sulfur bond). After that, the cells were incubated at 30 °C while shaking at 230 rpm for ~ 6 h followed by harvesting in 50 mL falcon tubes at 5000 *g* for 15 min. The pellets of cells were resuspended in 2.5 mL of resuspension buffer (50 mM Tris-HCl, and 0.02% (w/v) NaN_3 pH 7.4) for Sbh26GST and phosphate buffer saline (PBS) (137 mM NaCl, 2.7 mM KCl, 10 mM Na_2HPO_4, 2 mM KH_2PO_4, pH 7.4) for Sh28GST then stored at -80°C overnight to aid lysing. The respective frozen cell suspension was left to thaw at room temperature (20°C) and sonicated thoroughly on ice using 5-sec pulses for ten repeats at 40 Amp for a 1.5 mL microfuge tube. After that, 1 mL of the cell lysate was transferred into a 1.5 mL microfuge tube and centrifuged at 16 000 *g*, 4°C for 5 min to separate the soluble and insoluble fractions that SDS-PAGE analysed.

3.3.4. Qualitative analysis of Sbh26GST and Sh28GST on gels

The success of protein overexpression and purity at a later stage was established by sodium dodecyl sulfate-polyacrylamide gel electrophoresis (SDS-PAGE) according to Laemmli (1970). The principle behind this technique is about separating protein on a support matrix through an electric field making it possible to visualise different proteins in a sample upon staining with a dye like Coomassie blue. SDS achieves this, an anionic detergent that masks the net charge and shape by adding negative charges around the protein's backbone, thus denaturing it into individual linear polypeptides that can solely be separated based on size (Jafari *et al.*, 2018). Small molecules migrate faster than large ones due to less resistance from the gel (Moosavi-Movahedi, 2005). The support matrix used is polyacrylamide, which is acrylamide crossed linked with bis to create a sieving effect for small molecules like proteins. The PAGE setup is discontinuous, where the stacking gel is on top of the separating gel. The lower acrylamide percentage and pH of the stacking gel result in glycine with no net

charge. Therefore, causing constraints and collection of all the proteins at the same point before the initiation of separation in the resolving gel with negatively charged glycine, improving the resolution. A clear single band that represents the size of the monomeric protein structure would represent a homogenous mixture and the intensity correlates to concentration. Smeared bands usually represent degradation or a protein overload.

A 50 µL sample of the various supernatants were transferred into fresh 1.5 mL microfuge tubes and mixed with equivalent amount of reducing buffer (125 mM Tris-HCl pH 6.8, 2% (w/v) SDS, 20% (v/v) glycerol, 0.05% (w/v) bromophenol blue and 5% (v/v) β-mercaptoethanol). The pellets were washed 3X with deionised water using sonication and centrifugation. Thereafter, the pellets were resuspended in 1 mL of deionised water and 50 µL was transferred to 1.5 mL microfuge tubes of the reducing buffer. All samples were boiled at 100 °C for 5 mins and placed on ice before loading into the stacking gel wells (4 % (w/v) acrylamide, 0.36 % (w/v) bis-acrylamide, 0.1 M Tris-HCl pH 6.8, 0.1 % (w/v) SDS, 0.07 % (w/v) ammonium persulfate and 0.17 % (v/v) TEMED) that feeds the separating gel (12.5 % (w/v) acrylamide, 1.11 % (w/v) bis-acrylamide, 0.4 M Tris-HCl pH 6.8, 0.1 % (w/v) SDS, 0.07 % (w/v) ammonium persulfate and 0.67 % (v/v) TEMED) on the Bio-Rad mini protean electrophoresis system. The 3 µL of BLUeye Prestained Protein Ladder (Bio-Rad) was added to the wells to serve as the molecular weight marker (MWM). The electrophoresis ran with a glycine electrophoresis buffer, pH 8.3 (25 mM Tris,192 mM glycine and 0.1 % SDS) in the tank at 160 V for ~ 1 h. The gel was stained with Coomassie dye (0.1 % (w/v) Coomassie Brilliant Blue R-250 dye in 1:5:4 (v/v/v) acetic acid: methanol: water) and destained in 1:5:4 acetic acid: methanol: water solution for visualisation. The distances that the proteins travelled on the gel relative to the dye front known as the retention factor were used to interpolate the molecular weight of Sbh26GST and Sh28GST from a calibration curve of log molecular weight vs the distance migrated by the standard proteins created on GraphPad Prism version 8.0.2 (GraphPad Software, San Diego, California, USA) which shows a linear relationship.

3.3.5. Overexpression of Sbh26GST and Sh28GST

The expression trials showed that 0.5 mM IPTG at 30 °C, 230 rpm for ~ 6 h is sufficient for optimal overexpression of Sbh26GST and Sh28GST (no alterations required). Hence, proceedings to large-scale overexpression were made. Individual glycerol stock of the best colony was used for inoculating 50 mL 2X YT supplemented with 50 µg. mL^{-1} ampicillin and 35 µg. mL^{-1} chloramphenicol at 37 °C, 230 rpm overnight. After that, the cultures were

diluted 50X into 500 mL fresh 2X YT media with antibiotics in 2 L Erlenmeyer flasks equating to 2 L of each protein. IPTG inductions were performed as previously described (3.3.3). However, the cells were harvested by centrifugation at 5 000 *g*, 4 °C for 15 mins in 500 mL bottles and the pellets were weighed before resuspending in 50 mL of respective buffers per 1 L of culture. Thereafter, the cells were stored in 50 mL falcon tubes at -80 °C overnight before complete sonication at 60 Amp instead and centrifugation at 18 000 *g*, 4 °C for 20 min to separate the soluble and insoluble fraction. The supernatant was subsequently filtered with a 0. 2 µm syringe filter and used for purification of each protein.

3.3.6. Affinity chromatography purification of Sbh26GST and Sh28GST

The selective isolation and purification of proteins, Sbh26GST and Sh28GST were achieved by affinity chromatography. The technique efficiently exploits highly specific biological interactions between two molecules, enzymes, and substrates, to separate them from biochemical mixtures with high capacity. A substrate is immobilised on support to trap the enzyme. The enzyme's binding to the immobilised substrate can be reversed through competitive binding or by weakening the affinity with pH or ionic strength alterations. For instance, in the first round of purification of Sbh26GST, the MBP tag incorporated in the pMAL-c5x vector can be used to trap the protein in the amylose sepharose resin column since MBP has a natural affinity for α-(1–4) maltodextrin while the rest of the components in the cell lysate flow through. Immobilised Sbh26GST is then washed with salt or detergent to remove any bound DNA, proteins, and lipids as well as any weakly bound Sbh26GST. Thereafter, pure Sbh26GST can be freed through competitive binding with maltose (Duong-Ly and Gabelli, 2015).

On the other hand, immobilised metal affinity chromatography (IMAC) is used to purify Sh28GST and the second round of Sbh26GST takes advantage of metal chelators. Delocalised electrons in the ring of histidine-tagged to the proteins can bind nitrilotriacetic acid matrices with positively charged divalent metal ions such as nickel or cobalt (Arnau *et al.*, 2006). The interaction can be reversed through competitive binding with imidazole to release the recombinant protein. The mentioned tags can be removed with enzymatic proteases if they have significant effects on the structure and function of the protein e.g., thrombin can be facilitated by a thrombin cleavage site incorporated in the vector whereby it cuts between arginine and glycine residues thus releasing the recombinant protein (Waugh, 2011).

Gravity flow amylose-agarose affinity resin column connected to low pressure pump (Bio-Rad Model EP-1 Econo™) was equilibrated with 10X column volume of equilibration

buffer (50 mM Tris-HCl, 200 mM NaCl, 1mM EDTA and 0.02% (w/v) NaN_3, pH 7.4). Subsequently, 50 mL of the filtered supernatant from the soluble fraction of Sbh26GST's overexpression was loaded onto the column at 4 mL/min for MBP tag binding and the flowthrough was collected. This was followed by 3X contaminants' washing with 10X column volume of the equilibration buffer and the wash in-between had 0.5 % Tween-20. Subsequently, the protein was eluted with a 2X column volume of equilibration buffer with 10 mM maltose. The eluents were collected at fractions of 1 mL/min. While collecting fraction, 50 µL of the eluted fraction was added to 950 µL of Bradford dye (6% (v/v) β-mercaptoethanol, 10% (w/v) SDS, 30% (v/v) glycerol, 0.05% (v/v) Bromophenol Blue, 150 mM Tris-HCl, pH 7) which turns blue in the presence of protein thus used as an indicator of when to stop collecting fraction. Fractions with absorbance at 280 nm ≥ 1 were pulled together (11 mL) and dialysed with 10kDa cut-off snakeskin for 2X overnights against 5 L of 50 mM Tris-HCl, 5 mM $CaCl_2$ and 0.02% (w/v) NaN_3 pH 7.4 to prepare for thrombin cleavage since MBP weighed heavily on the protein of interest. Afterwards, ~ 3 µL of thrombin was added per 1 mL of dialysed protein (0.5 U/mg of recombinant protein) and left overnight at 20 °C on a gentle rotator. In addition, time-dependent trials of thrombin cleavage were performed under the above conditions to find the optimal duration and evaluate efficiency.

Similarly, His GraviTrap™ (Ni Sepharose® 6 Fast Flow) column was prepared with of 9.5 of sepharose resin and then washed with 100 mL of deionised water (10X column volume) to remove the ethanol that helps in preservation. The matrix was charged with Ni^{2+} bypassing 0.1 M $NiSO_4$ through gravity and washing with water, was equilibrated with the latter dialysis buffer, and loaded with the cleaved protein where only His-tagged Sbh26GST binds and other protein (thrombin and MBP) flows through. After that, the column was washed with the dialysate or 50 mM Tris-HCl, 200 mM NaCl, 50 mM imidazole, 0.5 % Tween-20 and 0.02% (w/v) NaN_3. pH 7.4. The protein was eluted with 50 mM Tris-HCl, 500 mM NaCl, 300 mM imidazole and 0.02% (w/v) NaN_3, pH 7.4 at a 1 mL/min flow rate under the control of Bradford reagent. Thereafter, the protein was dialysed against 1 L of 50 mM Tris-HCl, pH 7.4 and 0.02% (w/v) NaN_3 to remove the concentrated imidazole as it might interfere with subsequent studies. No cleavage was required since His-tag has an insignificant effect on the proteins due to their small size. All the different stages of the purification process were captured by collecting 1 mL samples and assessed on SDS-PAGE as described in 3.3.4. The purification of Sh28GST was performed according to the second purification of Sh26GST, IMAC but with a different buffer, PBS instead of Tris-HCl: equilibration buffer (137 mM NaCl, 2.7 mM KCl, 10 mM Na_2HPO_4, 2 mM KH_2PO_4, 25 mM imidazole and 0.02% (w/v)

NaN_3, pH 7.4). Wash buffer (equilibration buffer with 0.05 % Tween-20) and elution buffer (equilibration buffer with 300 mM imidazole). Each protein's final respective dialysis buffer is technically the storage buffer, and it was used for subsequent studies that require dilutions.

3.3.7. Protein concentration determination

Purified Sbh26GST and Sh28GST were quantified spectrophotometrically. Light is either absorbed or transmitted when it passes through a sample. In the case of proteins: tryptophan, tyrosine, and to some extent, phenylalanine tends to absorb light at 280 nm. Therefore, the absorbance can be used to calculate the concentration of a protein based on Beer Lambert's law,

$$A = \varepsilon_\lambda cl \tag{3.1}$$

Where A is the absorbance, ε_λ is the molar extinction coefficient at a specific wavelength ($M^{-1}.cm^{-1}$), c is the molar concentration (M), and l is the path length of light passing through the cuvette (cm). The extinction coefficient, 79 760 $M^{-1}.cm^{-1}$ for Sbh26GST's dimer and 45 840 $M^{-1}.cm^{-1}$ for Sh28GST's dimer at 280 nm in water was theoretically determined on Expasy's ProtParam (Gasteiger *et al.*, 2005) or calculated using the Perkins method,1986.

$$\varepsilon = 5550 \sum Trp\ residues + 1340 \sum Tyr\ residues + 150 \sum Cys\ residues \tag{3.2}$$

Where ε is the extinction coefficient, 5550 is the molar absorption coefficient of the residue Trp,1340 for Tyr and 150 for Cys and ∑ is the sum of the respective residues.

Doubling dilution series of the respective protein was prepared in 100 mm micro-QS quartz absorbance cuvettes and analysed on Jasco V-630 BIO UV/VIS spectrophotometer (Jasco Inc., Tokyo Japan) set at a data pitch of 1 nm, a scan speed of 200 nm/min for three accumulations. The monitored absorbances were on a 240 to 350 nm spectrum to make sure it assumes an ideal protein shape of no contamination. In particular, the ratio of $A_{260/280}$ is for nucleic acids' presence which needs to remain below 0.6 (Warburg and Christian, 1941) whereas protein aggregates are checked at 340 nm. Corrected absorbances for the buffer and aggregates were used to establish a calibration graph of absorbance vs dilution factor for obtaining the gradient required for concentration determination in the equation below:

$$C\ (^{mg}/_{mL}) = \frac{Slope\ \times MW\ (Da)}{\varepsilon\ (M^{-1}.cm^{-1})\ \times l\ (cm)}$$

(3.3)

3.4. Results

Ample amounts of proteins of interest, Sbh26GST and Sh28GST were recombinantly overexpressed with *E. coli* machinery and purified on the basic principle of affinity chromatography to get isolated enzymes.

3.4.1 Sbh26GST gene construct

Homology studies using Clustal Omega have shown that the partial sequence of 26 kDa GST from *Schistosoma haematobium* has a sequence identity of ~100% at both nucleotide and amino acids level with the 26 kDa GST from *Schistosoma bovis*, which is less incomplete as shown in Figure 3.1. Therefore, the partial sequence of 26 kDa GST from *Schistosoma bovis* was aligned with the closely related complete sequence of 26 kDa GST from *Schistosoma japonicum* and *mansoni* as depicted in Figure 3.2 to establish how the protein of interest varies from the typical sequence of *Schistosoma* GSTs that affect humans. The trend reflected a conserved amino acid sequence despite having different nucleotide sequences. However, it was observed that there are 12 unknown initial amino acids in the 26 kDa *Schistosoma bovis/haematobium* GST (Sbh26GST). The homologous organisms were used to generate a sequence logo in Figure 3.3 for the missing initial 12 amino acids motif using the CLC bio™ bioinformatics software. The established sequence was incorporated into the cDNA sequence of wild-type *Schistosoma bovis* to produce pseudo Sbh26GST along with a hexahistidine fusion tag and thrombin cleavage site at its N-terminal cap. The latter was inserted into an increased solubility pMAL-c5x vector.

A

```
Sb26kDa_GST.  LVQPTRLLLEYVGEVYEERLYDRNDGDVWRNEKFNLGLEFPNLPYYIDGDVKLTQSMAIL   60
Sh26kDa_GST.  LVQPTRLLLEYVGEVYEERLYDRNDGDVWRNEKFNLGLEFPNLPYYIDGDVKLTQSMAIL   60
              ************************************************************

Sb26kDa_GST.  RYIADKHNMLGGCPKERAEISMLEGAILDIRLGVSRIAYNKEFETLKVGFLNQLPGMLKM   120
Sh26kDa_GST.  RYIADKHNMLGGCPKERAEISMLEGAVLDIRLGVSRIAYNKEFETLKVGFLNQLPGMLKM   120
              ************************:***********************************

Sb26kDa_GST.  FENRLSHKIYLNGDNVTHVDFMLYDALDVVLYMDPKCLDAFPKLISFKQRIENLPPIKNY   180
Sh26kDa_GST.  FENRLSH-------------------------------------------------------   127
              *******

Sb26kDa_GST.  LNSDRHIKWPLQGWSAIFGGGDAPPK    206
Sh26kDa_GST.  --------------------------    127
```

B

```
ENA|RTG84353|RTG84353.1         CTTGTACAACCGACTCGTCTTCTTTTGGAATATGTTGGCGAAGTATATGAAGAGCGTTTG   60
ENA|KAF1314627|KAF1314627.1     CTTGTACAACCGACTCGTCTTCTTTTGGAATATGTTGGCGAAGTATATGAAGAGCGTTTG   60
                                ************************************************************

ENA|RTG84353|RTG84353.1         TATGATCGCAATGATGGTGATGTCTGGCGAAACGAAAAGTTCAATTTAGGTCTGGAATTT   120
ENA|KAF1314627|KAF1314627.1     TATGATCGCAATGATGGTGATGTCTGGCGAAACGAAAAGTTCAATTTAGGTCTGGAATTT   120
                                ************************************************************

ENA|RTG84353|RTG84353.1         CCTAATCTACCTTATTATATTGATGGTGATGTTAAATTAACACAGTCTATGGCTATTTTA   180
ENA|KAF1314627|KAF1314627.1     CCTAATCTACCTTATTATATTGATGGTGATGTTAAATTAACACAGTCTATGGCTATTTTA   180
                                ************************************************************

ENA|RTG84353|RTG84353.1         CGTTATATAGCTGATAAACACAATATGTTGGGTGGTTGTCCCAAAGAACGTGCAGAAATT   240
ENA|KAF1314627|KAF1314627.1     CGTTATATAGCTGATAAACACAATATGTTGGGTGGTTGTCCCAAAGAACGTGCAGAAATT   240
                                ************************************************************

ENA|RTG84353|RTG84353.1         TCTATGCTTGAGGGAGCCATTTTGGATATCAGACTTGGTGTTTCAAGAATTGCATATAAT   300
ENA|KAF1314627|KAF1314627.1     TCTATGCTTGAGGGAGCCGTTTTGGATATCAGACTTGGTGTTTCAAGAATTGCATATAAT   300
                                ****************.*******************************************

ENA|RTG84353|RTG84353.1         AAAGAATTTGAAACTCTCAAAGTTGGTTTTCTCAATCAACTCCCTGGAATGCTGAAAATG   360
ENA|KAF1314627|KAF1314627.1     AAAGAATTTGAAACTCTCAAAGTTGGTTTTCTCAACCAACTCCCTGGAATGCTGAAAATG   360
                                ********************************** ************************

ENA|RTG84353|RTG84353.1         TTTGAAAATCGTTTATCTCACAAAATATATTTGAATGGTGATAATGTGACTCATGTTGAC   420
ENA|KAF1314627|KAF1314627.1     TTTGAAAATCGTTTATCTCAC-----------------------------------------   381
                                *********************

ENA|RTG84353|RTG84353.1         TTCATGCTGTACGACGCTCTTGATGTAGTTTTATACATGGACCCAAAGTGCTTGGATGCA   480
ENA|KAF1314627|KAF1314627.1     ------------------------------------------------------------   381

ENA|RTG84353|RTG84353.1         TTTCCAAAACTAATTAGTTTCAAACAGCGTATAGAAAATTTACCACCAATCAAGAACTAC   540
ENA|KAF1314627|KAF1314627.1     ------------------------------------------------------------   381

ENA|RTG84353|RTG84353.1         CTGAATTCTGACAGGCACATAAAATGGCCTCTGCAAGGCTGGTCCGCCATTTTTGGTGGT   600
ENA|KAF1314627|KAF1314627.1     ------------------------------------------------------------   381

ENA|RTG84353|RTG84353.1         GGAGATGCTCCTCCAAAATAA  621
ENA|KAF1314627|KAF1314627.1     ----------------------  381
```

Figure 3.2. Sequence alignment of the putative 26 kDa GSTs from *S. bovis* and *S. haematobium* fragments. The partial sequence of *S. haematobium* (SCHHA, KAF1314627) is incorporated in the less incomplete sequence of *S. bovis* (SCHBO, RTG84353) as depicted by 99.9 % sequence identity at both amino acid (**A**) and nucleotide (**B**) level on Clustal Omega whereby the (*) represents common residues and (-) for incomplete sequence. This excludes the additional C-terminus region in *bovis*.

```
Sm26kDa_GST.   MAPKFGYWKVKGLVQPTRLLLEHLEETYEERAYDRNEIDAWSNDKFKLGLEFPNLPYYID 60
Sj26kDa_GST.   MSPILGYWKIKGLVQPTRLLLEYLEEKYEEHLYERDEGDKWRNKKFELGLEFPNLPYYID 60
Sb26kDa_GST.   ------------LVQPTRLLLEYVGEVYEERLYDRNDGDVWRNEKFNLGLEFPNLPYYID 48
                           **********:: * ***: *:*:: * * *.**:**************

Sm26kDa_GST.   GDFKLTQSMAIIRYIADKHNMLGACPKERAEISMLEGAVLDIRMGVLRIAYNKEYETLKV 120
Sj26kDa_GST.   GDVKLTQSMAIIRYIADKHNMLGGCPKERAEISMLEGAVLDIRYGVSRIAYSKDFETLKV 120
Sb26kDa_GST.   GDVKLTQSMAILRYIADKHNMLGGCPKERAEISMLEGAILDIRLGVSRIAYNKEFETLKV 108
               **.********:***********.**************:**** ** ****.*::*****

Sm26kDa_GST.   DFLNKLPGRLKMFEDRLSNKTYLNGNCVTHPDFMLYDALDVVLYMDSQCLNEFPKLVSFK 180
Sj26kDa_GST.   DFLSKLPEMLKMFEDRLCHKTYLNGDHVTHPDFMLYDALDVVLYMDPMCLDAFPKLVCFK 180
Sb26kDa_GST.   GFLNQLPGMLKMFENRLSHKIYLNGDNVTHVDFMLYDALDVVLYMDPKCLDAFPKLISFK 168
               .**.:**  *****:**.:* ****: *** ***************  **: ****:.**

Sm26kDa_GST.   KCIEDLPQIKNYLNSSRYIKWPLQGWDATFGGGDTPPK 218
Sj26kDa_GST.   KRIEAIPQIDKYLKSSKYIAWPLQGWQATFGGGDHPPK 218
Sb26kDa_GST.   QRIENLPPIKNYLNSDRHIKWPLQGWSAIFGGGDAPPK 206
               : ** :* *.:**:*.::* ******.* ***** ***
```

Figure 3.3. Protein sequence alignment of 26 kDa GSTs from *Schistosoma bovis* with homologous species. The partial sequence of *Schistosoma bovis* (SCHBO/Sb26GST) was compared to the complete closely related *S. japonicum* (Sj26GST) and *S. mansoni* sequence (Sm26GST) to establish the variation from typical *Schistosoma* GSTs. The results show 12 initial unknown amino acids in the N-terminus as represented by (-). The rest of the symbols represent common residues (*), different amino acids with similar properties (:) and different properties (.). Overall, this also confirms that the fragments are likely to be 26 kDa isoforms from *bovis* and/or *haematobium* and not the 28 kDa isoform.

Figure 3.4. Synthesized Sbh26GST. Sequence logo of the missing initial 12 amino acids of 26 kDa GST from *S. haematobium/bovis* was generated with CLC bio™ bioinformatics software by aligning five motifs that had top-scoring sequences from BLAST analysis using dendrogram clustering (implemented in the Clustal Omega algorithm), namely *Biomphalaria glabrata* (BIOGL), *Clonorchis Sinensis* (CLOSI), *S. mansoni* (SCHMA), *S. japonicum* (SCHJA) and *S. mekongi* (SCHME). The conserved amino acids (Web Logo analysis-consensus) are highlighted in yellow (MAP**A**LG**Y**WKIKG) represented by (*) for common residues whereby different amino acids with similar properties are represented by (:) and ones with different properties by (.). Alanine is the 4th amino acid, and the catalytic Tyr (in bold) is the 7th position.

3.4.2. Overexpression of Sbh26GST and Sh28GST

Sbh26GST and Sh28GST were recombinantly expressed at 30 °C for 6 h upon addition of 0.5 mM IPTG at OD_{600} of 0.5 to T7 cells transformed with pMAL c5X and pET-11a vector which respectively encodes for enzymes, MBP-His tagged Sbh26GST (~68 kDa) and His tagged Sh28GST (~27 kDa). The success of overexpression and solubility of the respective proteins were evaluated with SDS-PAGE, as depicted in Figure 3.4. The electrophoretogram shows thick bands in the supernatant (soluble fraction) of IPTG induced batch and small bands in the pellet whereas the uninduced culture had no overexpression. Therefore, the used concentration of IPTG was sufficient to overexpress Sbh26GST and Sh28GST without any alteration before proceeding with large-scale overexpression and purification processes.

3.4.3. Affinity chromatography purification of Sbh26GST and Sh28GST

The soluble fraction of each protein was subjected to respective affinity chromatography columns for purification. In the case of Sbh26GST, double purifications were performed whereby initially the agarose resin trapped the MBP tag. Bound protein was washed off impurities and eluted with 10 mM maltose. The eluents were collected in fractions of 1 mL/min and the ones with an A_{280} >1 were pooled together for thrombin cleavage studies. The optimal conditions in terms of time for thoroughly cleaving MBP with 0.5 U of thrombin per 1 mg of recombinant protein was approximately 3 h at 20 °C as shown in Appendix, Figure S1, less than that is not sufficient despite rapid cleaving at 30 min. The cleaved protein was then subjected to the Ni-IMAC column that binds His tagged Sbh26GST and then, released with 500 mM imidazole. The eluents were again measured at $A_{280,}$ and they displayed a single bell-shaped plot as expected for protein presence during purification processes.

Similarly, Sh28GST was isolated with the Ni-IMAC column. Samples of each protein were collected at every stage of purification and analysed on a 12% glycine SDS-PAGE gel as shown in Figure 3.5.A. Pure proteins were obtained without any contaminants as indicated by the single bands in orange and blue squares. All the columns were efficient in binding as no protein remnants were observed in the washes. The SDS-PAGE calibration curve in Figure 3.5 B was used to interpolate the monomeric size of Sbh26GST and Sh28GST. The proteins' molecular weights were experimentally found to be around 25 kDa and 29 kDa, respectively which correlates with the theoretical sizes of 26 kDa and 28 kDa as well as the general 25 kDa for GSTs (McTigue *et al*., 1995; Sheehan *et al.*, 2001; Rufer *et al*., 2005).

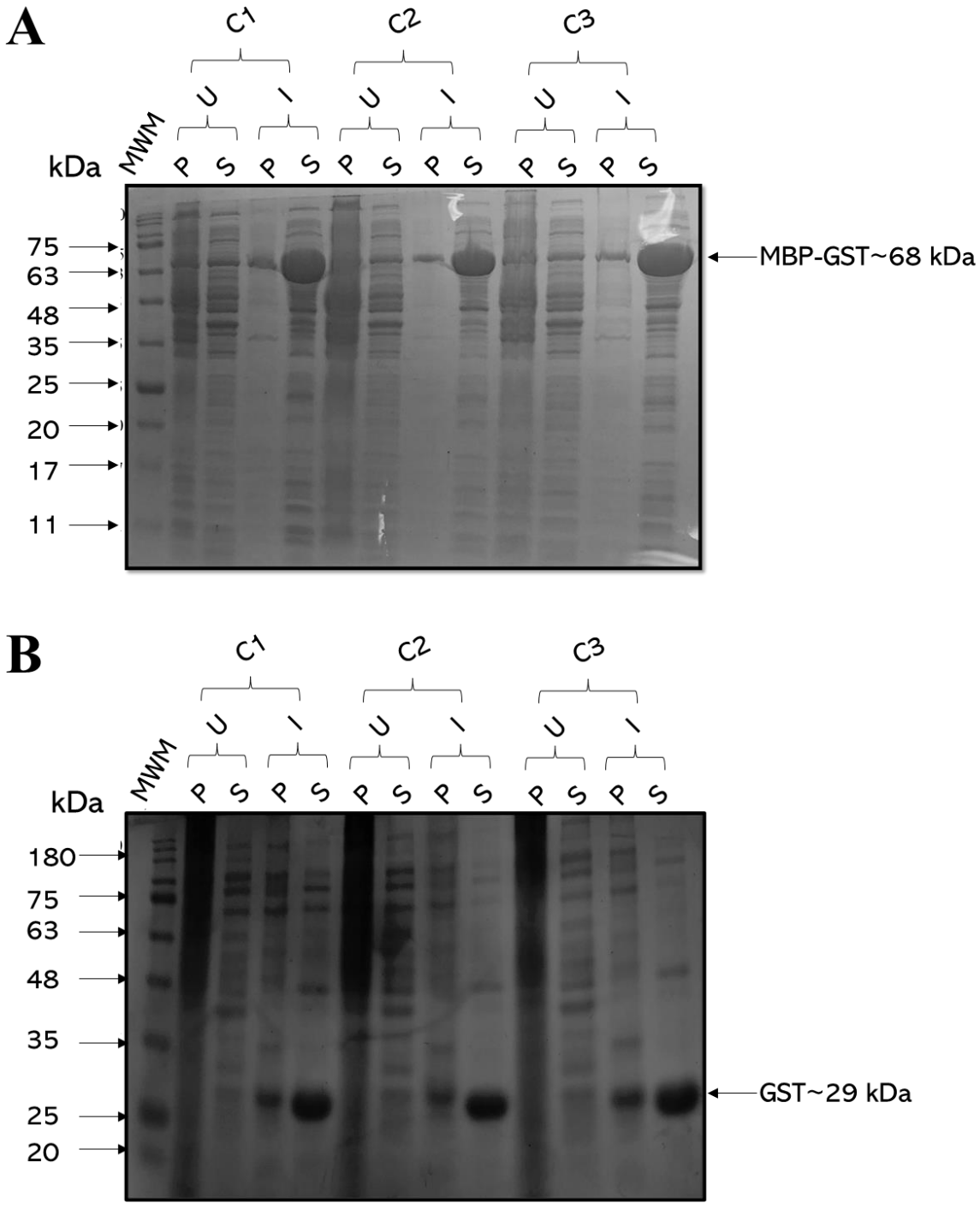

Figure 3.5. The overexpression of Sbh26GST and Sh28GST. T7 *E. coli* cells were transformed with **A**. pMAL-c5X encoding Sbh26GST and **B**. pET11 for Sh28GST. Three colonies (C1-3) were picked from the transformation colonies of each protein to check the success of recombinant overexpression at 30 °C for 6 h. The uninduced culture (U) showed no overexpression of the desired protein. However, the culture that was induced with 0.5 mM IPTG (I) showed thick bands in its soluble fraction, supernatant (S) and small bands in the insoluble fraction, pellet (P). The molecular weight marker (MWM) was used to track the expected molecular weight of the desired proteins.

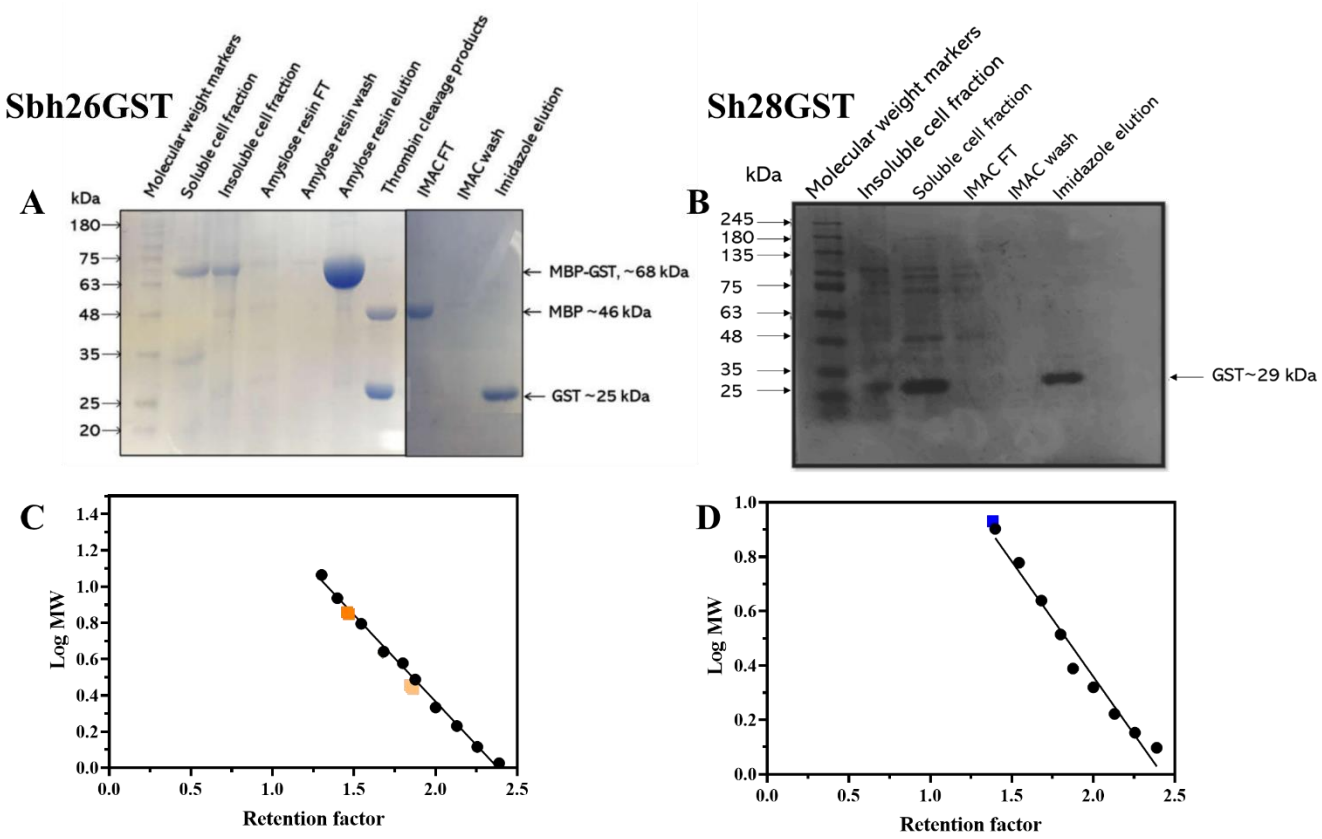

Figure 3.6. Affinity chromatography of Sbh26GST and Sh28GST. **A**. 12 % glycine SDS-PAGE showing the stages of purification from the cell lysate that was lysed and centrifuged to separate the soluble supernatant from the insoluble pellet. Thereafter, the respective protein solutions were subjected to an IMAC and MBP column to isolate Sbh26GST and Sh28GST from other bacterial proteins, respectively. Subsequently, several washes were performed to remove any impurities or weakly bound protein. Lastly, bound protein was released through competitive binding as observed in affinity chromatography. **A** Sbh26GST was firstly purified via agarose-MBP and then released with 10 mM maltose in (50 mM Tris-HCl, pH 7.4). Afterwards, the MBP tag was cleaved with thrombin before the second round of purification with ((Ni-IMAC)-His) where the bound protein was released with 500 mM imidazole. **B**. Similarly, Sh28GST was purified with (Ni-IMAC)-His but using PBS buffer. **C** The standard curve of Sbh26GST for molecular weight determination using SDS-PAGE, Y= -0.9570 + 2.279 and R^2= 0.9959. MBP-His-Sbh26GS (■) weighted 68 kDa compared to a theoretical 69.5 kDa. Whereby, the 46 kDa MBP tag (◆) opposed to the theoretical 42.5 kDa was cleaved to yield pure His-Sbh26GST (■) weighing 25 kDa experimentally and 26 kDa theoretically **D** Similarly, the molecular size of Sh28GST was experimentally determined to be 29 kDa compared to theoretical 28 kDa with Y= -0.8477 + 2.054 and R^2= 0.976.

3.4.4. Protein quantification

Pure proteins, Sbh26GST and Sh28GST were analysed with a JASCO V-630 spectrophotometer to confirm there are no impurities/ interferences before quantification Figure 3.6 shows an absorbance spectrum with a single peak at A_{280} which is indicative of proteins and the flat line at A_{340} means there are no protein aggregates or any particles that might cause light scattering. Lastly, the A_{280}/A_{260} ratio was 0.61 for Sbh26GST and 0.51 for Sh28GST which supports no presence of DNA contamination (Porterfield and Zlotnick, 2010). Once cleared, the pooled proteins' concentrations were determined to be 3.8 mg/mL for Sbh26GST and 4.2 mg/mL for Sh28GST by using the gradient of a serial dilution in the Beer-Lamberts' equation as depicted in Figure 3.7. The overall protein yield average was 4 mg/g for Sbh26GST and 8 mg/g for Sh28GST of wet cells per litre of culture.

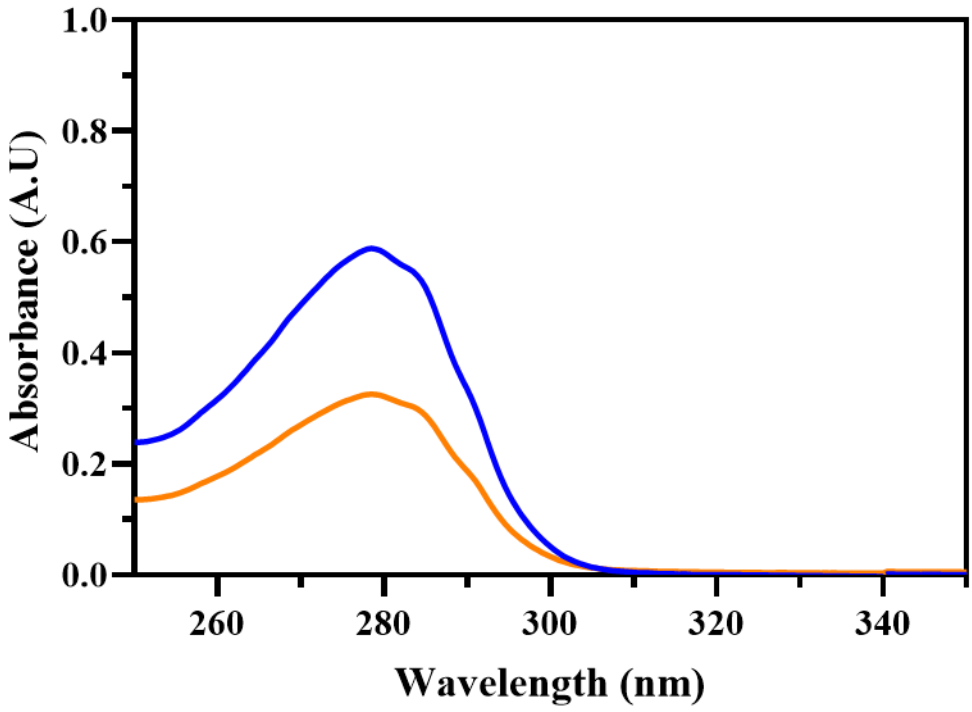

Figure 3.7. Absorbance spectra of Sbh26GST and Sh26GST. The purity of the respective proteins, Sbh26GST (orange) and Sh28GST (blue) were supported by the spectra taken from 250 -350 nm on the JASCO V-630 spectrophotometer. The peak at 280 nm indicates protein and the flat line at 340 nm shows that aggregates are negligible. In addition, the A_{280}/A_{260} ratio was 0.61 for Sbh26GST and 0.509 for Sh28GST, which implies there was insignificant DNA contamination.

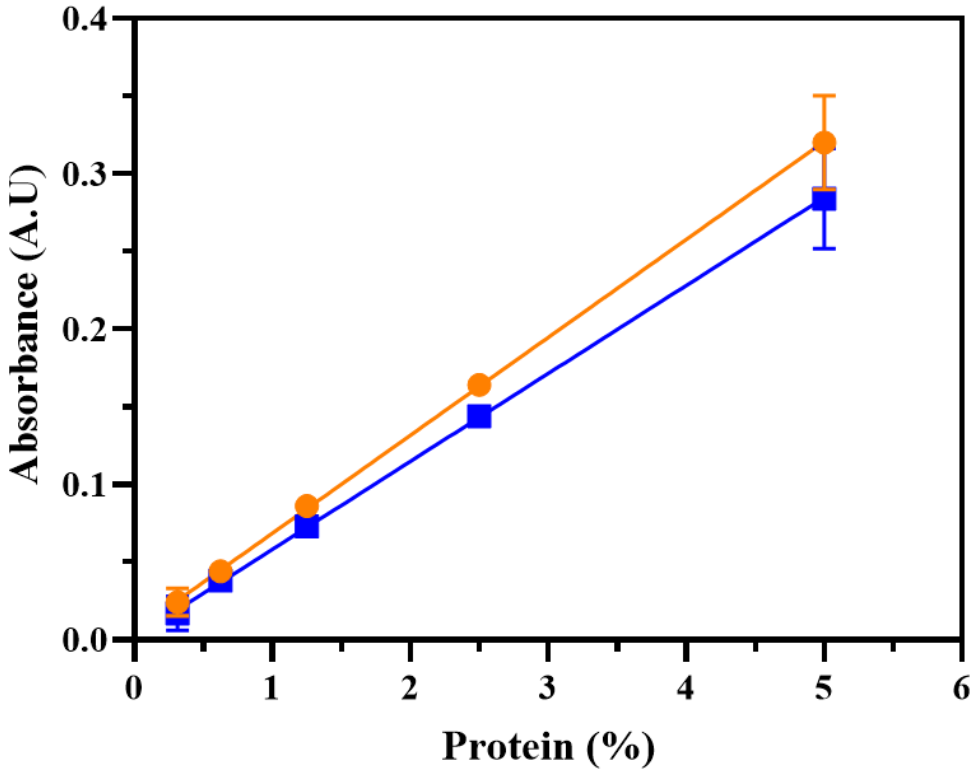

Figure 3.8. Protein quantification of Sbh26GST and Sh26GST. A doubling dilution series was performed for each protein on the JASCO V-630 spectrophotometer whereby A_{280} was monitored for protein presence and A_{340} was used to correct for any aggregates. The corrected absorbances were plotted against the dilution factor of the protein. The gradient from the line of best fit was then used in Beer-Lambert's equation to obtain concentration. The outcome was Y= 0.063x+0.0054, R^2=0.9999 for Sbh26GST (orange) meaning 3.78 mg/mL protein in storage buffer (50 mM Tris-HCl, pH 7.2, 0.02% NaN3) and Y= 0.057x+0.0015, R^2=0.9998 for Sh28GST (blue) meaning 4.20 mg/mL protein in PBS buffer (137 mM NaCl, 2.7 mM KCl, 10 mM Na2HPO4, 2 mM KH2PO4, pH 7.4).

3.5. Discussion

Recombinant overexpression of Sbh26GST was performed with a pMAL-c5X expression vector which employs MBP as a fusion tag in addition to the incorporated His-tag in the sequence of Sbh26GST to increase solubility and ease purification (Duong-Ly and Gabelli, 2015). In the case of Sh28GST, vector pET-11 expressed His-tagged Sh28GST. All in all, under optimised conditions, to produce respective proteins in higher than native concentrations. The SDS-PAGE profile of both proteins showed that they were only expressed under IPTG induction which supports the tight control of the P_{tac} promoter with no leaky/background overexpression, as expected. Furthermore, the proteins were mostly soluble with a minimal amount in the insoluble fraction of the cell lysate as firstly observed in previous studies of a related protein, Sj26GST by Smith and Johnson (1988). The high levels of soluble proteins were also supported by cold induction conditions that promoted proper pro-

tein folding by slowing down and cooling the protein expression machineries in *E. coli*. The overexpression follow-up step was isolating proteins of interest to characterise them.

Therefore, two-step purification using various affinity chromatography namely, MBP and IMAC for Sbh26GST and one-step purification of IMAC for Sh28GST were used to obtain pure proteins. Single, clear, and concentrated bands were predominant on SDS-PAGE electrophoretogram at theoretical and published molecular weights of approximately 25 kDa for Sbh26GST and 29 kDa for Sh28GST. The absence of over-expressed protein in the final flow-through and wash-up steps supports a strong selection of the trapped His-tagged protein with Ni^{2+} chelator resin column and removal of contaminants (Arnau et al., 2006). Moreover, no other bands were observed and respective buffers with Tween-20 did not disrupt the bound proteins.

The location of the tags were at the N-terminus of Sbh26GST and Sh28GST's sequence, influenced by the direction of purification and cleavage. The plasmid designs were in a manner whereby the MBP tag was initially expressed, followed by the thrombin cleavage site then His tag and lastly the expressed protein. The reason behind the design was to allow the initial purification to be based on the interaction of amylose and MBP and eliminate other proteins expressed by *E. coli*, followed by cleaving of the latter tag with thrombin. After that, the second round of purification would isolate cleaved His-Sbh26GST with IMAC from thrombin, cleaved MBP protein and uncleaved MBP-His-Sbh26GST protein as it will bind to the column while other proteins would be eradicated in the flow-through. This, then made it possible to collect pure His-Sbh26GST in a controlled single elution.

The cleavage was performed off-column to avoid aggregates but incurred minor protein loss or dilution due to additional steps of eluting uncleaved protein and loading cleaved protein to the column. Thrombin proved to be efficient in the cleavage as the results were seen within 30 min of incubation, but it was left overnight for maximum concentration of cleaved His-Sbh26GST.

On the other hand, purification of Sh28GST was straight forward and achieved with IMAC yielded the expected results. The protein production of Sh28GST was double the one for Sbh26GST. These may be accounted for by protein stability, the response of *E. coli* machineries and purification dilutions etc. Moreover, a different buffer was used for Sbh26GST due to its purification process whereby thrombin optimally works with calcium but forms calcium stones in the presence of PBS buffer, hence the use of Tris-HCl.

In terms of purification processes' quality, the 240 to 340 nm spectra showed a typical peak at 280 nm dominated by tryptophan residues and no peak at 340 nm, indicating no pro-

tein aggregation or other contaminants, thus yielding Sbh26GST and Sh28GST with homogeneity of greater than 95% purity. The above processes were crucial in laying the foundation for the study as protein yield, purity and activity are key prerequisites to any structural biology research.

Chapter 4

Structure-function characterisation of GSTs from *S. haematobium/bovis*

4.1. Introduction

Enzymes catalyse the rate of chemical reactions by optimising substrate conversion to products. It requires the correct structural conformation orientation of substrates to perform its role. However, some substrates or molecules can inhibit the process by compromising the ideal conditions for maximum catalytic efficiency. In this chapter, the structure of Sbh26GST and Sh28GST were analysed in the presence and absence of non-substrate PZQ, ART and BSP using various techniques and functional tests. The information was used to gain insights into possible binding conformations of the ligands as they interact with the enzyme.

4.2. Materials

Purchased from Sigma are as follows: GSH, CDNB, 8-anilino-1-naphthalenesulfonate (Vos et al.), PZQ, ART, BSP, Dithiothreitol (DTT), Tris (2-carboxyethyl) phosphine (TCEP), sodium phosphate, Tris-HCl, EDTA, NaN_3 and PBS reagents. Snakeskin™ dialysis membrane (10K MWCO, 22 mm) was purchased from Thermo scientific (South Africa). All other reagents used in the study were of analytical grade.

4.3. Methods

4.3.1. Enzyme activity studies

The biological activity of Sh26GST and Sh28GST were evaluated through the classical GSTs enzymatic performance, GSH-CDNB conjugation assay proposed by Habig and Jakoby, 1981 as depicted in Figure 4.1. The substrate, CDNB goes through a nucleophilic aromatic substitution of chlorine for the thiol group of GSH to yield a dinitrophenyl thioether chromophore, 1-(S-glutathionyl)-2,4 dinitrobenzene at a faster rate in the presence of an enzyme. This product absorbs light at 340 nm thus enabling spectrophotometric assay for GST activity. The activity of GST is defined as the amount of enzyme-producing 1 µmol of GS-DNB conjugate per minute.

Figure 4.1 Schematic description of CDNB conjugating assay. GSTs conjugate CDNB using GSH resulting in a chromogenic product, 1-(S-glutathionyl)-2,4 dinitrobenzene which absorbs light at 340 nm. https://www.biovision.com/documentation/datasheets/K263.pdf.

The catalytic activity of Sbh26GST and Sh28GST was assayed exclusive and inclusive of potential inhibitors, PZQ, ART and BSP. Samples were prepared by varying the concentration of the enzyme while the ligands remained constant at 0.05 mM in a final volume of 3 mL reaction buffer made up of 100 mM sodium phosphate, pH 6.5, 1 mM EDTA, 0.02% (w/v) NaN_3, 5.0 mM GSH and 1.0 mM CDNB. The rate of product formation was attained on the UV-visible light spectrophotometer (Jasco V-730 BIO, Jasco Inc., Tokyo Japan) by measuring the change in absorption as the reaction at 20 ℃, 340 nm (ε = 9600 $M^{-1}.cm^{-1}$) progresses for 60 s. The absorptions were converted to concentrations based on Beer Lambert's law in the equation below:

$$Activity\left(\mu mol/_{min}\right) = \frac{A_{340} \times 3000}{9600 \times 10^6} \quad (4.1)$$

All samples were measured in triplicates, blank corrected for non-enzymatic rates and standard deviation was used to measure variation for control. The specific activity ($\mu mol.min^{-1}.mg^{-1}$) was determined from the slope of initial velocity against the amount of enzyme (mg).

4.3.2. Inhibition analysis-IC_{50} of BSP

The half-maximal inhibitory concentration (IC_{50}) is a quantitative measure of the efficacy of a substance in inhibiting a specific biological process. It estimates the concentration of an inhibitor required to reduce the response (or binding) by 50%, thus measuring the potency of an antagonist drug (Neubig *et al.*, 2003). The IC_{50} of BSP towards the enzyme activity of Sbh26GST and Sh28GST was monitored by varying the concentrations of the potential inhibitors when performing the GSH-CDNB conjugation assay as described in section 4.3.1. All samples were analysed in triplicates using 100 nM of Sbh26GST and 64 nM of Sh28GST, all incubated for an hour in respective ligands. The progress curves were captured spectrophotometrically at 340 nm for 60 s and blank corrected. The data of activity (%) vs the

logarithm of inhibitors' concentration was then fitted on GraphPad Prism version 8.0.2 (GraphPad Software, San Diego, California, USA) using the non-linear regression curve fit with four parameters variable slope shown below:

$$Y = \frac{bottom + (top - bottom)}{1 + 10^{((\log IC_{50} - x) \times hillslope)}} \quad (4.2)$$

Where Y is the enzyme activity (%), bottom and top are the minimum and maximum of the plateaus of the graph (%), IC_{50} in respective units (µM), x is the log of inhibitor concentration and hillslope is the slope factor of the curve at its midpoint.

4.3.3. Enzyme steady-state kinetics

Measurements of the initial rates, V_0 of a catalysed reaction are prerequisites to understanding the mechanism by which enzymes work and estimating their activity in a biological system. The initial rate is the maximum rate for a given enzyme and substrate concentration under defined experimental conditions. For many enzymes, there is a hyperbolic relationship between the initial rate and substrate concentration expressed as the Michaelis-Menten (MM) equation,

$$V_o = \frac{V_{max}[S]}{K_M + [S]} \quad (4.3)$$

Where V_{max} is the maximum velocity, the reaction can reach when all the limiting active sites are occupied at initial rates, K_M is the Michaelis constant which represents the substrate concentration at which the reaction velocity is 50 % of the maximum velocity. The smaller the value, the higher the enzyme's affinity for the substrate, achieving low catalytic efficiency. [S] is the substrate concentration.

The enzyme kinetics of Sbh26GST and Sh28GST were measured using the GSH-CDNB conjugation assay as previously described in 4.3.1. However, the protein concentration remained the same at 100 nM for Sbh26GST and 64 nM for Sh28GST. In contrast, the concentration of GSH (natural substrate) was varied to obtain the apparent V_{max} and K_M from the Michalis-Menten (MM) model in GraphPad Prism version 8.0.2 (GraphPad Software, San

Diego, California, USA). In addition, the linear reciprocal of the MM equation, Lineweaver-Burk below was used to evaluate the type of inhibition that is taking place:

$$\frac{1}{V_o} = \frac{1}{K_M}\left(\frac{1}{[S]}\right) + \frac{1}{V_{max}} \tag{4.4}$$

Only the K_M is changed for competitive inhibition, V_{max} for non-competitive inhibition and both for uncompetitive inhibition. Another valuable catalytic constant is the turnover number, k_{cat} which is defined as the maximum number of moles of the substrate that can be converted to product per mole of the enzyme in unit time:

$$k_{cat} = \frac{V_{max}}{[E_t]} \tag{4.5}$$

Where [Et] is the total concentration of enzyme. However, since k_{cat} is the first-order reaction rate constant for conversion of the enzyme-substrate complex to a product, a true measure of catalytic efficiency would be the specificity constant, V_{max}/K_M .It is a second-order rate constant for the reaction of an enzyme converting substrate to produce the product at low substrate concentration. Therefore, the k_{cat} was obtained from the initial linear plot of enzyme velocity versus substrate concentration in the presence and absence of potential inhibitors. Whereby substrate concentration, GSH was kept far below its K_M value towards enzymes, Sbh26GST and Sh28GST, respectively.

4.3.4. Secondary structure

Circular dichroism is a phenomenon that measures the difference in absorption between left-and right-handed circular polarised light due to distinct structural asymmetry caused by the amide interactions in the polypeptide backbone and aromatic side chains (Greenfield, 1996). Consequently, it can give insights into proteins' folding and secondary structure content. When used in the far-UV range (250-170 nm), the absorption of the circularly polarised light is mainly due to the tryptophan and tyrosine in the backbone of the protein (Greenfield, 2006). Proteins that are dominated by α helices result in absorbance at 208 nm and 222 nm in a negative ellipticity and positive ellipticity at 190 nm. In contrast, β-

sheets absorb at 218 nm in negative ellipticity and 195 nm in positive ellipticity (Brahms and Brahms, 1980).

The far-UV CD spectrum of Sbh26GST and Sh28GST were obtained with a 2 mm path length flat quartz cuvette at 20 ℃ and wavelength range of 250-180 nm from Jasco J-810 spectropolarimeter connected to Spectra Manager software v1.5.00 (Jasco Inc., Tokyo, Japan). The used 2 µM of protein in native state was stored in 50 mM Tris-HCl, pH 7.2, 1 mM EDTA, 1 mM DTT and 0.02% (w/v) NaN_3 for Sbh26GST and PBS, pH 7.4, 1 mM EDTA, 1 mM DTT and 0.02% (w/v) NaN_3 for Sh28GST to reduce salt concentration for a better noise to signal ratio. All spectra readings were set at a bandwidth of 1 nm, a scan speed of 100 nm/min, data pitch of 0.5 nm and 1 sec response time for ten accumulations under continuous nitrogen flush to remove oxygen. Data was buffer corrected and normalised to mean residue ellipticity [θ] ($deg.cm^2.dmol^{-1}$)

$$[\theta] = \frac{100\ (signal)}{C.n.l} \tag{4.6}$$

The signal is the CD signal average for several accumulations in millidegrees after the correlation for the solvent baseline, C is the protein concentration (mM), n is the number of residues and l is the path length of light (cm). In addition, the percentages of the secondary structure content of Sbh26GST and Sh28GST were obtained from the Dichroweb algorithm server (Whitmore and Wallace, 2008).

4.3.5. Tertiary structure

4.3.5.1 Intrinsic tryptophan fluorescence spectroscopy

The phenomenon whereby molecules can absorb light or electromagnetic radiation and subsequently emit light is called fluorescence. The observed emission results from electrons returning to the stable ground state after being excited to higher energy states (shorter wavelengths) by light absorption. The difference in excitation and emission energy is known as the Stokes shift, and it is due to energy being lost to vibrational relaxation. Fluorescence spectroscopy measures the radiation energy emitted. Amongst the aromatic amino acids, tryptophan contributes to fluorescence due to delocalised electrons possessed in its indole ring that can solely be excited at 295 nm. The ring is also sensitive to solvent polarity and is a suitable intrinsic probe. This makes the emission maxima (300-350 nm) closely related to the occurrence and positioning of Trp residues within the protein matrix. Trp residues are usually

buried in hydrophobic environments which results in high quantum yield; hence high fluorescence intensity occurs (blue shift) (Ghisaidoobe and Chung, 2014).

The three-dimensional structure of Sbh26GST and Sh28GST in the presence and absence of co-substrates and potential inhibitors were characterised using the fluorescence spectra obtained on the Jasco FP-6300 spectrofluorometer with Spectra Manager software v1.5.00 (Jasco Inc., Tokyo, Japan). The used conditions were set at 20 °C in a 10 mm path length quartz cuvette, 300 to 400 nm using an excitation wavelength of 295 nm, 200 nm/min speed, 5.0 nm excitation and 2.5 nm emission slit width. The protein concentration used was 10 µM, where Sbh26GST was in 50 mM Tris-HCl buffer, and Sh28GST in PBS buffer, all with 1.0 mM DTT, 1.0 mM EDTA and 0.02% (w/v) NaN_3 at pH 7.2 were measured in triplicates of three accumulations. Similarly, the respective proteins were incubated in 1.0 mM co-substrate, GSH and a similar structure to the co-substrate, *S*-hexylglutathione (GTX), in the presence and absence of 100 µM PZQ, ART and BSP, respectively. All the spectra were buffer-corrected for any Raman peaks.

4.3.5.2 Extrinsic ANS fluorescence spectroscopy

The fluorescent dye, ANS as shown in Figure 4.2 was used as a probe for hydrophobic cavities in Sbh26GST and Sh28GST. ANS has a characteristic increase in fluorescence intensity when bound to solvent-accessible non-polar regions which are few in native proteins or unavailable in denatured proteins. Free ANS electrons are excited to a higher energy state by absorbing light in the interaction. However, processes such as vibrational relaxation and/or internal conversion, intramolecular charge transfer and solvent relaxation result in energy losses that compete with fluorescence thus wavelength redshift is observed. Consequently, any change in ANS' polarity increases quantum yield (ΔΦ) and intensity, resulting in a blueshift between the wavelengths of 500 nm and 480 nm (Hawe *et al.*, 2008).

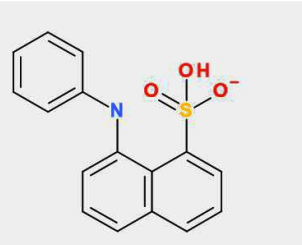

Figure 4.2. 2D illustration of the structures of 8-anilino-1-naphthalenesulfonate.

Stock ANS was prepared in 20 mM sodium phosphate, 1.0 mM EDTA, 0.02% (w/v) NaN_3, pH 7.4 and its concentration was measured spectroscopically at 372 nm (Ɛ= 7800 $M^{-1}cm^{-1}$). The solution was wrapped in foil and stored at 4℃ to prevent photodecomposition. Freshly diluted 100 µM of ANS with respective buffer was incubated for 30 min in the dark with 10 µM Sbh26GST and Sh28GST, 1.0 mM of ligand GSH and GTX in the presence and absence of 100 µM potential inhibitors (PZQ, ART and BSP) to enhance proper binding in mimicked natural conditions. All samples were analysed using Jasco FP-6300 fluorimeter with excitation at 390 nm, 20 ℃, with 5 nm slit widths, emission at 400-600 nm and a scan speed of 200 $nm.min^{-1}$. The readings were corrected by subtracting the spectra of free ANS from ANS bound to Sbh26GST and Sh28GST. Furthermore, the contribution of the inner filter effect by ligands whereby they would absorb excitation (primary) or emission (secondary) light was corrected by using the equation below (Lakowicz, 1999)

$$F_{corr} = F_{obs} \times 10^{\left(\frac{OD_{ex}+OD_{em}}{2}\right)} \quad (4.7)$$

Where F_{obs} is the observed, uncorrected fluorescence intensity, OD_{ex} and OD_{em} are the inhibitor optical densities at the emission and excitation wavelengths respectively.

4.4. Results

Structural characterisation techniques (far-UV CD, Trp and ANS fluorescence) and functional ones (GSH-CBNB assay for activity, IC_{50} and kinetics) were used in the presence and absence of non-substrates, PZQ; ART and BSP to determine the effects of these ligands to the structure-function of pseudo Sbh26GST in comparison to the known Sh28GST.

4.4.1 Functional characterisation

The function of Sbh26GST and Sh28GST was characterised by GSTs' ability to catalyse GSH-CDNB conjugation which speaks more to their role in metabolism. The interest was in investigating the reaction rates under different conditions, which reveals the mechanism of action, substrate specificity and how agonists inhibit the enzyme.

4.4.1.1 Catalytic activity of Sbh26GST and Sh28GST

The functionality of the enzymes, Sbh26GST and Sh28GST were evaluated through the GSH-CBNB conjugation assay in the presence and absence of 0.5 mM potential inhibitor, BSP and PZQ. The progress curve of product formation from 5 mM GSH and 1.0 mM CDNB

in 100 mM $NaHPO_4$, pH 6,5, 1 mM EDTA, 0.02% (w/v) NaN_3 buffer was monitored in triplicates at an absorbance of 340 nm for 60 seconds as shown in Appendix, Figure S3. The slopes of the reaction curves, which are the initial velocity, were plotted against enzyme concentration to determine the enzyme activity. The latter measure is required to determine specific activity, whereby it is plotted against enzyme mass as shown in Figure 4.3. The specific activity of 13 µmol/min/mg for Sbh26GST was consistent with Sj26GST studies (Kaplan *et al.*, 1997; Pooe et al., 2021), and 44 µmol/min/mg for Sh28GST was high but within ranges of GSTs. Both enzyme activities were halted by ~ 99% in the presence of BSP, whereas PZQ and ART had an insignificant impact.

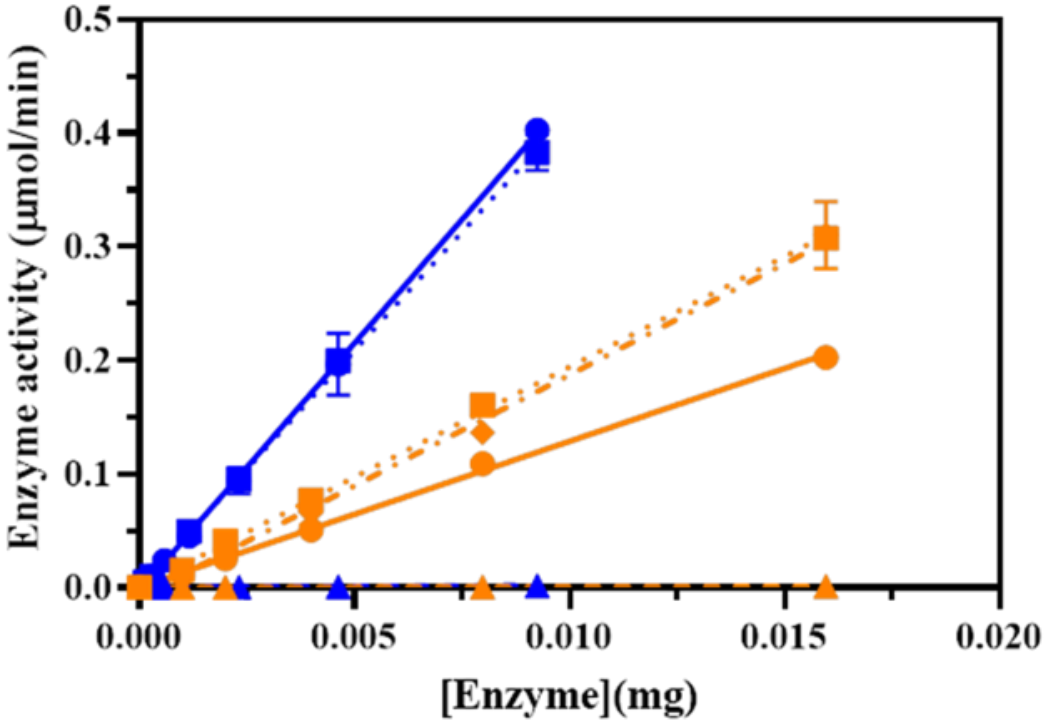

Figure 4.3. Specific activity towards GSH-CDNB conjugation. An activity plot of GSH-CDNB conjugation by GSTs against the amount of enzyme. The product, 1-(S-glutathionyl)-2, 4 dinitrobenzene formation, was monitored on absorbance spectroscopy at 340 nm for 60 sec in reaction buffer (1 mM sodium phosphate, pH 6.5, 5 mM GSH and 1.0 mM CDNB). All measurements were performed in triplicates in the absence or presence of 0.5 mM ligand, whereby standard deviation was used to account for error bars. The following slopes were obtained from the plot for specific activity determination: 13 µmol/min/mg, R^2= 0.9984 for Sbh26GST (●) with insignificant increase to 19 µmol/min/mg in both cases of Sbh26GST +PZQ (■), R^2= 0.9992 and Sbh26GST +ART (◆), R^2= 0.9961 but a complete knock-out to 0.07 µmol/min/mg, R^2=0.9715 for Sbh26GST +BSP (▲). Similarly, 44 µmol/min/mg, R^2=0.9997 for Sh28GST (●) with insignificant change to 42 µmol/min/mg, R^2= 0.9994 for Sh28GST +PZQ (■) and knockout to 0.17 µmol/min/mg, R^2=0.9994 for Sh28GST +BSP (▲).

4.4.1.2 Inhibition studies for IC_{50} determination

The observed halt of GSH-CDNB conjugation by BSP in respective enzymes was studied further by determining the ligand's half-maximal inhibitory concentration (IC_{50}) to understand its effect. This was established from a plot of GSTs' activity as the reaction progresses vs the logarithmic concentration of BSP, Figure 4.4. The data was fitted on GraphPad Prism 8.0.2 (GraphPad Software, San Diego, California, USA) with the four-parameter-linear regression for sigmoidal curves. The IC_{50} calculation for Sbh26GST was 27 µM and 0.88 µM for Sh28GST.

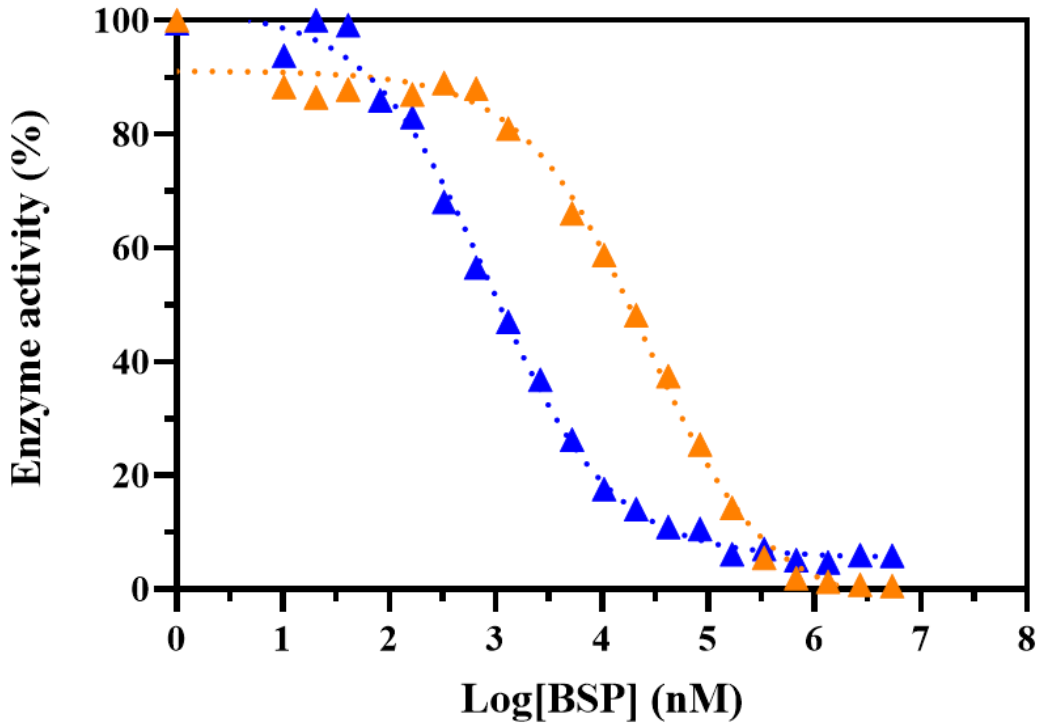

Figure 4.4. The inhibitory concentration of BSP on Sbh26GST and Sh28GST. CDNB-GSH conjugation was performed in 100 mM NaHPO4, pH 6,5, 1 mM EDTA, 0.02% (w/v) NaN3 buffer containing 5 mM GSH and 1 mM CDNB in the presence of 100 nM Sbh26GST (orange) and 64 nM Sh28GST (blue). The product formation was monitored at 340 nm for 60 sec after 30 min of incubation in the presence of a varying concentration of BSP. The enzymes' recorded percentage activities were plotted against the log of BSP's concentrations for the interpolation of IC_{50} values, which were found to be 27 µM, R^2=0.9938 and 0.88 µM, R^2= 0.9961, respectively. The error bars represent ± SD for the triplicates.

4.4.1.3 Enzyme kinetics of GSTs' GSH-CDNB conjugation

The evaluation of the GSH-CBNB conjugation assay was conducted continuously to measure product formation. This was performed in the absence and presence of varying BSP concentrations. The GSH-CDNB conjugation by Sbh26GST and Sh28GST, followed a Michaelis-Menten hyperbolic curve of reaction velocity as a function of substrate concentration, as

depicted in Figure 4.5. The plots were used to determine the V_{max} and K_M of GSH towards the enzymes, as shown in Table 4.1 with the non-linear regression enzyme kinetics feature in GraphPad Prism. The V_{max} of Sbh26GST was comparatively lower than the one in Sh28GST, but the K_M of Sbh26GST was higher than Sh28GST.

Furthermore, the V_{max} and K_M in the case of Sbh26GST catalysis were decreased by 84 and 70 % in the presence of BSP. Similarly, both K_M and V_{max} of Sh28GST catalysis was significantly decreased by 98 and 92 %. However, when Sbh26GST was exposed to ART it decreased K_M by 52 % but the V_{max} change was insignificant (6%). Additionally, a more accurate linear plot of Lineweaver-Burk, Hanes-Woolf and Eadie-Hofstee was used to support K_M and V_{max} predictions in addressing the mode of inhibition of BSP towards GSH as shown in Appendix, Figure S4 and Table S1. Overall, the liner plots were in comparable ranges with the GraphPad predictions in the order of Hanes-Woolf, Eadie-Hofstee and Lineweaver-Burk. The effects of BSP interaction on the enzymes were probed further to evaluate catalytic efficiency, k_{cat} and the rate of product formation k_{cat}/K_M. Whereby the focus was below K_M of GSH at the first-rate linear order on the Michaelis-Menten curves. In all cases, the catalytic efficiency of Sbh26GST and Sh28GST were reduced as depicted in Table 4.1 and Appendix, Figure S5, whereby Sh28GST experienced more deteriorative impact from BSP binding, about 90%% than Sbh26GST at 80%.

Table 4.1. Kinetic parameters of Sbh26GST and Sh28GST. GSH-CDNB conjugation assay was performed under varying concentrations of GSH at different conditions of BSP exposure.

Kinetic parameters	Sbh26GST			Sh28GST		
BSP (µM)	0	2.7	27	0	0.08	0.8
V_{max} (µmol/min)	0.19 ± 0.02	0.28 ± 0.013	0.03 ± 0.001	0.34 ± 0.06	0.021 ± 0.021	0.0061 ± 0.04
K_M (µM)	120 ± 0.03	322 ± 0.011	36.5 ± 0.006	176 ± 0.08	11 ± 0.072	19 ± 0.9
k_{cat} (s^{-1})	9.80 ± 0.06	21.6 ± 0.064	1.20 ± 0.130	29 ± 0.04	1.5 ± 0.042	0.34 ± 0.05
k_{cat}/K_M ($M^{-1}s^{-1}$)	0.08 ± 0.04	0.11 ± 0.027	0.03 ± 0.003	0.16 ± 0.04	0.12 ± 0.085	0.022 ± 0.03

*Value ± SD

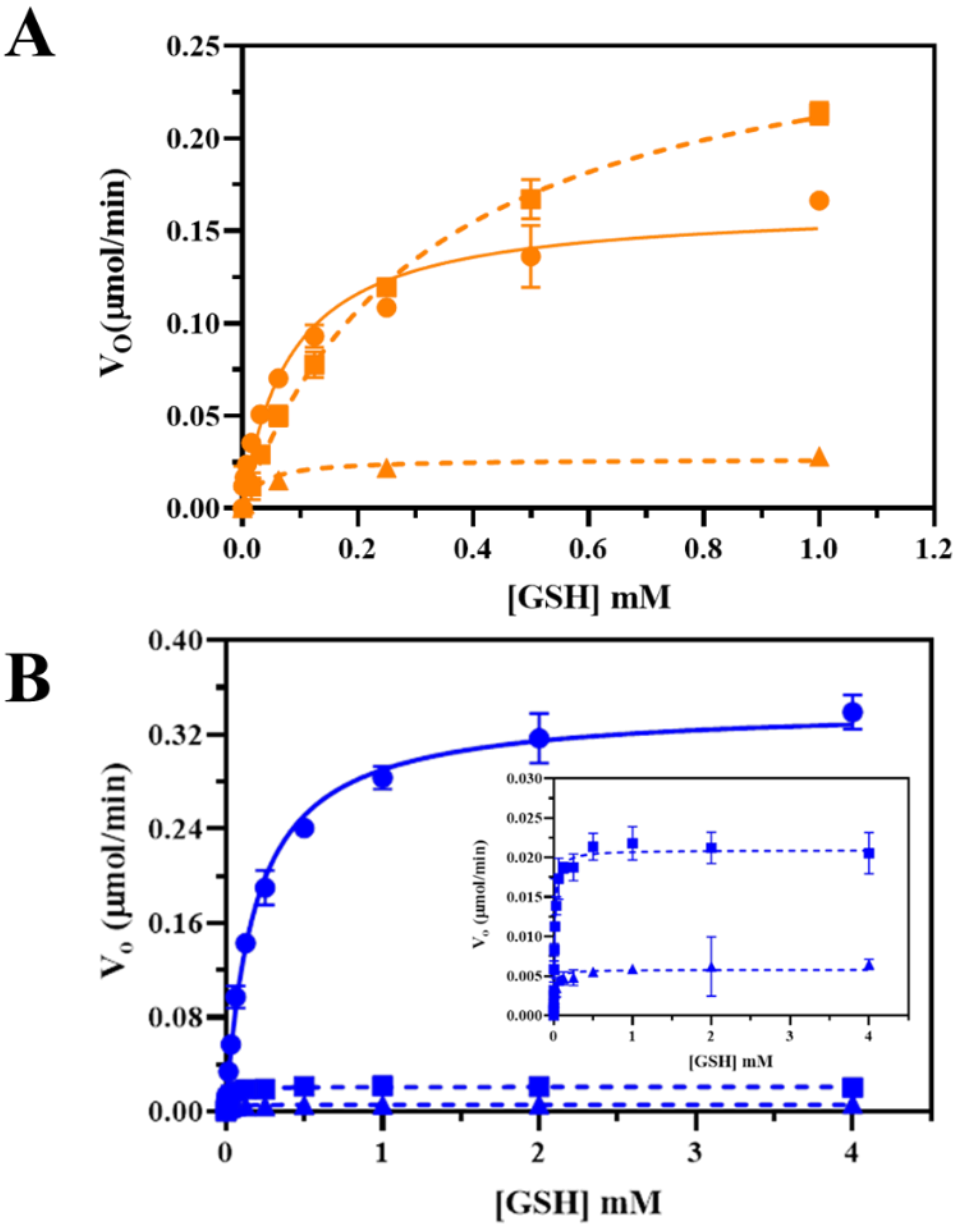

Figure 4.5. Michaelis-Menten curve of Sbh26GST and Sh28GST towards GSH. The GSH-CBNB conjugation assay was conducted in 100 mM $NaHPO_4$, pH 6,5, 1 mM EDTA, 0.02% (w/v) NaN_3 buffer containing variable amounts of GSH and 1 mM CDNB. The product formation was monitored at A_{340} for 60 s. The orange plots in **A**. are for Sbh26GSH, whereas the blue plots in **B**. are for Sh28GST. The hyperbolic curves in plots of reaction velocity vs GSH concentration (, ,) represent no drug, 2.7 µM BSP and 27µM BSP, respectively. Similarly, (, ,) represent no drug, 0.08 µM BSP and 0.8 µM BSP. The error bars are ±SD of each replicate experiment.

4.4.2 Structural characterisation

The structural integrity of Sbh26GST and Sh28GST in the presence and absence of PZQ, ART and BSP were analysed at the secondary level using Far-UV CD and tertiary level using intrinsic tryptophan fluorescence spectroscopy as well as ANS spectroscopy.

4.4.2.1 Far-UV circular dichroism spectropolarimetry

The secondary structure of Sbh26GST and Sh28GST are mainly stabilised by hydrogen bonding of the proteins' backbone was assessed through far-UV CD. The spectrum of Sbh26GST as depicted in Figure 4.6 shows a trough at 219.5 and 208 nm which is close to the expected troughs at 208 and 222 nm, plus a peak at 195 nm for such folds (Kelly *et al.*, 2005). However, the peak at 195 nm was disturbed by the high voltage compensation signalled by the HT spectrum (data not shown). Similarly, Sh28GST has a peak at 220, 215.5 and lastly at 212 nm. In addition, Dichroweb was used to calculate the secondary structure content fit of the submitted data to the actual secondary structure. The results showed NRMSD (normalized root mean square deviation) within the typical range of accurate good fits in both cases (Whitmore and Wallace, 2004) and it agrees with the CD data.

4.4.2.2 Intrinsic tryptophan fluorescence

The tertiary structure of Sbh26GST and Sh28GST in the presence and absence of PZQ, ART and BSP were analysed with fluorescence spectroscopy using Trp residues as a probe for the polarity of the microenvironment of the enzyme. The indole rings of these Trp residues were selectively excited at a wavelength of 295 nm and the emission was monitored between 300 and 500 nm as depicted in Figure 4.7. The fluorescence spectra show the maximum emission wavelength as 342 nm for Sbh26GST with higher intensity compared to the 341 nm of Sh28GST, all in the absence of ligands compared to free Trp that emits at 350 nm (Lakowicz, 2006). The introduction of PZQ to the systems had no significant impact. However, when BSP was introduced, it changed the polarity and completely knocked down the respective microenvironment. The fluorescence intensities decreased by 82 % for Sbh26GST with no wavelength shift. The latter trend was also observed when ART was added with a 79 % decrease. Concerning Sh28GST, BSP resulted in an over 95 % decrease in intensity accompanied by a redshift in wavelength.

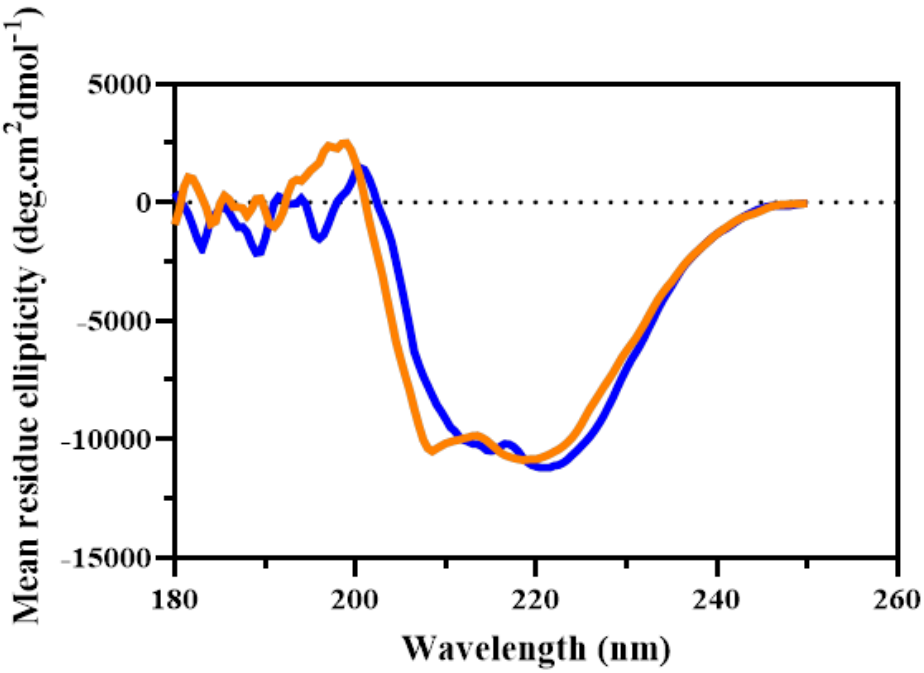

Figure 4.6. Far-UV CD spectra of Sbh26GST and Sh28GST. The spectrums were recorded at 20 ℃ on Jasco J-810 spectropolarimeter using a 2mm path length cuvette containing 2 µM of protein, namely Sbh26GST (orange) in 50 mM Tris-HCl, pH 7.4 and Sh28GST (blue) in PBS buffer. The profiles are characteristic of predominantly α-helical protein with a trough at ~ 208 and 222 nm.

Table 4.2. Dichroweb data for secondary structure content of Sbh26GST and Sh28GST. The CONTILL algorithm was used to determine the NRMSD (Normalised Root-Mean-Square Deviation) which is a measure of goodness of fit for calculated data compared to obtained experimental data whereby a value below 0.1 is accepted as a good fit (Sreerama and Woody, 2000).

Protein (%)	Sbh26GST	Sh28GST
α-Helix	52.0	48.4
β-Strand	0.70	5.10
β-Turn	17.9	17.4
Uunordered	29.4	29.1
NRMSD	0.23	0.18

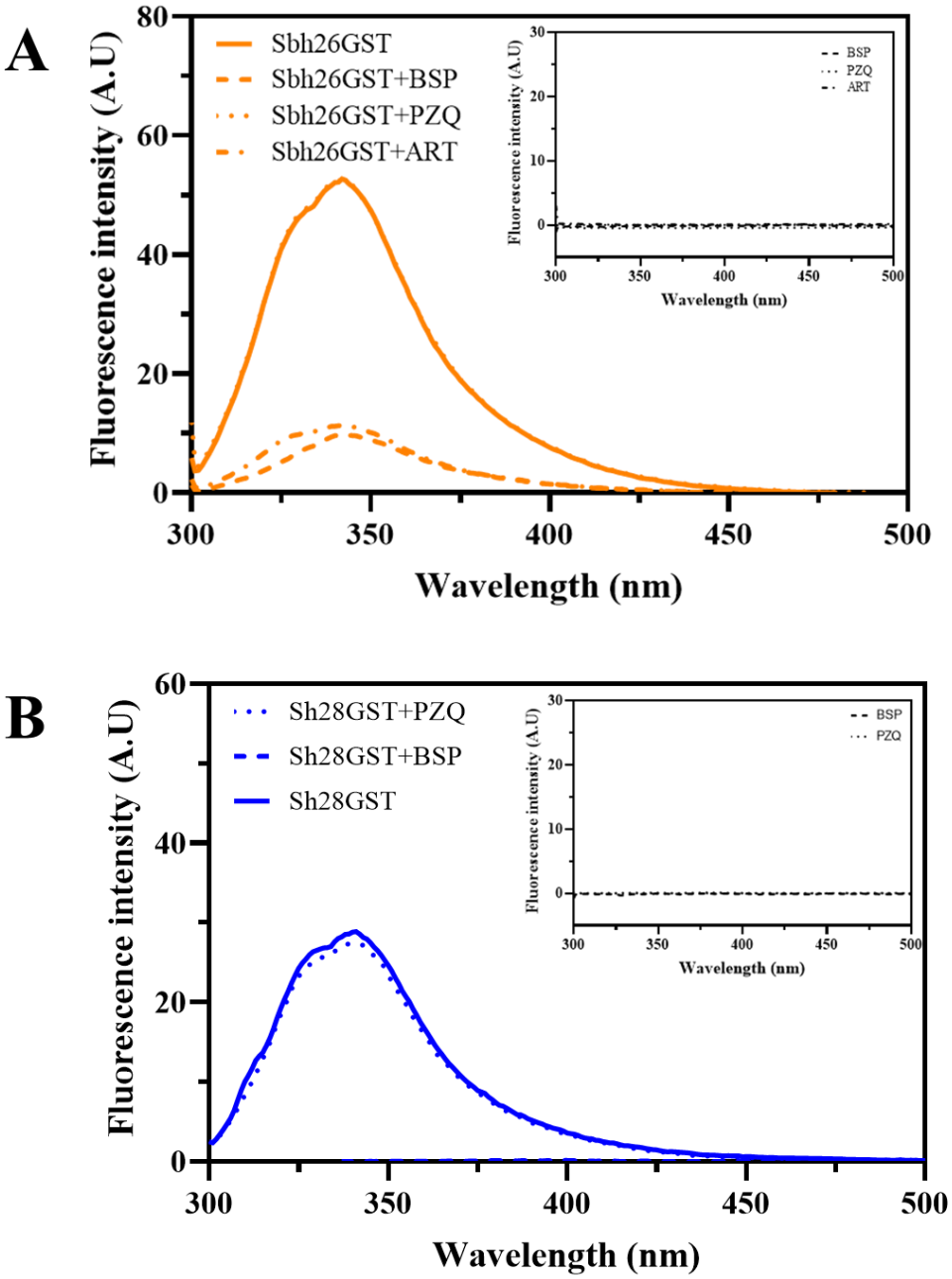

Figure 4.7. Trp fluorescence emission spectrum of Sbh26GST vs Sh28GST. The fluorescence emission spectrum of 10 µM of Sbh26GST in Tris-HCl (A) and Sh28GST in PBS buffer (B) after selectively exciting Trp residues at 295 nm. The maximum emission for Sbh26GST was at 342 nm with higher intensities, whereas for Sh28GST it was at 341 nm. Furthermore, 100 µM of ligands PZQ, ART and BSP were added. The results show that PZQ has no significant impact as sole Sbh26GST overlays on top of Sbh26GST+PZQ. Similarly, sole Sh28GST and Sh28GST+PZQ had negligible differences. On the other hand, it was observed that BSP shows a significant decrease in fluorescence intensities in the case of Sbh26GST+BSP and a knockout in Sh28GST+BSP along with a redshift in wavelength from 341 nm to 377 nm. The insert graphs show that sole ligands had an insignificant contribution to the fluorescence intensities at studied wavelengths.

In addition, the natural co-substrate GSH and its analogue GTX were introduced to the systems. Overall, similar trends in the presence and absence of ligands were followed as depicted in Appendix, Figure S6. The differences observed were higher intensities in the presence of GSH and even higher in the presence of GTX, and negligible wavelength changes (±1 or 2 nm). GSH (in the presence of BSP) had even greater disturbance (90 %) and ART had an 80 % impact, whereas PZQ had no significant change for Sbh26GST. GTX, on the other hand, decreased Trp environment disturbance to 72 % in the presence of BSP and no change for ART but increased the disturbance by 9 % in the presence of PZQ. In terms of Sh28GST, the presence of GSH was the one that resulted in a 17% decreased intensity of PZQ, while GTX had similar trends that were mentioned earlier.

4.4.2.3 Extrinsic ANS fluorescence

The tertiary structure of Sbh26GST and Sh28GST was further extrinsically studied using ANS as a probe for hydrophobic patches and a ligand for possible binding sites. The emission spectrums of the respective protein in the presence of ANS resulted in a significant increase in quantum yield and slight blueshift in wavelength concerning free ANS that maximally emit at 520 nm as shown in Figure 4.8. The conclusion was made based on the maximum emission of Sbh26GST+ANS at 493 nm and Sh28GST+ANS at 490 nm. This trend is characteristic of ANS interacting with a hydrophobic pocket of a protein (Gasymov and Glasgow, 2007). When BSP and ART were introduced to the reference, ANS-bound proteins, these ligands outcompeted ANS, which decreased its quantum yield and a 9 and 21 nm redshift for Sbh26GST and Sh28GST, respectively (Appendix, Table S3). However, the binding of PZQ exposed more hydrophobic patches that were not available to ANS, increasing its quantum yield accompanied by a 3 and 7 nm redshift for Sbh26GST and Sh28GST. All the conditions were repeated in the presence of co-substrate, GSH and its similar structure, GTX as shown in Appendix, Figure S7. The trends followed were similar to those above except for GSH having slightly the lowest fluorescence intensity, relative to Apo native proteins and GTX being the one with the highest intensities. Furthermore, it was also noted that in the presence of GSH and GTX, PZQ had a blueshift in wavelength (±2 or 3 nm) relative to ANS-bound protein and not the observed redshift in Apo conditions, thus speaking to the degree of folding.

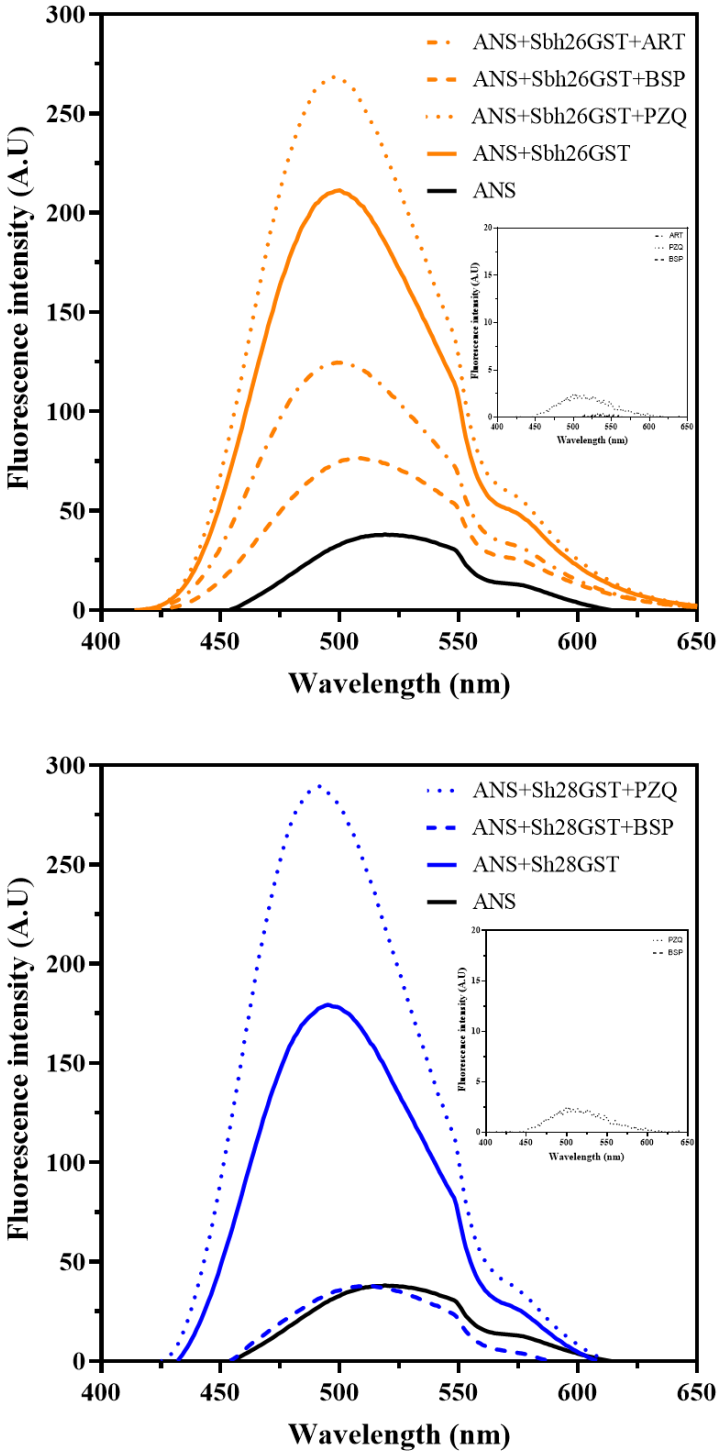

Figure 4.8. ANS fluorescence emission spectrum of Sbh26GST vs Sh28GST. The fluorescence emission spectra of 10 µM Sbh26GST and Sh28GST in 20 mM sodium phosphate, 1 mM EDTA, 0.02% (w/v) NaN3, pH 7.4 after excitation at 395 nm were analysed between 400 and 600 nm. The maximum emission for Sbh26GST was at 493 nm while Sh28GST was at 490 compared to free ANS at 520 nm. Therefore, blueshift in wavelength was accompanied by decreased intensities in the presence of ART and BSP but increased one in the presence of PZQ. The insert graphs show the additional contribution of the drugs towards the studied ANS spectrum which was insignificant and corrected.

4.5. Discussion

The study of enzyme kinetics which are rates of reactions gives insights into how the respective enzymes achieve their role in catalysis. This study used the catalysis of GSH-CDNB conjugation by Sbh26GST and Sh28GST to determine the activity of the enzymes and mechanism of action for the introduced drugs (PZQ, ART and BSP) as potential inhibitors. The active site of cytosolic GSTs has an allosteric site at the dimer interface of the two subunits. In each subunit, a site that accommodates the GSH (G-site) is positioned towards the N-terminus while the hydrophobic site that accommodates CDNB (H-site) is at the C-terminus.

Both enzymes were active and the specific activity of Sh28GST was established to be higher than Sbh26GST. This suggests a better selectivity fit/ affinity driver of certain substrates in the active site of one enzyme than the other. Furthermore, the introduction of BSP proved to decrease enzyme activity and has a higher affinity towards Sh28GST than Sbh26GST as shown by a factor of 10 decreases in IC_{50} values. Upon further analysis of the reaction through kinetic studies, it was observed that BSP binds non-competitively to Sbh26GST and Sh28GST with respect to GSH and electrophilic substrates. This supports studies that agree with such non-substrates partially occupying the H-site and or an allosteric L-site at the dimer interface (van Bladeren and van Ommen, 1991; Bico *et al.*, 1995; Lyon *et al.*, 2003; Pooe et al., 2021). The catalytic mechanism observed was a random substrate-binding due to the formation of a ternary complex and it agrees with what is available in the literature about Sj26GST (Stefanidis et al., 2018; Akumadu et al., 2020). The latter inference was made based on the ability of non-competitive inhibitors to bind the enzyme or enzyme-substrate complex with equal affinity.

The binding of GSH to Sbh26GST and Sh28GST showed high affinity as expected since it is the natural co-substrate for these enzymes, and it is found in high abundance (1-10 mM) in the cytosol. In terms of the rate constant, k_d for conversion of the enzyme-substrate complex to product, it showed a non-rapid process that correlates to moderate affinity for substrates and aligns with observations of Fabrini *et al.* (2010). Overall, Sh28GST is more sensitive to BSP inhibition, or it is more indirectly proportional to catalytically efficiency than Sbh26GST concerning GSH-CDNB conjugation. Moreover, these observation supports previous decreased enzyme activity upon BSP binding. On the contrary, ART and arguable PZQ had increased kinetics which correlates with increased activity. There is limited information on the kinetics of cytosolic GSTs for comparison to our study. When it came to the kinetic parameters of CDNB, they were not analysed as it is not a natural substrate for GSTs, and it does not reach saturation. Yet, in previous studies, non-substrates such as EA have

shown to bind uncompetitively at the H-site, which also speaks to such ligands binding elsewhere e.g. L-site at the dimer interface (Akumadu *et al*., 2020). Therefore, in our study, we resorted to other substrates to probe H-site characterisation as explained in 4.3.5.2. Otherwise, K_M and V_{max} values were compared across several linear plots of Michaelis-Menten kinetics. All the data yielded values with negligible differences and few outliers, but they were fairly according to similar studies (Walker et al., 1993; Akumadu et al., 2020). The primary goal of the CDNB-GSH assay was to test and check whether the functionality of the respective enzymes was intact. Followed by a detailed understanding of how catalysis is achieved which helps in ligands designs for therapeutic response upon cracking structural conformations.

Regarding the structural integrity of Sbh26GST and Sh28GST, the secondary profile from CD data has shown that both proteins support the established GST structure, which is predominately α-helical. Furthermore, Sbh26GST had more β-sheet than Sh28GST due to a higher quantity of amino acids such as Trp residues which are more susceptible to such folds. The observed variation is imperative for substrate recognition and catalysis of GSTs. Hence the conserved three-dimensional fold of GSTs is crucial for the interaction of the α-helices and β-strands with co-substrate GSH while the H-site and L-site have more variations that enable these closely related enzymes to bind a vast range of substrates. Moreover, the flexibility of these structural elements also drives substrate-dependent catalysis. The CD data was supported by DichroWeb analysis which gave secondary structure content percentages within acceptable NRMSD that aligned with the experimental data. However, a considerable percentage of unordered regions were not flagged on the CD spectrum at 200 nm. Nonetheless, the data still correlates and comes down to a high-resolution structure of predominantly α-helical GST enzymes.

In Sbh26GST, there are four Trp residues per monomer (Trp 20,53,213 and 218) but only two are situated near the active sites, whereas Sh28GST has only two conserved Trp residues (Trp 49 and 75) critical to binding near the active site. Therefore, this explains the higher intensities observed in Sbh26GST than in Sh28GST as the polarities of the Trp environment are slightly different. However, it is not easy to differentiate individual spectral contributions. Trp residues in both cases show an overall slight blue shift (<10 nm) in the emission wavelength relative to free Trp. It can be concluded that the Trp residues are mostly buried in non-polar regions of correctly folded Sbh26GST and Sh28GST whereas unfolding exposes the Trp residues to the polar environment. The introduction of BSP and ART decreased intensities related to Trp residues being more exposed to the polar solvent and not necessary a

change in the global structure. Moreover, Sh28GST showed more exposure to Trp residues than Sbh26GST which has Trp residues situated in hydrophobic patches or clefts. However, the presence of co-substrate GSH and its analogue, GTX with a bulky side chain would otherwise impede the exposure to some extent due to non-covalent interactions with amino acids lining the dimer interface.

The tertiary structure of Sbh26GST and Sh28GST was further probed with an anionic dye, ANS, which is sensitive to hydrophobic clefts or pockets, whereby upon binding, its quantum yield increases. Indeed, ANS in the presence of sole Sbh26GST and Sh28GST had a higher quantum yield than free ANS accompanied by blueshift in wavelength. The observations of hydrophobic binding sites are consistent with Sj26GST and GSTs class Mu studies (Kinsley *et al.*, 2008; Akumadu *et al*., 2020). Furthermore, Sbh26GST had higher intensities than Sh28GST, meaning hydrophobic patches were more accessible in Sbh26GST. In Sh28GST they tend to be more buried and less exposed to the aqueous solvent. It has been established that ANS tends to mostly bind at the H-site of GSTs (Mannervik and Danielson, 1988; Oakley *et al.*, 1997; Dirr *et al.*, 2005) but not exclusively as ANS has also been shown to bind elsewhere in Sj26GST, possibly the L-site in the dimer interface and not the highly specific G-site for GSH (Yassin *et al*., 2004). Therefore, since ART and BSP outcompeted ANS and decreased its intensity, these ligands could potentially bind at these sites. The obtained results agreed with a similar study by Yassin *et al*. (2004) showed Sj26GST has a low affinity for ANS as a strong binder, and BSP outcompeted it. More so, ANS in cytosolic GSTs tends to bind at the H-site (Litwack *et al.*, 1971). Previous studies have shown that non-substrates such as BSP, indanyloxyacetic acid 94 (IAA-94) and ellagic acid (EA) can bind at the H-site and/or the L-site of GSTs, which concur with our findings (Yassin et al., 2004; Akumadu et al., 2020; Pooe et al., 2021). Conversely, PZQ promoted ANS binding. More specifically, it was shown to bind at the dimer interface of Sj26GST with no inhibition (McTigue et al., 1995). The binding sites occupied and orientations of the mentioned ligands are different, but GSTs hydrophobic binding site is very promiscuous and can accommodate a wide range of substrates, including weak and highly transient interactions (Dirr et al., 1994; Atkinson and Babbitt, 2009).

The introduction of co-substrates in both proteins showed that GSH had better interactions with all ligands (PZQ, ART and BSP) or more contacts than GTX as it had the lowest intensities; thus, the minimal hydrophobic room was left for ANS to bind. This depicts induced fitting as alkyl groups of GTX make non-specific apolar contacts while GSH makes specific ones with H-site, rendering additional binding energy and subsequently tighter binds

(Quesada-Soriano *et al*.,2006). The proteins' hydrophobic sites were more buried (folded) in the case of PZQ than in BSP and ART that exposed/lost these regions upon unfolding/ solvent interaction. Overall, Sh28GST had a more wavelength shift than Sbh26GST when BSP was introduced in all cases. Hence Sh28GST has an effect of more structural changes or an induced fit towards the ligand that reconfigures side chains of amino acids aligning the active site for optimal interactions in a closed active site that is less polar covering most of the bound product to allow tight interactions. This could potentially affect the enzyme's function as supported by the observation of BSP having a higher affinity for Sh28GST than Sbh26GST in enzyme activity studies mentioned earlier. This also supports the different mechanisms of binding observed in Sbh26GST and Sh28GST since the enzymes experience ligand-induced fitting.

Chapter 5
Thermodynamics of BSP-Sbh26GST/Sh28GST interaction

5.1. Introduction

Thermodynamic parameters of the interaction between BSP binding towards Sbh26GST and Sh28GST in the presence and absence of GSH were monitored to determine drivers of these chemical reactions as a function of temperature effects on the structures and how they will affect the equilibrium properties of the molecule's population. Isothermal titration calorimetry (ITC) takes advantage of the universal heat transfer when molecules bind whereby heat is either absorbed or released thus giving insights into binding equilibriums (Pierce *et al.*, 1999). The ITC machine setup has two cells called the reference cell and the sample cell in an adiabatic jacket with no heat transfer with the surroundings. Their temperature differences are constantly monitored to be uniform with every injection of ligand to protein in the sample cell via internal power compensation by the Peltier cooler/heater controlled by the reference cell. The observed peaks of heat compensations are associated with binding energies. The areas underneath the peaks are then integrated to produce isotherms of the Wiseman plot that can be used to directly determine thermodynamic parameters (Wiseman *et al.*, 1989). This includes affinities (associate constant (K_a) and dissociation constant), enthalpy (ΔH) and stoichiometry (n). Whereas entropy (ΔS) and Gibbs free energy (ΔG) can be calculated using the equations below:

$$\Delta G = -RTlnKa \; or \; -RT\ln(1/Kd) = \Delta H - T\Delta S \tag{5.1}$$

Where ΔG represent the change in Gibbs free energy (kJ/mol), R is the gas constant (8.3145 J/mol/K), T is the absolute temperature (K), and K_a is the binding affinity (association) constant (M^{-1}) which is the inverse of the dissociation constant K_d (M). Furthermore, ΔH represents the change in enthalpy (kJ/mol), the heat released or absorbed during a reaction under constant pressure and ΔS represents a change in entropy (kJ/mol. K). All the information on ITC set-up and thermodynamic parameters is illustrated in Figure 5.1.

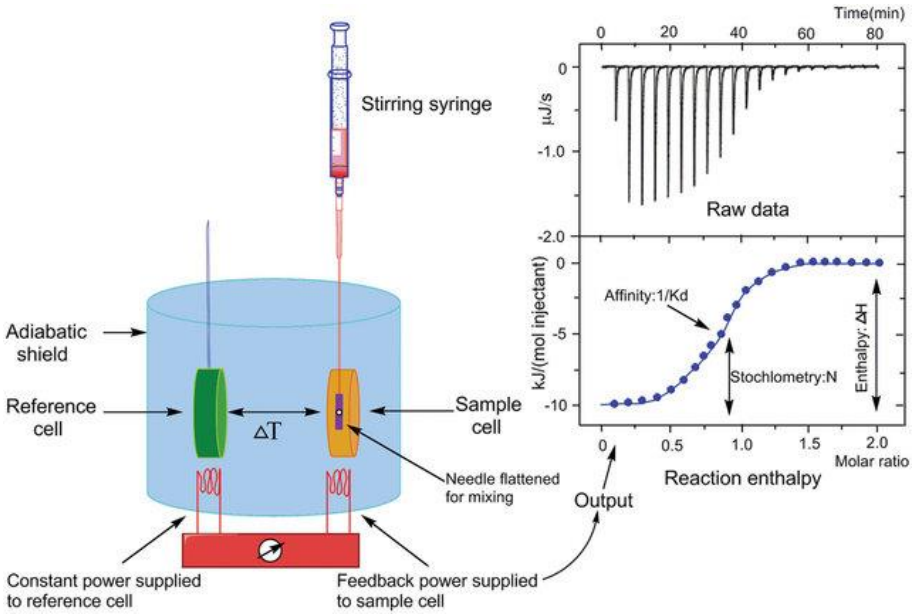

Figure 5.1. Schematic diagram of ITC concept. An ITC machine set-up of an adiabatic jacket with an injection that titrates a molecule to the substance in a sample cell, controlled by the reference cell that takes note of temperature changes and corrects it with internal power provided by the system. The output is a thermogram showing heat peaks generated as the two molecules (e.g., protein and ligand) interact until they reach saturation. doi: 10.3389/fmicb.2015.01049

5.2. Materials

All reagents used were purchased from Sigma-Aldrich: Tris-HCl, EDTA, TCEP, NaN_3, GSH, DMSO and BSP.

5.3. Methods

Thermodynamic parameters of Sbh26GST and Sh28GST were studied via the Nano ITC standard volume instrument (TA® Instruments, New Castle, DE, USA). Sbh26GST and Sh28GST were individually dialysed into two batches of 50 mM Tris-HCl, pH 7.2, 2 mM EDTA, 0.02% (w/v) NaN_3 and 1 mM TCEP in the presence and absence of 1 mM GSH overnight at 4°C. The respective buffers were used to prepare 2 mL of 50 µM Sbh26GST and Sh28GST as well as 1.0 mM of the ligand, BSP with 1% (v/v) of dimethyl sulfoxide (DMSO) (from a stock of 500 mM BSP in 100% (v/v) DMSO) to help with solubility. Furthermore, an equivalent amount of DMSO was added to the protein samples to prevent any buffer mismatches or organic solvent damage. The ITC machine was appropriately cleaned, and samples were filtered and degassed at a vacuum of 635 mmHg for ~20 min before conducting the experiments. The reference cell was filled with deionised water, the sample cell was loaded with respective protein and the syringe was filled with 250 µL of 1 mM BSP. The machine was set to equilibrate and automatically titrated 5 µL of the ligand into 1.5 mL of protein in

the sample cell except for the initial 2 µL to initiate the reaction. This occurred at 25°C (298.15 K) and a 310-rpm stirring rate with 300s between 30 incremental injections. The data were analysed with the NanoAnalyze ™ software (TA® Instruments, New Castle, DE, USA). Whereby the integrated heats per injection were corrected for heats of dilution and the independent binding model was fitted to the data. In addition, due to several binding sites in GSTs, multiple binding sites were used for comparison.

5.4. Results

ITC was used to study the thermodynamics of the interaction between BSP and proteins, Sbh26GST and Sh28GST, respectively in the presence and absence of GSH under controlled conditions. The obtained binding thermograms and fitted isotherms, as depicted in Figure 5.2, show curves that are not the popular, clear sigmoidal shape. The reaction of BSP into Sbh26GT is exothermic ($\Delta H<0$), spontaneous ($\Delta G<0$), entropically favoured ($\Delta S>0$) with a stoichiometry (n) of one and dissociation of 35 nM for moderately tight binding as shown in table 5.1 of thermodynamic parameters. On the other, the reaction of BSP into Sh28GST is exothermic, spontaneous, and enthalpically favoured but entropically unfavoured with a K_d of 9.9 µM for tight binding and stoichiometry of one. The shape of the isotherm curve speaks more to the type of binding taking place, and the drivers are different in Sbh26GST and Sh28GST. Furthermore, the introduction of GSH in both systems resulted in a decreased $K_{d,}$ thus higher affinity for BSP as also supported by plots in (Appendix, Figure S8. Conversely, the reaction drivers responded differently despite a slight variation of ΔG throughout different conditions. The entropy of Sbh26GST-BSP increased further in the favourable direction, whereas the entropy opposition of Sh28GST-BSP was decreased but still not favourable overall. Nonetheless, the heat released by the systems was decreased. The multiple binding site model showed one site is favoured over the other while maintaining the latter trends (Appendix, Table S4).

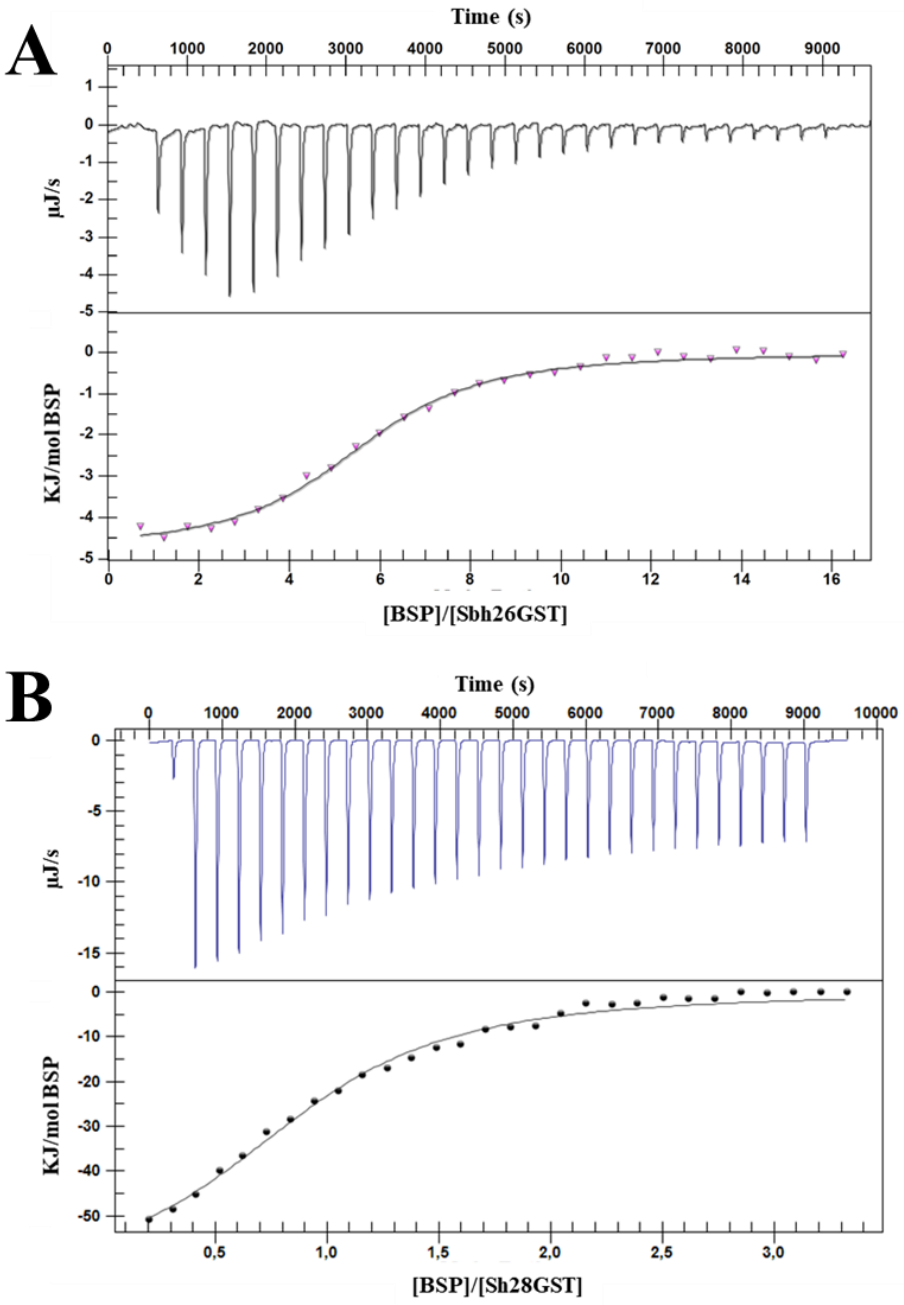

Figure 5.2. ITC titration of BSP into Sbh26GST and Sh28GST.**A**. Thermogram and isotherm respectively showing the interaction between 1 mM BSP and 50 µM Sbh26GST while **B**. shows the binding of 1 mM BSP to 50 µM Sh28GST. The experiments were performed at 25˚C (298.15 K) in 50 mM Tris-HCl, 2 mM EDTA and 1 mM TCEP at pH 7.2 at a 310 rpm stirring rate with 300s in-between 30 injections. The baselines were corrected for heats of dilutions. The integration points were fitted with the independent model on the Nano Analyzer software.

Table 5. 1 Thermodynamic parameters of the interaction between BSP and protein, Sbh26GST and Sh28GST in the presence and absence of GSH (co-substrate), respectively.

Thermodynamic parameters	Sbh26GST		Sh28GST	
Independent model	**No GSH**	**With GSH**	**No GSH**	**With GSH**
K_d (μM)	0.0351 ± 0.01	17.1 ± 0.03	99.9 ± 1.14	5.25 ± 1.2
ΔH (kJ/mol)	-23.4 ± 0.28	-7.63 ± 0.41	-65.6 ± 0.23	-32.6 ± 0.3
ΔS (J/mol·K)	26.1	65.6	-124	-2.43
ΔG (kJ/mol)	-31.1	-27.2	-28.5	-30.1
n/dimer	1.13 ± 0.02	1.01 ±0.02	0.902 ± 0.13	1.38 ± 0.9

* The readings are captured as value ± SD at 95% confidence level. The residual plot deviations around fit for Sbh26GST were 3.2 and 4.6 in the presence and absence of 1 mM GSH respectively then for Sh28GST it was 2.7 and 4.8

5.5. Discussion

BSP interact differently between Sbh26GST and Sh28GST which speaks to the different roles they play in schistosomes, hence the need for both. Binding specificity is driven by hydrogen bond donors and acceptors, electrostatic interactions as well as dipole contacts. All towards favourable interaction of BSP with head groups available for binding in studied enzymes, then the individual entities interacting with the solvent or set orientations within an entity (e.g., forces between atoms within the protein chain). One molecule of BSP binding to the proteins correlates to the one available site at the dimer interface, which is open and solvent-exposed (Reinemer *et al.*, 1991; Dirr et al., 1994). Moreover, BSP binds Sbh26GST with a higher affinity than Sh28GST in the absence of GSH. But, when GSH was introduced to the system, Sh28GST slightly binds BSP more tightly than Sbh26GST, whereby the 10^{th} unit differences seen in IC_{50} values are also reflected in K_d values, which are all in the micromolar range. The multiple-site model also showed that one site is preferred over the other, while the hydrophobic binding site in each monomer is not preferred. This observation is supported by other studies that showed non-substates such as PZQ binds at the dimer interface of Sj26GST (McTigue *et al*., 1995), a conjugate of GSH in a class Sigma GST (Ji *et al.*, 1996) and EA in Sj26GST (Akumadu *et al*., 2020) as observed in their crystal structures.

Enthalpic contributions are dominated by an entity's hydrophilicity through optimal hydrogen bonds donors-acceptor geometry, and distance which favours Van der Waals interactions bond formation or breaking. In contrast, entropic contributions have to do with the number of states or accessible conformational changes of the protein and the ligand as they interact, all towards stable low energies (Connelly *et al*., 1994). The solvent-bound water is released into the bulk solvent which destroys the ordered water molecules (solvation shell) around each entity, thus exposing hydrophobic groups of Sbh26GST and Sh28GST to form

non-covalent interactions with the hydrophobic BSP that has bulky aromatic benzene and furanone ring. However, the binding decreases the conformation and rotational freedom of the highly dynamic protein when the hydrogen bonding network of the carbonyl backbone is rearranged due to the presence of BSP which also comes with steric hindrances caused by the bulky rings. The difference in energy between the two determines the feasibility of the reaction. In Sh28GST-BSP, the binding of BSP results in an organised system (decrease in microstates) because of bond formation thus an enthalpic driver is observed and that makes the reaction exergonic be it in the presence or absence of GSH. On the other hand, Sbh26GST-BSP has a chaotic and disorderly state that is less exothermic in the presence of GSH. Critical contacts that could contribute to hydrogen bonding in the active sites include Asp and Glu in the L-site and Tyr, Ser and Arg in the H-site as seen by inhibiting moles such as EA in Sj26GST (Akumadu *et al*., 2020), but it all comes to the structure, size and nature of the ligand at hand (Yassin *et al*., 2004). The entropy opposition in Sh28GST could be accounted for by hydrophobic interactions of Trp and Phe residues in the active site that are not large enough to be favoured as they are at work stabilising BSP binding. On the other hand, in Sbh26GST the entropy is favoured since some of the water molecules are not fully liberated from BSP

Lastly, the free energies of the interaction of BSP with Sbh26GST and Sh28GST have respectively shown not to require an input of energy for the reactions to proceed, the products are favoured at equilibrium. In all cases, the enthalpy and entropy compensations maintain the free energy, and it is comparable to other studies of Sj26GST (Yassin *et al*., 2004; Akumadu *et al*., 2020; Pooe *et al*., 2021). In addition, the structural variations are also highlighted by energy differences in response to the ligands. Sh28GST has a better therapeutic response than SBh26GST. Likewise, it has been shown that the obtained kJ/mol has a limited antioxidant capacity compared to its counterpart in the human host (Huang *et al.*, 2012).

Above all, the studied energies only generalised the type of interactions taking place between BSP and Sbh26GST/Sh28GST under set conditions. Further analysis into enthalpic and entropic contributions can accurately be determined upon known positions of various residues and water molecules via crystal or molecular modelling. The knowledge would aid in designing a drug with increased affinity to the binding sites due to water molecule adaptations (Ladbury, 1996).

It is also essential to consider the *c*-value which gives insights into the reliability of binding isotherms obtained from ITC data, thus ensuring thermodynamic parameters (Wiseman et al., 1989).

$$c = n \times Ka \times [M]$$

(5.2)

Where n is the stoichiometry, K_a is the binding affinity association constant (M^{-1}), and [M] is the total concentration of the molecules in the sample cell e.g., protein (M). Thermodynamic parameters had a c-value of 3.22 and 5.61 for Sbh26GST and Sh28GST respectively, but in the presence of GSH, it was 2.70 and 8.78. Therefore, the readings are dependable as they fall within the recommended range of 1-1000.

Chapter 6
Stability of GSTs from *S. haematobium/bovis*

6.1. Introduction

The study was based on pseudo-Sbh26GST, which was crucial to observe its conformational stability based on its construction. Protein stability describes the balance of forces as the protein spontaneously folds in a cooperative manner. It requires enough intermolecular interactions (hydrogen bonding, Van der Waals interactions, hydrophobic packing, and disulfide bonds) to overcome the single activation free energy barrier between the native folded state and inactive unfolded state that is dominated by entropic interactions (Vajda *et al.*, 1994; Breiten *et al.*, 2013). It is also important to note the interactions of the solvent with the protein as it creates a solvation shell that affects the interaction forces at play. The technique used to probe protein stability was fluorescence-based thermal shift assay (TSA), an all-purpose method for identifying inhibitors from compound libraries due to its advantageous character of measuring a small number of multiple proteins simultaneously. TSA measures thermal denaturation, hence determining the melting temperature (T_m), the temperature at which 50% of the protein has denatured. It is at the inflexion point of the unfolding curve. The T_m is directly proportional to the thermal stability of proteins. Over time, the increase in temperature results in the unfolding of the protein, thus exposing hydrophobic regions that become accessible to the environment-sensitive, bulky SYPRO® Orange fluorescent dye that yields a higher quantum when bound. Moreover, as the protein loses its structure and then precipitates and aggregates due to an intolerable high temperature, the dye dissociates. This results in decreased fluorescence of the dye which can also be accounted for by the natural decrease in quantum yield due to high temperature.

6.2. Materials

The equipment used for TSA was purchased as a kit from Bio-Rad, which included the SYPRO® Orange dye, Microseal 'B' PCR plate Sealing Film, 96-well plates, and mixing trays. Buffer components (PBS: NaCl. KCl, Na_2HPO_4 and KH_2PO_4), GSH, EDTA, and DTT were bought from Sigma-Aldrich as well as ligands used, PZQ and BSP. The supplier of the 10 kDa molecular weight cut-off dialysis tubing was Thermo Scientific (South Africa).

6.3. Methods

Stability studies of Sbh26GST by TSA were performed in the presence and absence of natural co-substrate, GSH and ligands PZQ and BSP, respectively using the CFX96

Touch-Real-Time PCR detection system. Stock 50 µM of Sbh26GST was dialysed overnight at 4 °C against PBS buffer, pH 7.2 supplemented with 1.0 mM DTT and 1.0 mM EDTA. The various buffers used in the study for respective conditions included PBS, pH 7.2 with and without 0.5 mM GSH and IC_{50} value of PZQ or BSP (25 µM) for Sbh26GST as outlined in the visual representation of the 96-well plate (Figure 6.1). All the wells were filled with a final reaction volume of 25 µL, which contained 10 µL of buffer, 10 µL of protein (20 µM) and 5 µL of 10X SYPRO® Orange dye (3X). The plate was then covered with Microseal 'B' PCR Plate Sealing Film to minimise evaporation. The reaction components were mixed thoroughly through a brief (30 sec) centrifugation before running in a Real-Time PCR Detection System. The effects of potential inhibitors on the stability of the proteins were further studied by varying the concentration of PZQ and BSP in the presence and absence of 0.5 mM GSH in PBS, pH 7.2.

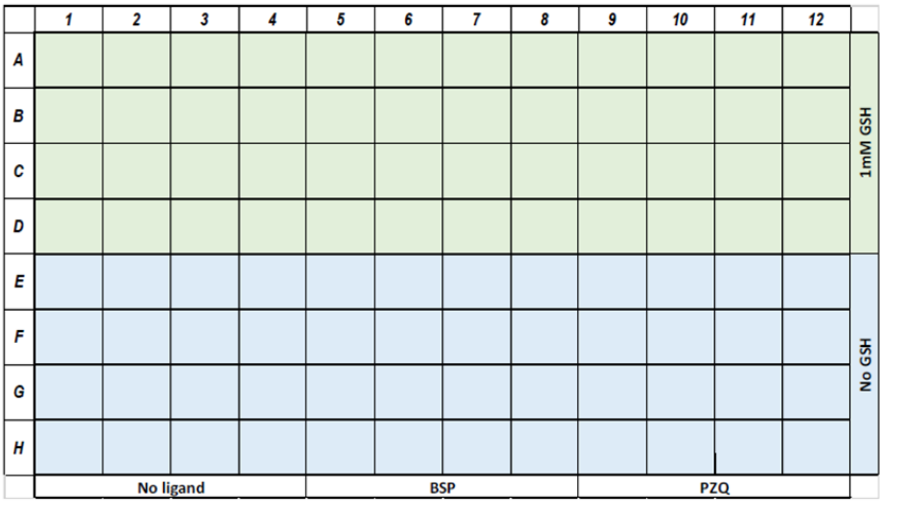

Figure 6.1 Visual representation of thermal shift assay layout in the 96-well PCR microplate on the effect of PZQ and BSP on the stability of the pseudo-Sbh26GST.

The PCR machine was set up to heat the samples at increments of 0.5 °C for 10 sec starting at 10 °C to 95 °C upon excitation at 470 nm and emission at 570 nm. The melting curves of the relative fluorescence unit (RFU) and its derivative concerning temperature (°C), -d(RFU)/dT were viewed on the CFX Maestro software. Sample replicates were averaged and corrected with buffer blanks. Thereafter, T_m was obtained from the lowest point of the derivative plot. Furthermore, the final plots were represented as a fraction of unfolded protein accessible to the dye over folded protein against temperature.

6.4. Results

The binding of SYPRO® Orange to proteins is such that as the temperature increases, the protein unfolds, thereby allowing the dye to access more hydrophobic pockets, consequently increasing its fluorescence. Specifics as captured in the sigmoidal curve; Figure 6.2 exhibited that Apo Sbh26GST follows cooperative unfolding as shown by the asymmetric single transition point with a T_m of 56.5 ± 0.35 °C. This was comparable with other GSTs of similar structure such as the highly reproducible T_m of Sj26GST at 53.0 ± 0.02 °C (Lo *et al.*, 2004; Quesada-Soriano *et al.*, 2006). In addition, the presence of GSH increased the stability of Apo Sbh26GST to T_m 57.5 ±0.46 °C correlating with a similar study that showed a 4 °C thermal shift of Sj26GST in the presence of 2 mM GSH (Lo *et al*., 2004). The introduction of BSP slightly increased the T_m in the presence and absence of GSH whereas PZQ had no significant effect as depicted in Figure 6.2. Furthermore, when BSP concentration was varied, it resulted in a higher initial unfolding transition at high concentrations with parallel inflexion points (Appendix, Figure S9).

6.5. Discussion

All equilibrium unfolding experiments were performed with 50 µM Sbh26GST at varying temperatures in PBS buffer, pH 7.2 supplemented with 1.0 mM EDTA and DTT using SYPRO Orange dye as a probe for hydrophobicity. The studied conditions were in the presence and absence of ligands; co-substrate GSH, BSP and PZQ. The denaturation in TSA is not reversible and thus cannot be defined as thermodynamic properties. Nonetheless, T_m was measured and all the transition curves for Sbh26GST had a characteristic single sigmoidal transition supporting the absence of thermodynamically stable intermediates. Therefore, the plots illustrated a two-state model of significant concentration of folded and unfolded conformation states of proteins at equilibrium. The findings showed that Sbh26GST had the greatest stability in the presence of GSH and BSP, whereby GSH enhance BSP effects of increased enzyme stability. On the other hand, PZQ has a negligible effect. Thermal shift assay results of Sh28GST were not persuaded further as they did not show a clear melt transition (data not shown).

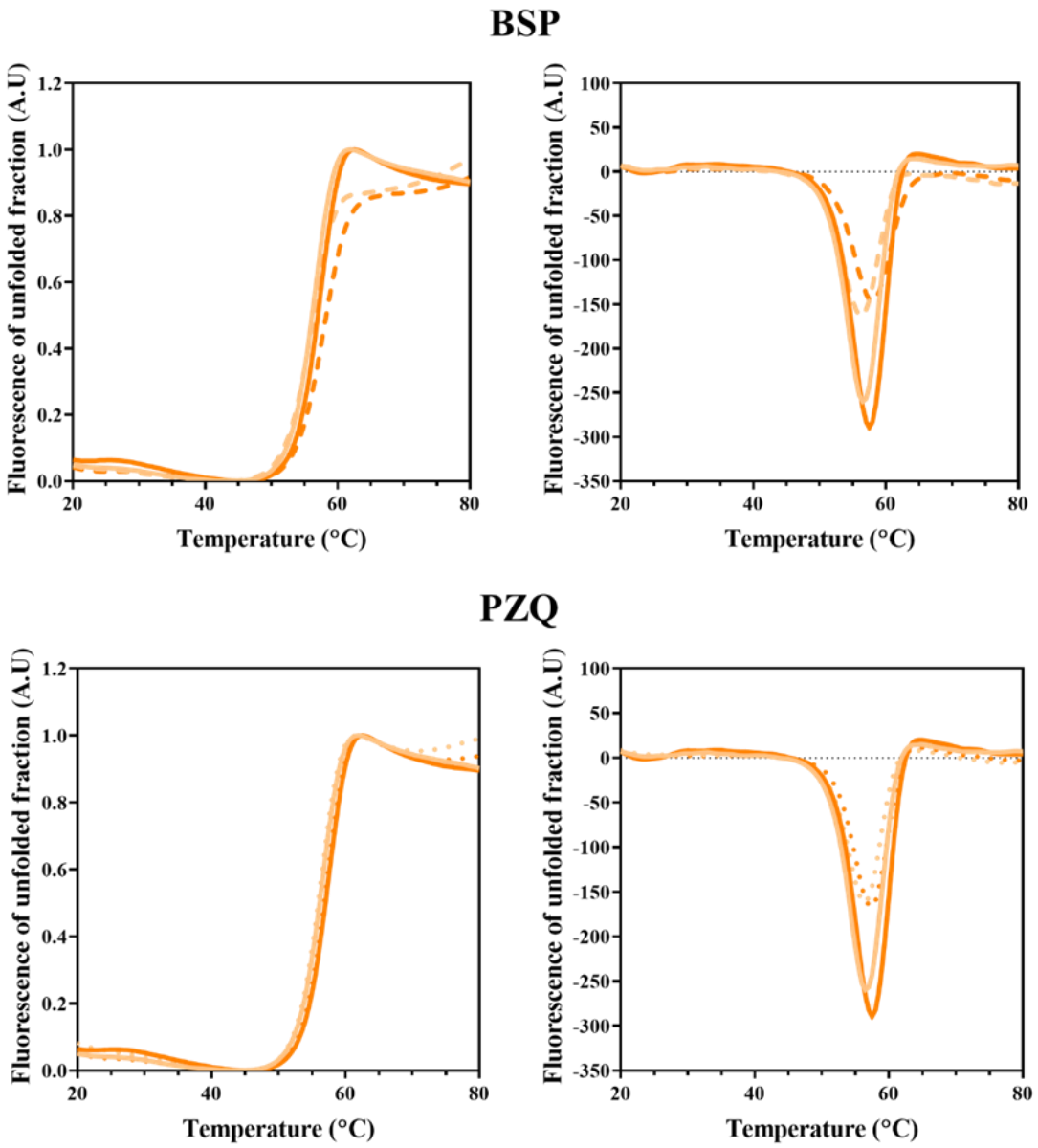

Figure 6.2. Thermographs of Sbh26GST. The stability of Apo Sbh26GST in the presence (bold orange solid lines) and absence (faded orange solid lines) of co-substrate, 0.5 mM GSH and 25 mM of non-substrate BSP (dashed lines) and PZQ (dotted lines) were monitored with SYPRO Orange dye in PBS buffer, pH 7.2 supplemented with 1 mM DTT and 1 mM EDTA. The thermal unfolding plots show that as the temperature increases, the protein transition from folded to unfolded as shown by the sigmoidal curve thus enabling the dye to bind hydrophobic pockets and increase the quantum yield of the dye at emission maxima of 570 nm. The rightward shift of unfolding transition and melting peaks when ligands bind indicate increased stability.

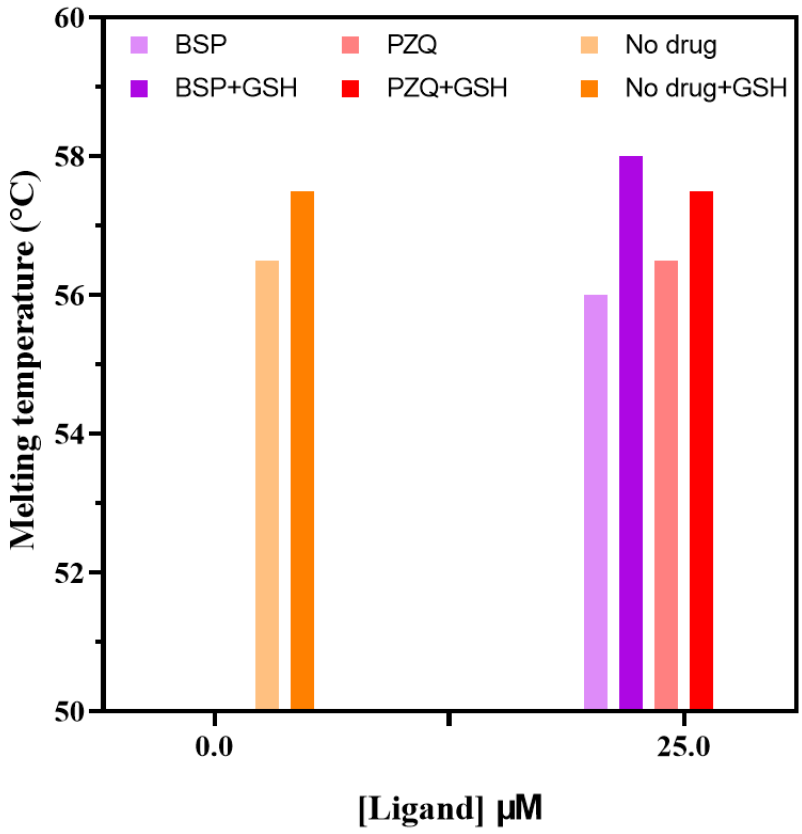

Figure 6.3. Melting temperatures for Sbh26GST in varying ligands. The melting temperature of Apo-Sbh26GST (faded orange) slightly increased in the presence of GSH (bold orange). The introduction of ligands such as PZQ has an insignificant effect on the melting temperature in the absence (faded red) and presence (bold red) of GSH whereas BSP (faded purple) increases it in the presence of GSH (bold purple).

Stability thermal shift is affected by several factors which include the concentration of the ligands, binding affinity, enthalpy, and heat capacity (Matulis *et al.*, 2005; Vedadi *et al.*, 2006). Observations in this study support ligand binding being the driver as it disrupts the interactions of amino acids (bonds, orientation, and exposure to solvent) (Pantoliano *et al.*, 2001). The binding of most inhibitors to enzymes tends to stabilise the protein as it forms high-affinity bonds with internal residues rather than weak external interactions with the solvent, which was also seen in our case of the Sbh26GST-BSP interaction. Furthermore, these results are supported by postulations from its strong interaction with pseudo-Sbh26GST from enzyme inhibition studies, thermodynamic parameters, and fluorescence studies. The coupling of protein unfolding to ligand binding is usually associated with increased Gibbs free energy that results in the observed increased $T_{m.}$

The interaction of Sbh26GST-BSP was further enhanced in the presence of GSH where slightly increased stabilisation was observed, accompanied by a slight rightward shift in the unfolding curve. No published data were available to compare our results, but the determined T_m was within ranges of homologous organisms, SjGST and the overall 60 °C for most. Moreover, the T_m derived from TSA is comparable with other techniques, Sj26GST was determined to have T_m of 51 °C with residual enzyme activity after heating (Kaplan *et al*., 1997) and 55.15 - 58.96 °C at pH 7.5 with differential scanning calorimetry (Quesada-Soriano *et al*., 2006).

The BSP concentration-dependent study of Sbh26GST-BSP stability in the absence and presence of GSH proved to have a directly proportion and inversely proportion relationship, respectively. An inference made is that BSP could potentially be supported to be modified as a drug candidate as it disturbs conformational dynamics that affect enzyme functionality which was shown by rigidifying stable interactions made with available binding sites in Sbh26GST. The knowledge can also be used to help with refinements of increasing the likelihood of protein crystallisation which has been reported to be crucial insights for specific ligand binding affinity or stoichiometry (Matulis *et al*., 2005).

Chapter 7
Summary, conclusion, and possible future directions

Schistosomiasis is a parasitic NTD caused by blood flukes, affecting over 230 million people worldwide (prevalent in sub-Saharan Africa), with chronic morbidities that negatively impact the socio-economic states of affected regions. Moreover, available treatment for schistosomiasis (PZQ) is under pressure due to the mass administration of the drug for over 10 decades, thus calling for new therapeutic approaches.

In schistosomes, GSTs are critical for their survival as they are mainly responsible for detoxification processes, without the support of alternative phase I enzymes such as cytochrome P-450. Therefore, GSTs tend to be overexpressed during drug treatment to combat metabolic interference and account for the observed drug resistance. Hence, *Schistosoma* GSTs are labelled as good targets for a new generation of anthelmintics plus they have considerable structural variation compared to human GSTs which lays a developmental backbone for the study. However, out of the three species that mainly infect humans, 26 kDa isoform and not 28 kDa of *S. haematobium* GST is the only one with an incomplete ORF which previously hindered research and underappreciated the impact of urogenital schistosomiasis. Furthermore, its ability to form heterosis hybrids with animal schistosomes (*S. bovis*), added to the burdening threat of drug resistance and formed the basis of this study. The study aimed to characterize the structural and functional relations of Sbh26GST and Sh28GST in response to potential inhibitors, namely PZQ, ART and BSP. All in light of insights into a possible drug therapy for the alleviation of schistosomiasis burden.

The first breakthrough was completing the sequence of Sh26GST through homologous species using several sequence analyses tools. A consensus sequence of the initial twelve amino acids was added to the native sequence of Sh26GST which has 100% similarity to Sb26GST, hence the name Sbh26GST. The successful overexpression of Sbh26GST and Sh28GST using *E. coli* machinery under optimized conditions in the soluble fraction was easily purified with affinity chromatography to homogeneity and laid the foundation for downstream applications. Structural characterisations have shown that both proteins are predominantly α-helical with stability T_m of 56.5 °C for Sbh26GST. Trp residues in the active sites of both proteins are not readily exposed to the solvent in accordance with reported literature. Moreover, PZQ binding has insignificant disturbance to the Trp environment, whereas ART

and BSP disrupt it, irrespective of the presence or absence of natural co-substrate GSH and its analogue GTX. Functional characterisation using GSH-CDNB conjugation, ANS binding, and ITC have shown BSP tightly binds Sbh26GST and Sbh26GST, resulting in inhibition of the enzymes' activity whereas PZQ has negligible impact and ART slight increases it. The mode of action is non-competitive at the dimer interface with more detrimental effects on Sh28GST, especially in the presence of GSH where the has a higher affinity for BSP and increased stability that negatively affect protein functionality due to decreased dynamics. In addition, BSP is a stronger binder of Sbh26GST and Sh28GST than ANS, thus outcompeting it. Energies around the interaction of BSP with Sbh26GST and Sh28GST are both spontaneous and enthalpically favoured. On the contrary, the interaction is entropically favoured in Sbh26GST but not in Sh28GST. The one molecule binding Sh28GST becomes constrained due to more contacts than in Sbh26GST being made and overall unfavored compactness of the protein, but the energy released drives the interaction.

The observed variation in the two enzymes from the explored techniques that give insights about a specific activity, ligand interactions, structural conformations, and stability elaborated that one enzyme isoform is better at catalyzing some reactions than the other. Hence, the need for both isoforms in schistosomes. Overall, this study introduces BSP as a newly rationalized inhibitor with therapeutic potential or guide for the treatment of schistosomiasis thus lessening the time and money that would be required in search of a new cure (drug repurposing). Alternatively, the knowledge about the enzymes could be used for novel applications or molecular basis for further evaluation.

The limitation of the study includes, (I) inferences made were based on a pseudo model and not 100% true reflection of the native enzyme. (Board *et al*.) The activity of the enzyme was measured based on GSH-CDNB conjugation, but CDNB is not a natural substrate of the enzyme thus no saturation. Therefore, the kinetics were not explored for the H-site. The compensation was ANS binding but it is not exclusive to the H-site (III) Some ligands were difficult to solubilize at high concentrations hence resorting to an organic solvent, DMSO at a non-detrimental concentration to protein but that came with a cost of CD studies of ligands effects on secondary structure elements. (IV) Buffer differences were due to different purification procedures. Despite all of that, the study still supports that BSP binds and inhibits *Schistosoma* GSTs at the dimer interface. Future studies would be understanding what makes the dimer interface unique from the common three-dimensional fold of GSTs. Does it have to do with the respective residues type, position and orientation or evolution towards stabilizing this region? This could be unpacked through structural studies with molecular

modelling and X-ray crystallography to know critical contacts and see how the enzymes would respond to the ligands if they were manipulated.

References

Abraham, D., Kaliappan, S.P., Walson, J.L., Rao Ajjampur, S.S., (2018). Intervention strategies to reduce the burden of soil-transmitted helminths in India. *The Indian journal of medical research* 147, 533-544.

Agnew, A.M., Murare, H.M., Lucas, S.B., Doenhoff, M.J., (1989). Schistosoma bovis as an immunological analogue of S. haematobium. *Parasite immunology* 11, 329-340.

Akumadu, B.O., Pandian, R., Olfsen, J., Worth, R., Thulo, M., Mentor, T., . . . Achilonu, I., (2020). Molecular basis of inhibition of Schistosoma japonicum glutathione transferase by ellagic acid: Insights into biophysical and structural studies. *Molecular and biochemical parasitology* 240, 111319.

Alger, H.M., Williams, D.L., (2002). The disulfide redox system of Schistosoma mansoni and the importance of a multifunctional enzyme, thioredoxin glutathione reductase. *Molecular and biochemical parasitology* 121, 129-139.

Anisuzzaman, Tsuji, N., (2020). Schistosomiasis and hookworm infection in humans: Disease burden, pathobiology and anthelmintic vaccines. *Parasitology international* 75, 102051.

Arnau, J., Lauritzen, C., Petersen, G.E., Pedersen, J., (2006). Current strategies for the use of affinity tags and tag removal for the purification of recombinant proteins. *Protein expression and purification* 48, 1-13.

Arthur, J.R., (2000). The glutathione peroxidases. *Cellular and molecular life sciences: CMLS* 57, 1825-1835.

Atkinson, H.J., Babbitt, P.C., (2009). Glutathione transferases are structural and functional outliers in the thioredoxin fold. *Biochemistry* 48, 11108-11116.

Baiocco, P., Gourlay, L.J., Angelucci, F., Fontaine, J., Hervé, M., Miele, A.E., . . . Bellelli, A., (2006). Probing the mechanism of GSH activation in Schistosoma haematobium glutathione-S-transferase by site-directed mutagenesis and X-ray crystallography. *Journal of molecular biology* 360, 678-689.

Bico, P., Erhardt, J., Kaplan, W., Dirr, H., (1995). Porcine class pi glutathione S-transferase: anionic ligand binding and conformational analysis. *Biochimica et biophysica acta* 1247, 225-230.

Board, P.G., (2011). The omega-class glutathione transferases: structure, function, and genetics. *Drug metabolism reviews* 43, 226-235.

Board, P.G., Baker, R.T., Chelvanayagam, G., Jermiin, L.S., (1997). Zeta, a novel class of glutathione transferases in a range of species from plants to humans. *The Biochemical journal* 328 (Pt 3), 929-935.

Boyland, E., Chasseaud, L.F., (1969). The role of glutathione and glutathione S-transferases in mercapturic acid biosynthesis. *Advances in enzymology and related areas of molecular biology* 32, 173-219.

Brahms, S., Brahms, J., (1980). Determination of protein secondary structure in solution by vacuum ultraviolet circular dichroism. *Journal of molecular biology* 138, 149-178.

Breiten, B., Lockett, M.R., Sherman, W., Fujita, S., Al-Sayah, M., Lange, H., . . . Whitesides, G.M., (2013). Water networks contribute to enthalpy/entropy compensation in protein-ligand binding. *Journal of the American Chemical Society* 135, 15579-15584.

Buetler, T.M., Eaton, D.L., (1992). Glutathione S-transferases: Amino acid sequence comparison, classification and phylogenetic relationship. *Journal of Environmental Science & Health Part C* 10, 181-203.

Burke, M.L., Jones, M.K., Gobert, G.N., Li, Y.S., Ellis, M.K., McManus, D.P., (2009). Immunopathogenesis of human schistosomiasis. *Parasite immunology* 31, 163-176.

Caffrey, C.R., (2007). Chemotherapy of schistosomiasis: present and future. *Current opinion in chemical biology* 11, 433-439.

Cardoso, R.M., Daniels, D.S., Bruns, C.M., Tainer, J.A., (2003). Characterization of the electrophile binding site and substrate binding mode of the 26-kDa glutathione S-transferase from Schistosoma japonicum. *Proteins* 51, 137-146.

Chitsulo, L., Engels, D., Montresor, A., Savioli, L., (2000). The global status of schistosomiasis and its control. *Acta tropica* 77, 41-51.

Cioli, D., Pica-Mattoccia, L., Basso, A., Guidi, A., (2014). Schistosomiasis control: praziquantel forever? *Molecular and biochemical parasitology* 195, 23-29.

Colley, D.G., Bustinduy, A.L., Secor, W.E., King, C.H., (2014). Human schistosomiasis. *Lancet (London, England)* 383, 2253-2264.

Connelly, P.R., Aldape, R.A., Bruzzese, F.J., Chambers, S.P., Fitzgibbon, M.J., Fleming, M.A., . . . et al., (1994). Enthalpy of hydrogen bond formation in a protein-ligand binding reaction. *Proceedings of the National Academy of Sciences of the United States of America* 91, 1964-1968.

De Bont, J., Vercruysse, J., (1997). The epidemiology and control of cattle schistosomiasis. *Parasitology today (Personal ed.)* 13, 255-262.

Dirr, H., Reinemer, P., Huber, R., (1994). X-ray crystal structures of cytosolic glutathione S-transferases. Implications for protein architecture, substrate recognition and catalytic function. *European journal of biochemistry* 220, 645-661.

Dirr, H.W., Little, T., Kuhnert, D.C., Sayed, Y., (2005). A conserved N-capping motif contributes significantly to the stabilization and dynamics of the C-terminal region of class Alpha glutathione S-transferases. *The Journal of biological chemistry* 280, 19480-19487.

Djuikwo-Teukeng, F.F., Kouam Simo, A., Allienne, J.F., Rey, O., Njayou Ngapagna, A., Tchuem-Tchuente, L.A., Boissier, J., (2019). Population genetic structure of Schistosoma bovis in Cameroon. *Parasites & vectors* 12, 56.

Doenhoff, M.J., Cioli, D., Utzinger, J., (2008). Praziquantel: mechanisms of action, resistance and new derivatives for schistosomiasis. *Current opinion in infectious diseases* 21, 659-667.

Downs, J.A., van Dam, G.J., Changalucha, J.M., Corstjens, P.L., Peck, R.N., de Dood, C.J., . . . Fitzgerald, D.W., (2012). Association of Schistosomiasis and HIV infection in Tanzania. *The American journal of tropical medicine and hygiene* 87, 868-873.

Duong-Ly, K.C., Gabelli, S.B., (2015). Affinity Purification of a Recombinant Protein Expressed as a Fusion with the Maltose-Binding Protein (MBP) Tag. *Methods in enzymology* 559, 17-26.

Fabrini, R., Bocedi, A., Pallottini, V., Canuti, L., De Canio, M., Urbani, A., . . . Ricci, G., (2010). Nuclear shield: a multi-enzyme task-force for nucleus protection. *PloS one* 5, e14125.

Feldmeier, H., Chitsulo, L., (1999). Therapeutic and operational profiles of metrifonate and praziquantel in Schistosoma haematobium infection. *Arzneimittel-Forschung* 49, 557-565.

Fenwick, A., Savioli, L., Engels, D., Robert Bergquist, N., Todd, M.H., (2003). Drugs for the control of parasitic diseases: current status and development in schistosomiasis. *Trends in parasitology* 19, 509-515.

Froger, A., Hall, J.E., (2007). Transformation of plasmid DNA into E. coli using the heat shock method. *Journal of visualized experiments : JoVE*, 253.

Frova, C., (2006). Glutathione transferases in the genomics era: new insights and perspectives. *Biomolecular engineering* 23, 149-169.

Gasteiger, E., Hoogland, C., Gattiker, A., Wilkins, M.R., Appel, R.D., Bairoch, A., (2005). Protein identification and analysis tools on the ExPASy server. *The proteomics protocols handbook*, 571-607.

Gasymov, O.K., Glasgow, B.J., (2007). ANS fluorescence: potential to augment the identification of the external binding sites of proteins. *Biochimica et biophysica acta* 1774, 403-411.

Ghisaidoobe, A.B., Chung, S.J., (2014). Intrinsic tryptophan fluorescence in the detection and analysis of proteins: a focus on Förster resonance energy transfer techniques. *International journal of molecular sciences* 15, 22518-22538.

Greenfield, N.J., (1996). Methods to estimate the conformation of proteins and polypeptides from circular dichroism data. *Analytical biochemistry* 235, 1-10.

Greenfield, N.J., (2006). Using circular dichroism spectra to estimate protein secondary structure. *Nature protocols* 1, 2876-2890.

Habig, W.H., Jakoby, W.B., (1981). Assays for differentiation of glutathione S-transferases. *Methods in enzymology* 77, 398-405.

Hawe, A., Sutter, M., Jiskoot, W., (2008). Extrinsic fluorescent dyes as tools for protein characterization. *Pharmaceutical research* 25, 1487-1499.

Hotez, P.J., Alvarado, M., Basáñez, M.G., Bolliger, I., Bourne, R., Boussinesq, M., . . . Naghavi, M., (2014). The global burden of disease study 2010: interpretation and implications for the neglected tropical diseases. *PLoS neglected tropical diseases* 8, e2865.

Hsu, S.Y., Li Hsu, H.F., Chu, K.Y., Tsai, C.T., Eveland, L.K., (1966). Immunization against Schistosoma haematobium in rhesus monkeys by administration of cercariae of Schistosoma bovis. *Zeitschrift fur Tropenmedizin und Parasitologie* 17, 407-412.

Huang, H.H., Rigouin, C., Williams, D.L., (2012). The redox biology of schistosome parasites and applications for drug development. *Current pharmaceutical design* 18, 3595-3611.

Huyse, T., Webster, B.L., Geldof, S., Stothard, J.R., Diaw, O.T., Polman, K., Rollinson, D., (2009). Bidirectional introgressive hybridization between a cattle and human schistosome species. *PLoS pathogens* 5, e1000571.

Jafari, M., Mehrnejad, F., Rahimi, F., Asghari, S.M., (2018). The Molecular Basis of the Sodium Dodecyl Sulfate Effect on Human Ubiquitin Structure: A Molecular Dynamics Simulation Study. *Scientific reports* 8, 2150.

Jakobsson, P.J., Thorén, S., Morgenstern, R., Samuelsson, B., (1999). Identification of human prostaglandin E synthase: a microsomal, glutathione-dependent, inducible enzyme, constituting a potential novel drug target. *Proceedings of the National Academy of Sciences of the United States of America* 96, 7220-7225.

Jakoby, W.B., Ziegler, D.M., (1990). The enzymes of detoxication. *The Journal of biological chemistry* 265, 20715-20718.

Ji, X., von Rosenvinge, E.C., Johnson, W.W., Armstrong, R.N., Gilliland, G.L., (1996). Location of a potential transport binding site in a sigma class glutathione transferase by x-ray crystallography. *Proceedings of the National Academy of Sciences of the United States of America* 93, 8208-8213.

Kallestrup, P., Zinyama, R., Gomo, E., Butterworth, A.E., van Dam, G.J., Gerstoft, J., . . . Ullum, H., (2006). Schistosomiasis and HIV in rural Zimbabwe: efficacy of treatment of schistosomiasis in individuals with HIV coinfection. *Clinical infectious diseases : an official publication of the Infectious Diseases Society of America* 42, 1781-1789.

Kaplan, W., Hüsler, P., Klump, H., Erhardt, J., Sluis-Cremer, N., Dirr, H., (1997). Conformational stability of pGEX-expressed Schistosoma japonicum glutathione S-transferase: a detoxification enzyme and fusion-protein affinity tag. *Protein science : a publication of the Protein Society* 6, 399-406.

Kelly, S.M., Jess, T.J., Price, N.C., (2005). How to study proteins by circular dichroism. *Biochimica et biophysica acta* 1751, 119-139.

Kesik-Brodacka, M., Romanik, A., Mikiewicz-Sygula, D., Pluciennicza k, G., Pluciennicza k, A., (2012). A novel system for stable, high-level expression from the T7 promoter. *Microbial cell factories* 11, 109.

King, C.H., Dangerfield-Cha, M., (2008). The unacknowledged impact of chronic schistosomiasis. *Chronic illness* 4, 65-79.

King, C.H., Dickman, K., Tisch, D.J., (2005). Reassessment of the cost of chronic helmintic infection: a meta-analysis of disability-related outcomes in endemic schistosomiasis. *Lancet (London, England)* 365, 1561-1569.

Kinsley, N., Sayed, Y., Mosebi, S., Armstrong, R.N., Dirr, H.W., (2008). Characterization of the binding of 8-anilinonaphthalene sulfonate to rat class Mu GST M1-1. *Biophysical chemistry* 137, 100-104.

Kramer, C.V., Zhang, F., Sinclair, D., Olliaro, P.L., (2014). Drugs for treating urinary schistosomiasis. *The Cochrane database of systematic reviews* 2014, Cd000053.

Krishna, S., Bustamante, L., Haynes, R.K., Staines, H.M., (2008). Artemisinins: their growing importance in medicine. *Trends in pharmacological sciences* 29, 520-527.

Ladbury, J.E., (1996). Just add water! The effect of water on the specificity of protein-ligand binding sites and its potential application to drug design. *Chemistry & biology* 3, 973-980.

Laemmli, U.K., (1970). Cleavage of structural proteins during the assembly of the head of bacteriophage T4. *Nature* 227, 680-685.

Lakowicz, J.R., (1999). Introduction to fluorescence, Principles of fluorescence spectroscopy. Springer, pp. 1-23.

Lakowicz, J.R., (2006). Principles of fluorescence spectroscopy. Springer.

Litwack, G., Ketterer, B., Arias, I.M., (1971). Ligandin: a hepatic protein which binds steroids, bilirubin, carcinogens and a number of exogenous organic anions. *Nature* 234, 466-467.

Lo, M.C., Aulabaugh, A., Jin, G., Cowling, R., Bard, J., Malamas, M., Ellestad, G., (2004). Evaluation of fluorescence-based thermal shift assays for hit identification in drug discovery. *Analytical biochemistry* 332, 153-159.

Lyon, R.P., Hill, J.J., Atkins, W.M., (2003). Novel class of bivalent glutathione S-transferase inhibitors. *Biochemistry* 42, 10418-10428.

Maina, C.V., Riggs, P.D., Grandea, A.G., 3rd, Slatko, B.E., Moran, L.S., Tagliamonte, J.A., . . . Guan, C.D., (1988). An Escherichia coli vector to express and purify foreign proteins by fusion to and separation from maltose-binding protein. *Gene* 74, 365-373.

Mannervik, B., Alin, P., Guthenberg, C., Jensson, H., Tahir, M.K., Warholm, M., Jörnvall, H., (1985). Identification of three classes of cytosolic glutathione transferase common to several mammalian species: correlation between structural data and enzymatic properties. *Proceedings of the National Academy of Sciences of the United States of America* 82, 7202-7206.

Mannervik, B., Danielson, U.H., (1988). Glutathione transferases--structure and catalytic activity. *CRC critical reviews in biochemistry* 23, 283-337.

Matulis, D., Kranz, J.K., Salemme, F.R., Todd, M.J., (2005). Thermodynamic stability of carbonic anhydrase: measurements of binding affinity and stoichiometry using ThermoFluor. *Biochemistry* 44, 5258-5266.

McManus, D.P., Dunne, D.W., Sacko, M., Utzinger, J., Vennervald, B.J., Zhou, X.N., (2018). Schistosomiasis. *Nature reviews. Disease primers* 4, 13.

McTigue, M.A., Williams, D.R., Tainer, J.A., (1995). Crystal structures of a schistosomal drug and vaccine target: glutathione S-transferase from Schistosoma japonica and its complex with the leading antischistosomal drug praziquantel. *Journal of molecular biology* 246, 21-27.

Meshnick, S.R., (2002). Artemisinin: mechanisms of action, resistance and toxicity. *International journal for parasitology* 32, 1655-1660.

Meyer, D.J., Coles, B., Pemble, S.E., Gilmore, K.S., Fraser, G.M., Ketterer, B., (1991). Theta, a new class of glutathione transferases purified from rat and man. *The Biochemical journal* 274 (Pt 2), 409-414.

Milhon, J.L., Thiboldeaux, R.L., Glowac, K., Tracy, J.W., (1997). Schistosoma japonicum GSH S-transferase Sj26 is not the molecular target of praziquantel action. *Experimental parasitology* 87, 268-274.

Mkoji, G.M., Smith, J.M., Prichard, R.K., (1988). Antioxidant systems in Schistosoma mansoni: evidence for their role in protection of the adult worms against oxidant killing. *International journal for parasitology* 18, 667-673.

Moosavi-Movahedi, A.A., (2005). Thermodynamics of protein denaturation by sodium dodecyl sulfate. *Journal of the Iranian Chemical Society* 2, 189-196.

Neubig, R.R., Spedding, M., Kenakin, T., Christopoulos, A., (2003). International Union of Pharmacology Committee on Receptor Nomenclature and Drug Classification. XXXVIII. Update on terms and symbols in quantitative pharmacology. *Pharmacological reviews* 55, 597-606.

Oakley, A.J., Lo Bello, M., Battistoni, A., Ricci, G., Rossjohn, J., Villar, H.O., Parker, M.W., (1997). The structures of human glutathione transferase P1-1 in complex with glutathione and various inhibitors at high resolution. *Journal of molecular biology* 274, 84-100.

Pantoliano, M.W., Petrella, E.C., Kwasnoski, J.D., Lobanov, V.S., Myslik, J., Graf, E., . . . Salemme, F.R., (2001). High-density miniaturized thermal shift assays as a general strategy for drug discovery. *Journal of biomolecular screening* 6, 429-440.

Pemble, S.E., Wardle, A.F., Taylor, J.B., (1996). Glutathione S-transferase class Kappa: characterization by the cloning of rat mitochondrial GST and identification of a human homologue. *The Biochemical journal* 319 (Pt 3), 749-754.

Pierce, M.M., Raman, C.S., Nall, B.T., (1999). Isothermal titration calorimetry of protein-protein interactions. *Methods (San Diego, Calif.)* 19, 213-221.

Plaa, G.L., (2010). Evaluation of hepatotoxicity: Physiological and biochemical measures of hepatic function in animals.

Ploemen, J.H., van Ommen, B., Bogaards, J.J., van Bladeren, P.J., (1993). Ethacrynic acid and its glutathione conjugate as inhibitors of glutathione S-transferases. *Xenobiotica; the fate of foreign compounds in biological systems* 23, 913-923.

Pooe, K., Worth, R., Iwuchukwu, E.A., Dirr, H.W., Achilonu, I., (2021). An empirical and theoretical description of Schistosoma japonicum glutathione transferase inhibition by bromosulfophthalein and indanyloxyacetic acid 94. *Journal of Molecular Structure* 1223, 128892.

Porterfield, J.Z., Zlotnick, A., (2010). A simple and general method for determining the protein and nucleic acid content of viruses by UV absorbance. *Virology* 407, 281-288.

Quesada-Soriano, I., García-Maroto, F., García-Fuentes, L., (2006). Kinetic study on the irreversible thermal denaturation of Schistosoma japonicum glutathione S-transferase. *Biochimica et biophysica acta* 1764, 979-984.

Ramsay, E.E., Dilda, P.J., (2014). Glutathione S-conjugates as prodrugs to target drug-resistant tumors. *Frontiers in pharmacology* 5, 181.

Reinemer, P., Dirr, H.W., Ladenstein, R., Schäffer, J., Gallay, O., Huber, R., (1991). The three-dimensional structure of class pi glutathione S-transferase in complex with glutathione sulfonate at 2.3 A resolution. *The EMBO journal* 10, 1997-2005.

Ressurreição, M., Elbeyioglu, F., Kirk, R.S., Rollinson, D., Emery, A.M., Page, N.M., Walker, A.J., (2016). Molecular characterization of host-parasite cell signalling in Schistosoma mansoni during early development. *Scientific reports* 6, 35614.

Ricciardi, A., Ndao, M., (2015). Still hope for schistosomiasis vaccine. *Human vaccines & immunotherapeutics* 11, 2504-2508.

Rollinson, D., (2009). A wake up call for urinary schistosomiasis: reconciling research effort with public health importance. *Parasitology* 136, 1593-1610.

Rosano, G.L., Ceccarelli, E.A., (2014). Recombinant protein expression in microbial systems. *Frontiers in microbiology* 5, 341.

Ross, A.G., Bartley, P.B., Sleigh, A.C., Olds, G.R., Li, Y., Williams, G.M., McManus, D.P., (2002). Schistosomiasis. *The New England journal of medicine* 346, 1212-1220.

Rufer, A.C., Thiebach, L., Baer, K., Klein, H.W., Hennig, M., (2005). X-ray structure of glutathione S-transferase from Schistosoma japonicum in a new crystal form reveals flexibility of the substrate-binding site. *Acta crystallographica. Section F, Structural biology and crystallization communications* 61, 263-265.

Sangweme, D.T., Midzi, N., Zinyowera-Mutapuri, S., Mduluza, T., Diener-West, M., Kumar, N., (2010). Impact of schistosome infection on Plasmodium falciparum Malariometric indices and immune correlates in school age children in Burma Valley, Zimbabwe. *PLoS neglected tropical diseases* 4, e882.

Schneider, T.D., Stephens, R.M., (1990). Sequence logos: a new way to display consensus sequences. *Nucleic acids research* 18, 6097-6100.

Secor, W.E., (2012). The effects of schistosomiasis on HIV/AIDS infection, progression and transmission. *Current opinion in HIV and AIDS* 7, 254-259.

Sheehan, D., Meade, G., Foley, V.M., Dowd, C.A., (2001). Structure, function and evolution of glutathione transferases: implications for classification of non-mammalian members of an ancient enzyme superfamily. *The Biochemical journal* 360, 1-16.

Sluis-Cremer, N., Wallace, L., Burke, J., Stevens, J., Dirr, H., (1998). Aflatoxin B1 and sulphobromophthalein binding to the dimeric human glutathione S-transferase A1-1: a fluorescence spectroscopic analysis. *European journal of biochemistry* 257, 434-442.

Smith, D.B., Johnson, K.S., (1988). Single-step purification of polypeptides expressed in Escherichia coli as fusions with glutathione S-transferase. *Gene* 67, 31-40.

Stefanidis, L., Scinto, K.V., Strada, M.I., Alper, B.J., (2018). Bisubstrate kinetics of glutathione S-transferase: a colorimetric experiment for the introductory biochemistry laboratory. *Journal of Chemical Education* 95, 146-151.

Steinmann, P., Keiser, J., Bos, R., Tanner, M., Utzinger, J., (2006). Schistosomiasis and water resources development: systematic review, meta-analysis, and estimates of people at risk. *The Lancet. Infectious diseases* 6, 411-425.

Studier, F.W., (1991). Use of bacteriophage T7 lysozyme to improve an inducible T7 expression system. *Journal of molecular biology* 219, 37-44.

Stutzer, C., Richards, S.A., Ferreira, M., Baron, S., Maritz-Olivier, C., (2018). Metazoan Parasite Vaccines: Present Status and Future Prospects. *Frontiers in cellular and infection microbiology* 8, 67.

Taylor, M.G., (1970). Hybridisation experiments on five species of African schistosomes. *Journal of helminthology* 44, 253-314.

Toh, S.Q., Glanfield, A., Gobert, G.N., Jones, M.K., (2010). Heme and blood-feeding parasites: friends or foes? *Parasites & vectors* 3, 108.

Torres-Rivera, A., Landa, A., (2008). Glutathione transferases from parasites: a biochemical view. *Acta tropica* 105, 99-112.

Trottein, F., Godin, C., Pierce, R.J., Sellin, B., Taylor, M.G., Gorillot, I., . . . Capron, A., (1992). Inter-species variation of schistosome 28-kDa glutathione S-transferases. *Molecular and biochemical parasitology* 54, 63-72.

Utzinger, J., N'Goran, E.K., N'Dri, A., Lengeler, C., Shuhua, X., Tanner, M., (2000). Oral artemether for prevention of Schistosoma mansoni infection: randomised controlled trial. *The Lancet* 355, 1320-1325.

Utzinger, J., Raso, G., Brooker, S., De Savigny, D., Tanner, M., Ornbjerg, N., . . . N'Goran E, K., (2009). Schistosomiasis and neglected tropical diseases: towards integrated and sustainable control and a word of caution. *Parasitology* 136, 1859-1874.

Vajda, S., Weng, Z., Rosenfeld, R., DeLisi, C., (1994). Effect of conformational flexibility and solvation on receptor-ligand binding free energies. *Biochemistry* 33, 13977-13988.

van Bladeren, P.J., van Ommen, B., (1991). The inhibition of glutathione S-transferases: mechanisms, toxic consequences and therapeutic benefits. *Pharmacology & therapeutics* 51, 35-46.

Vedadi, M., Niesen, F.H., Allali-Hassani, A., Fedorov, O.Y., Finerty, P.J., Jr., Wasney, G.A., . . . Edwards, A.M., (2006). Chemical screening methods to identify ligands that promote protein stability, protein crystallization, and structure determination. *Proceedings of the National Academy of Sciences of the United States of America* 103, 15835-15840.

Vos, T., Flaxman, A.D., Naghavi, M., Lozano, R., Michaud, C., Ezzati, M., . . . Memish, Z.A., (2012). Years lived with disability (YLDs) for 1160 sequelae of 289 diseases and injuries 1990-2010: a systematic analysis for the Global Burden of Disease Study 2010. *Lancet (London, England)* 380, 2163-2196.

Walker, J., Crowley, P., Moreman, A.D., Barrett, J., (1993). Biochemical properties of cloned glutathione S-transferases from Schistosoma mansoni and Schistosoma japonicum. *Molecular and biochemical parasitology* 61, 255-264.

Wang, W., Wang, L., Liang, Y.S., (2012). Susceptibility or resistance of praziquantel in human schistosomiasis: a review. *Parasitology research* 111, 1871-1877.

Warburg, C., Christian, W., (1941). Determination of DNA content. *Biochem Z* 310, 384.

Waugh, D.S., (2011). An overview of enzymatic reagents for the removal of affinity tags. *Protein expression and purification* 80, 283-293.

Whitmore, L., Wallace, B.A., (2004). DICHROWEB, an online server for protein secondary structure analyses from circular dichroism spectroscopic data. *Nucleic acids research* 32, W668-673.

Whitmore, L., Wallace, B.A., (2008). Protein secondary structure analyses from circular dichroism spectroscopy: methods and reference databases. *Biopolymers* 89, 392-400.

Wiseman, T., Williston, S., Brandts, J.F., Lin, L.N., (1989). Rapid measurement of binding constants and heats of binding using a new titration calorimeter. *Analytical biochemistry* 179, 131-137.

Wright, M.D., Harrison, R.A., Melder, A.M., Newport, G.R., Mitchell, G.F., (1991). Another 26-kilodalton glutathione S-transferase of Schistosoma mansoni. *Molecular and biochemical parasitology* 49, 177-179.

Yassin, Z., Ortiz-Salmerón, E., García-Maroto, F., Barón, C., García-Fuentes, L., (2004). Implications of the ligandin binding site on the binding of non-substrate ligands to Schistosoma japonicum-glutathione transferase. *Biochimica et biophysica acta* 1698, 227-237.

Zelck, U.E., Von Janowsky, B., (2004). Antioxidant enzymes in intramolluscan Schistosoma mansoni and ROS-induced changes in expression. *Parasitology* 128, 493-501.

Zhan, B., Perally, S., Brophy, P.M., Xue, J., Goud, G., Liu, S., . . . Hotez, P., (2010). Molecular cloning, biochemical characterization, and partial protective immunity of the heme-binding glutathione S-transferases from the human hookworm Necator americanus. *Infection and immunity* 78, 1552-1563.

Appendix

Supplementary material

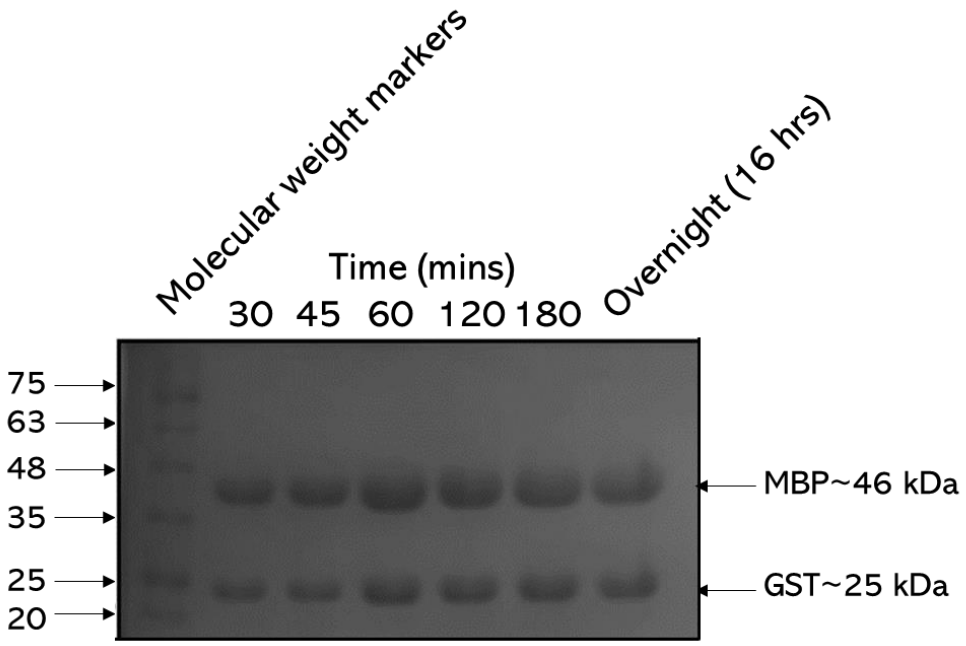

Figure S1. Thrombin cleavage trials. 12% SDS-PAGE showing MBP-His-Sbh26GST construct being cleaved into MBP and His-Sbh26GST by thrombin at variable times. It takes as little as 5 min for the cleavage to occur. However, the optimal condition that yielded the most protein was ~ after 2 h.

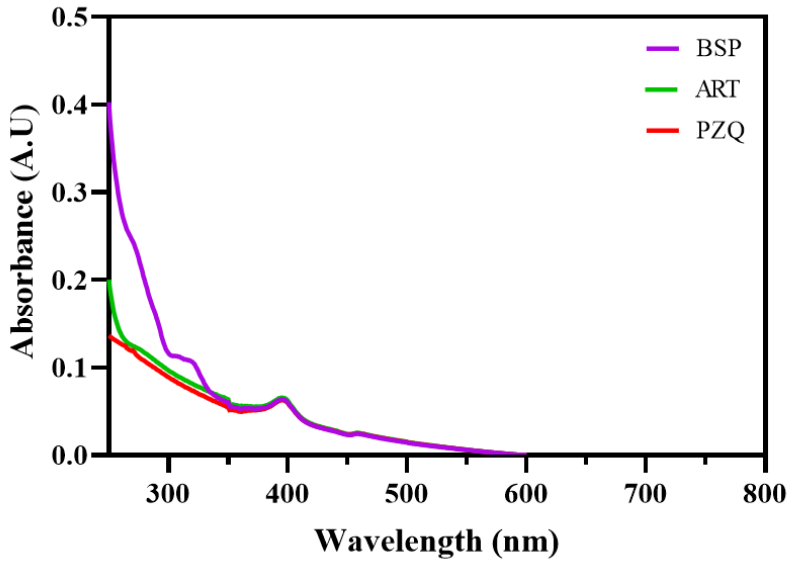

Figure S2. Absorbance spectrum of ligands used in the study (PZQ, ART and BSP). The ligands of interest insignificantly absorbed light at a wavelength that was used to measure the activity of the enzyme or structural changes at the tertiary structure level (295 nm, 340 nm, and 395 nm).

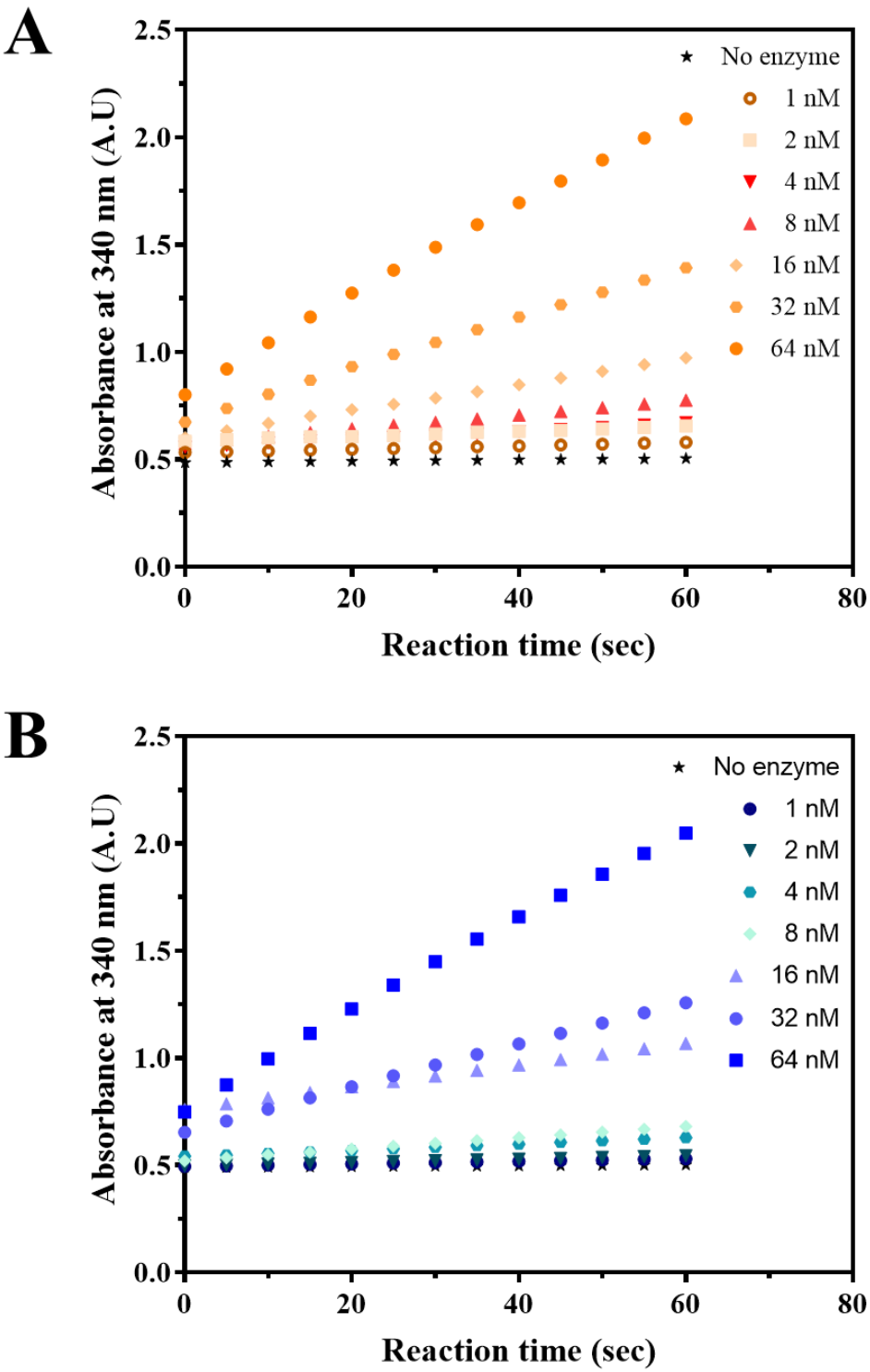

Figure S3. Progress curves of GSH-CDNB conjugation by Sbh26GST (A) and Sh28GST (B). The activities of the enzymes were measured by monitoring the product formation of 1-(S-glutathionyl)-2,4 dinitrobenzene for the 60s upon initiating the reaction by adding 1 mM CDNB to the GSH buffer of the proteins. It showed an increasing A_{340} reading over time. Thereafter, the slope of linear regression was used to calculate initial velocities (V_o). The data fit of the linear regression lines in all cases was about R^2= 0.98.

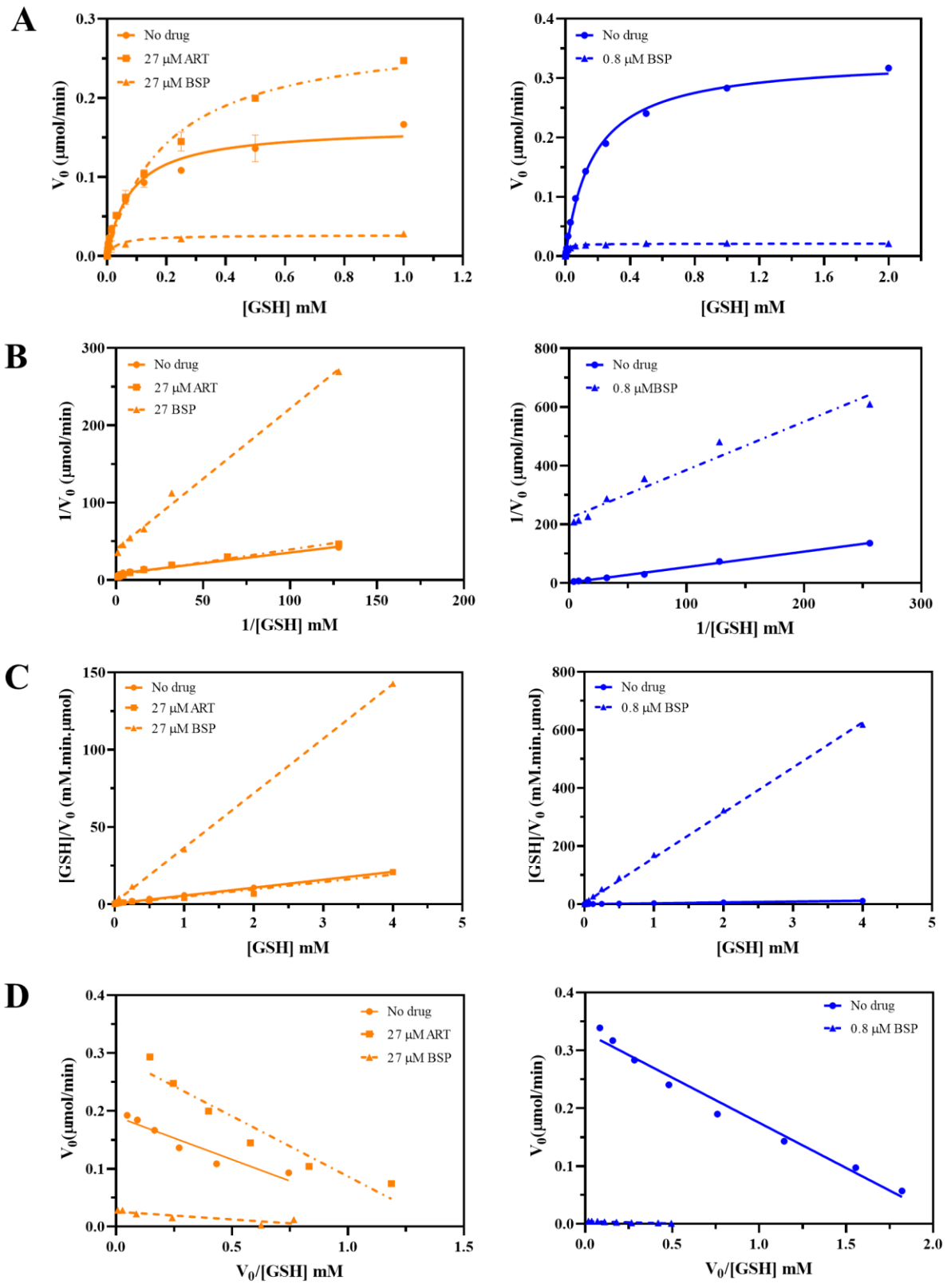

Figure S4. Linear-plots of Michaelis-Menten kinetics for Sbh26GST and Sh28GST. A Reference point of the hyperbolic curve of Sbh26GST in orange and Sh28GST in blue**. B** Lineweaver-Burke plot. **C**. Hanes-Woolf plot and, **D**. Eddie-Hofstee. All the plots show that the binding of BSP decreases the enzyme activity of Sbh26GST and Sh28GST by decreasing both the V_{max} and K_M whereas ART enhances the activity of the enzymes.

Table S1. The variation of Michaelis-Menten Kinetic parameters of Sbh26GST and Sh28GST based on different arrangements of the linear plots for error analysis.

		Sbh26GST			Sh28GST	
Kinetic parameter	**Type of plot**	**No drug**	**27 ART**	**27 BSP**	**No drug**	**0.8 BSP**
V_{max} (µmol/min)	Michaelis-Menten	0.190 ± 0.021	0.320 ± 0.014	0.0300 ± 0.001	0.34 ± 0.063	0.0061 ± 0.041
	Lineweaver-Burk	0.136 ± 0.047	0.147 ± 0.072	0.0345 ± 0.011	0.28 ± 0.041	0.0048 ± 0.330
	Hanes-Woolf	0.194 ± 0.380	0.210 ± 1.150	0.0283 ± 1.280	0.34 ± 0.160	0.0064 ± 0.570
	Eadie-Hofstee	0.190 ± 0.290	0.295 ± 0.420	0.0258 ± 0.053	0.33 ± 0.310	0.0070 ± 0.004
K_M (µM)	Michaelis-Menten	120 ± 0.034	250 ± 0.011	36.5 ± 0.006	176 ± 0.082	13.9 ± 0.092
	Lineweaver-Burk	33.3 ± 0.087	39.1 ± 0.140	37.2 ± 0.070	136 ± 0.250	7.80 ± 0.150
	Hanes-Woolf	101 ± 0.097	37.1 ± 0.091	36.2 ± 0.075	155 ± 0.310	28.8 ± 0.050
	Eadie-Hofstee	148 ± 0.051	208 ± 0.110	26.8 ± 0.018	156 ± 0.046	7.94 ±0.009

*Value ± SD

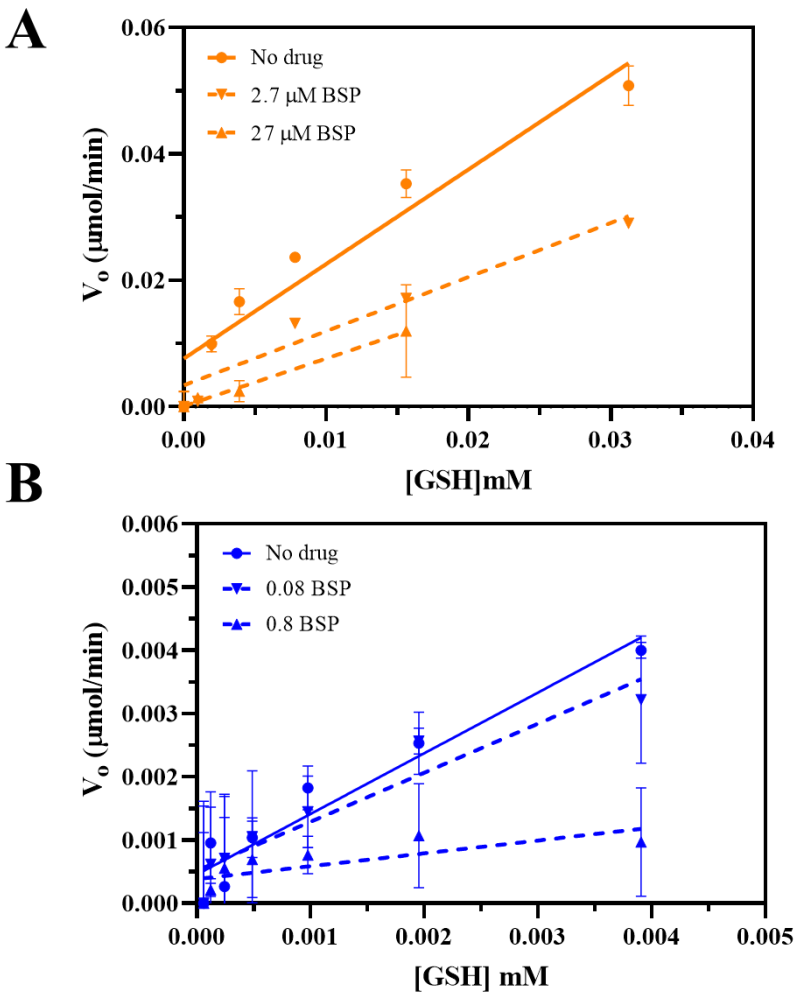

Figure S5. k_{cat} determination of Sbh26GST and Sh28GST. GSH-CDNB conjugation was performed with varying concentrations of GSH far below the K_M values of Sbh26GST (orange) and Sh28GST (blue) in the absence and presence of BSP at IC_{50} value and 10x less than the value. The introduction of BSP disrupts catalytic efficiency as it decreases the affinity of GSH required for GSH-CDNB conjugation.

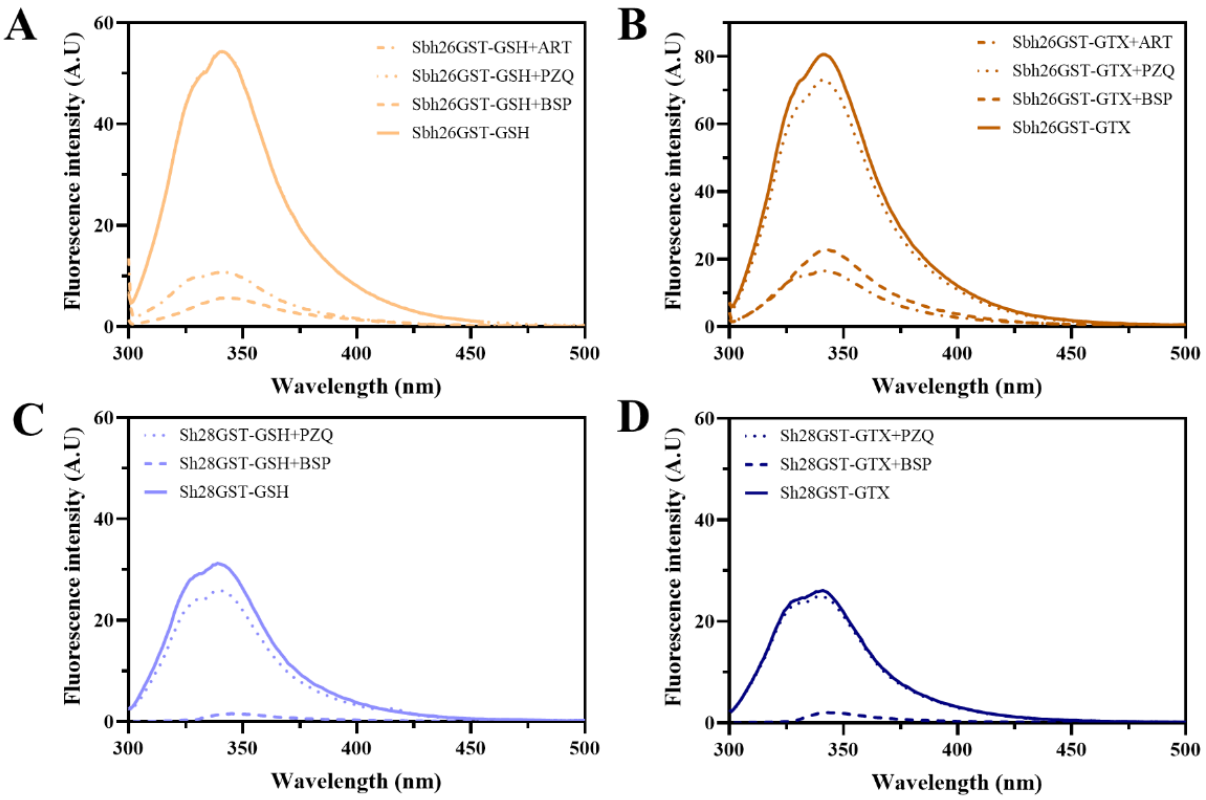

Figure S6. Trp fluorescence emission spectra of Sbh26GST in the presence of GSH (A) and GTX (B) as well as Sh28GST in the presence of GSH (C) and GTX (D). Trp residues of 10 µM of Sbh26GST in 50 mM Tris-HCl and Sh28GST in PBS buffer, all with 1 mM DTT, 1 mM EDTA and 0.02% (w/v) NaN_3 at pH 7.2 were excited at 295 nm and emissions were analysed between 300 and 500 nm. Thereafter 1 mM of co-substrates and 100 µM of ligands were added for comparison to the native proteins. Overall, PZQ had an insignificant impact whereas BSP and ART resulted in decreased intensities which correspond to exposed Trp residues.

Table S2. Impact of ligand binding on Trp fluorescence emission of Sbh26GST and Sh28GST with respect to PZQ, ART and BSP in the presence and absence of GSH and GTX.

A

Trp fluorescence	Sbh26GST				Sh28GST		
In the absence of ligands	**Apo**	**PZQ**	**ART**	**BSP**	**Apo**	**PZQ**	**BSP**
Maximum emission wavelength (nm)	342	342	342	342	341	340	377
Quantum yield	52.7	52.5	11.3	9.72	28.9	27.4	0.15
Shift relative to Apo (nm)	-	0	0	0	-	1	36
Type of shift relative to Apo	-	N/A	N/A	N/A	-	Blue	Red

B

Trp fluorescence	Sbh26GST				Sh28GST		
In the presence of GSH	**Apo**	**PZQ**	**ART**	**BSP**	**Apo**	**PZQ**	**BSP**
Maximum emission wavelength (nm)	341	342	341	343	339	339	348
Quantum yield	54.3	54.4	10.9	5.73	31.2	25.8	1.58
Shift relative to Apo (nm)	-	1	0	2	-	0	9
Type of shift relative to Apo	-	Red	N/A	Red	-	N/A	Red

C

Trp fluorescence	Sbh26GST				Sh28GST		
In the presence of GTX	**Apo**	**PZQ**	**ART**	**BSP**	**Apo**	**PZQ**	**BSP**
Maximum emission wavelength (nm)	341	340	341	343	342	340	344
Quantum yield	80.6	72.9	16.6	22.8	25.9	24.9	2.01
Shift relative to Apo (nm)	-	1	0	2	-	2	2
Type of shift relative to Apo	-	Red	N/A	Red	-	Blue	Red

The baseline or reference point is indicated by (–) and cases where they were no changes are indicated with N/A for not applicable.

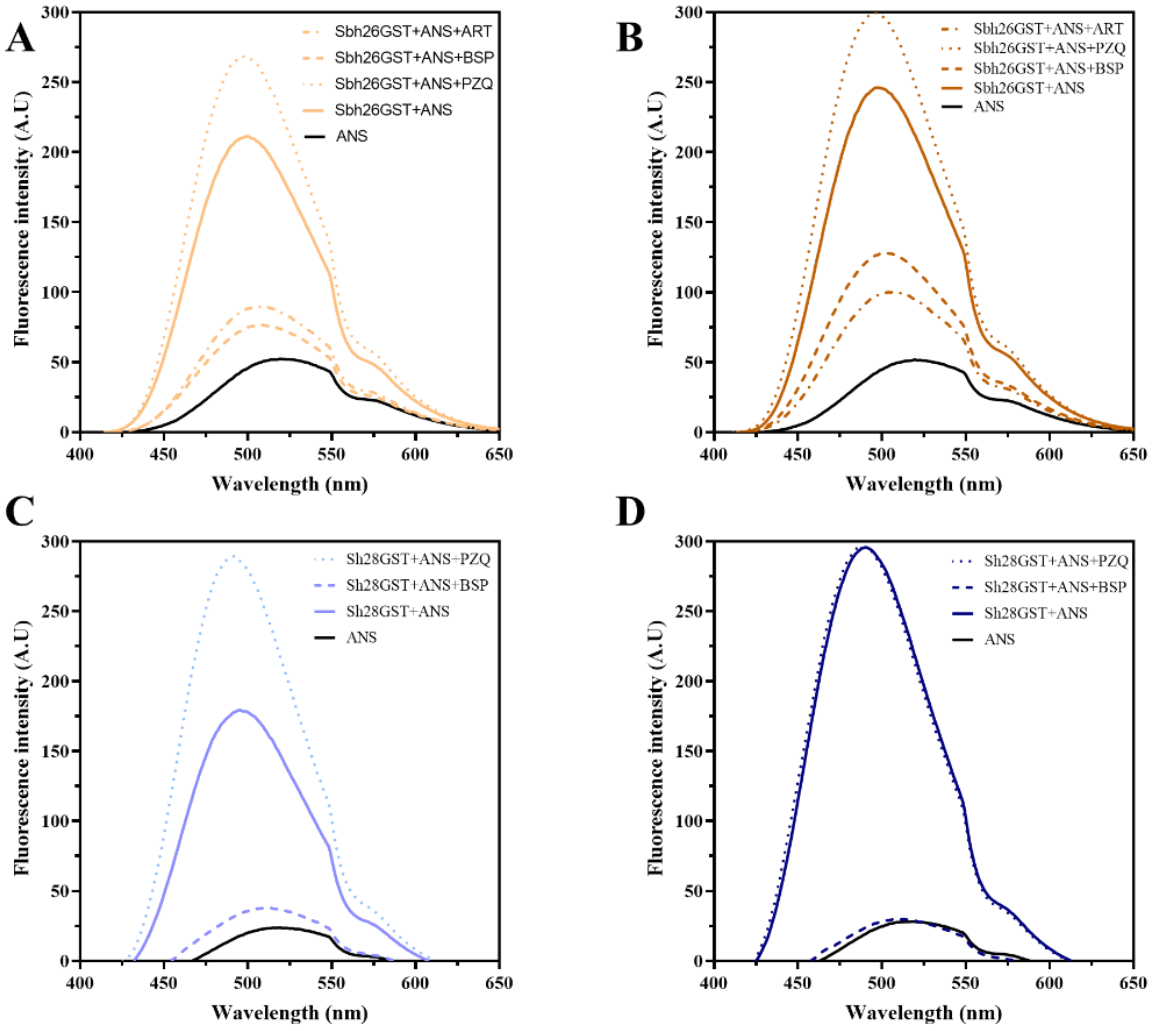

Figure S7. ANS fluorescence emission spectra of Sbh26GST in the presence of GSH (A) and GTX (B) as well as Sh28GST in the presence of GSH (C) and GTX (D). An anionic dye, ANS was used as a probe for proteins' hydrophobicity and ligand binding insights of PZQ, ART and BSP. 10 µM Sbh26GST in 50 mM Tris-HCl and Sh28GST in PBS buffer, all with 1 mM DTT, 1 mM EDTA and 0.02% (w/v) NaN_3 at pH 7.2 were excited at 395 nm and emissions were analysed between 400 and 600 nm. Thereafter, 1 mM of co-substrates (GSH and GTX) and 100 µM of ligands were added for comparison to the native structures. Overall, PZQ had an insignificant impact whereas BSP and ART resulted in decreased intensities accompanied by a slight blueshift in wavelength with respect to free ANS.

Table S3. Impact of ligand binding on ANS fluorescence emission of Sbh26GST and Sh28GST with respect to PZQ, ART and BSP in the presence and absence of GSH and GTX.

A

ANS fluorescence	Sbh26GST				Sh28GST		
In the absence of ligands	**Apo**	**PZQ**	**ART**	**BSP**	**Apo**	**PZQ**	**BSP**
Maximum emission wavelength (nm)	493	496	502	502	490	497	511
Quantum yield	281	424	124	101	225	376	34.3
Shift relative to Apo (nm)	-	3	9	9	-	7	21
Type of shift relative to Apo	-	Red	Red	Red	-	Red	Red

B

ANS fluorescence	Sbh26GST				Sh28GST		
In the presence of GSH	**Apo**	**PZQ**	**ART**	**BSP**	**Apo**	**PZQ**	**BSP**
Maximum emission wavelength (nm)	500	497	506	506	495	492	511
Quantum yield	211	268	89.5	76.7	179	288	37.9
Shift relative to Apo (nm)	-	3	6	6	-	3	16
Type of shift relative to Apo	-	Blue	Red	Red	-	Blue	Red

C

ANS fluorescence	Sbh26GST				Sh28GST		
In the presence of GTX	**Apo**	**PZQ**	**ART**	**BSP**	**Apo**	**PZQ**	**BSP**
Maximum emission wavelength (nm)	498	496	508	501	490	487	510
Quantum yield	246	299	100	128	295	296	29.3
Shift relative to Apo (nm)	-	2	10	3	-	3	20
Type of shift relative to Apo	-	Blue	Red	Red	-	Blue	Red

The baseline or reference point is indicated by (–)

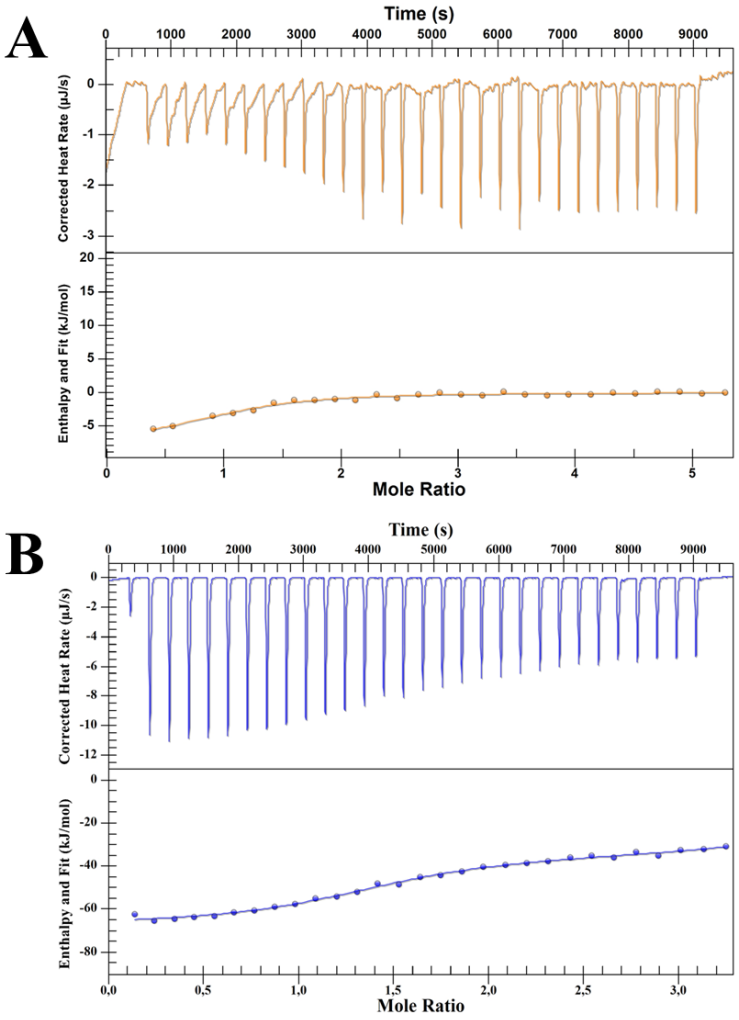

Figure S8. Thermogram and isotherm of Sbh26GST and Sh28GST interacting with BSP. Thermodynamic parameters of BSP-Sbh26GST (**A**) and BSP-Sh28GST (**B**) were determined in the presence of 50 µM protein, 1 mM BSP and 1 mM GSH under the following conditions: 50 mM Tris-HCl, 2 mM EDTA and 1 mM TCEP at pH 7.2, 25 °C and 310 rpm stirring every 300s until 30 injections.

Table S4. Thermodynamic parameters of BSP interaction with Sbh26GST and Sh28GST in the presence and absence of GSH based on multiple sites model fitting (H-site vs L-site).

Thermodynamic parameters	Sbh26GST		Sh28GST	
Multiple sites model	No GSH	With GSH	No GSH	With GSH
K_{d1} (µM)	0.001 ± 0.01	17.2 ± 0.006	23.3 ± 0.067	0.19 ± 0.018
K_{d2} (µM)	0.0538 ± 0.81	0.001 ± 003	95.8 ± 0.023	4.6 ± 0.048
ΔH_1 (kJ/mol)	-24.2 ± 0.33	-7.65 ± 1.63	-100 ± 1.37	-67.8 ± 2.14
ΔH_2 (kJ/mol)	0.53 ± 1.20	0.629 ± 1.23	168 ± 1.61	-36.3 ± 3.55
ΔS_1 (J/mol·K)	91.1	65.6	-247	-98.4
ΔS_2 (J/mol·K)	141	59.4	-642	-19.6
ΔG_1 (kJ/mol)	-51.4	-27.2	-26.4	-38.5
ΔG_2 (kJ/mol)	-41.5	-17.1	-22.9	-30.5
n_1/dimer	1.12 ± 0.05	1.01 ± 0.39	0.92 ± 0.13	1.34 ± 0.16
n_2/dimer	4.83 ± 0.70	0.10 ±0.48	0.26 ± 0.26	2.93 ± 0.97

* The readings are captured as value ± SD at 95% confidence level. The residual plot deviations around fit for Sbh26GST were 3.8 and 4.6 in the presence and absence of 1 mM GSH respectively then for Sh28GST it was 2.9 and 4.3

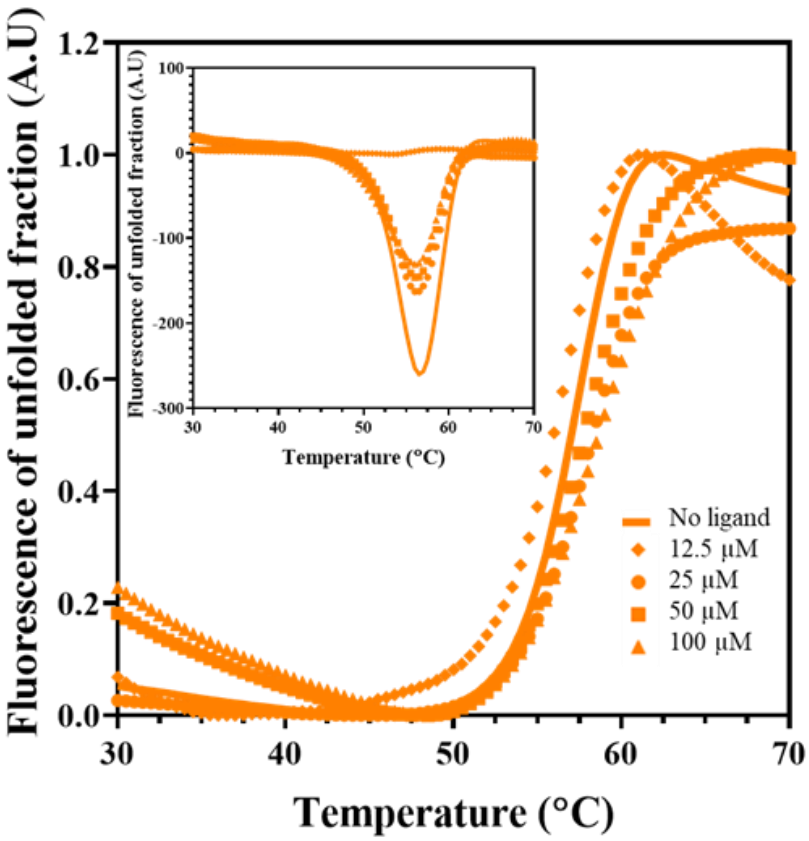

Figure S9. Thermogram of Sbh26GST. A thermal shift assay was performed using SYPRO Orange dye as a probe for hydrophobicity. The protein was in PBS buffer, pH 7.2 supplemented with 1 mM DTT and EDTA, where it was unfolded with increasing temperature at varying concentrations of BSP. These make room for the bulky dye to bind and increase its fluorescence. Thereafter, when the protein loses its structure at high temperature (denature), the dye unbinds thus a decrease in quantum yield. The plot shows a higher initial unfolding transition with high concentrations of BSP, despite increased stability.